Advancing Indoor Multi-person Localisation System based on Sensor Fusion Method

Renjie Wu
20319414

Thesis submitted to the University of Nottingham for the degree of Doctor of Philosophy, 2024.

Supervised by
Dr. Boon Giin Lee
Dr. Matthew Pike
Dr. Liang Huang

I, Renjie Wu, hereby confirm that the work presented in this thesis is my own. Where information has been derived from other sources, I confirm that this has been indicated in the thesis. This thesis is written by LaTeX based on the template provided by Chao Zhang [1].

Abstract

Indoor positioning systems (IPS) have garnered increasing attention in the field of positioning research in emergency services such as firefighting scenarios. The capability to deliver precise and comprehensible positioning information for multiple firefighters in harsh environments is a promising technology. It will effectively save their lives via timely and accurate location information for evacuation and reinforcement. The sensor fusion-based dead reckoning (DR) method is one of the typical techniques in IPS. Due to its little reliance on layout knowledge and pre-installed positioning hardware in the building, it is regarded as one of the most promising methods for IPS in firefighting. Existing research on DR has not adequately addressed the challenges of positioning accuracy, surrounding reconstruction, and multi-person positioning in firefighting scenarios. In order to address these problems, this thesis explores advanced DR based multi-person localisation and mapping. The research work consists of five associated studies that aim to answer the formulated research questions. The first three studies explore the novel approaches in gait analysis-based heading estimation, dual foot synergistic step detection and dynamic minimum stride length constraint-based positioning optimisation. The objective of these studies is to improve the precision of positioning by optimising parameters in the DR calculation process. The next study presents a geometry algorithm that utilises a polar projection strategy to determine the coordinates of map points and reconstruct the user's surrounding map. The last study explores an innovative approach for integrating multiple trajectories via online magnetic fingerprint matching. By doing so, the position of each individual is updated by combining fingerprint information. This thesis conducts experiments to evaluate the performance of the systems proposed in each study. Each experiment is tailored with specifically designed realistic indoor scenarios, data collection hardware, and evaluation metrics. The quantitative assessment results illustrate improved positioning accuracy in comparison to conventional methods. The displayed trajectory and map demonstrate accurate results that exhibit high consistency with the ground truth.

Key Words: Indoor positioning system (IPS); Dead reckoning (DR); Gait analysis; Sensor fusion; Kalman Filter; Multi-person localisation; Firefighting Scenarios.

Acknowledgements

I wish to convey my profound appreciation to my team of supervisors for their invaluable support throughout every phase of the research endeavour. Dr. Boon Giin Lee and Dr. Matthew Pike actively participated in my brainstorming sessions, experimental implementations, and academic presentation and writing. Their assistance helped me become acquainted with research activity and advance significant contributions to my project. I would like to express my gratitude to Dr. Liang Huang for his invaluable technical assistance during my study. I would like to express my gratitude to the members of the Artificial Intelligence and Optimisation (AIOP) research groups for organising various research activities that have significantly expanded my understanding in the field of computer science. I also want to express my gratitude to my friends, lab mates, colleagues, and research team for the valuable and enjoyable time we spent together in the laboratory and during social interactions. Finally, I would like to convey my appreciation to my parents. Without their profound comprehension and unwavering support in recent years, it would be unattainable for me to successfully conclude my academic pursuits.

Contents

List of Tables

List of Figures

Chapter 1

Introduction

1.1 Overview

Indoor positioning system (IPS) [2] is a promising technology which aims to locate people where the widely used global navigation satellite system (GNSS) [3] lacks precision or fails entirely, such as inside multistory buildings and underground locations. IPS exhibits significant application potential in various scenarios involving industry [4], extended reality [5] and emergency services [6] which has garnered considerable attention from the research community.

IPS methods can be categorised into two groups: building dependent and building independent techniques. The majority of building dependent IPS requires hardware or pre-installation of hardware during the building construction with the dedicated layout information acknowledged. These methods track the targeted people and objects by triangulation and trilateration [7] using the measured geographic distance or angle between the transmitters (within the building) and the receiver (placed on the moving platforms e.g. people and vehicles). Various wireless sensor network (WSN) approaches using different radio frequency (RF) based measurement tools, including wireless local area network (WLAN) [8], Bluetooth low energy (BLE) [9], ultra-wide band (UWB) [10], radio frequency identification (RFID) [11] and narrow band internet of things (Nb-IoT) [12].

Building independent IPS methods, however, do not require prior information about the building or placing any hardware in the building. Typical building independent IPS methods include simultaneous localisation and mapping (SLAM) [13, 14] and dead reckoning (DR) approaches [15, 16]. SLAM based building independent methods use cameras [17], light detection and ranging (Lidar) [18] and millimetre wave radio detection and ranging (mmWave Radar) [19] for optical, laser and radio imaging, enabling the simultaneous indoor structure reconstruction or updating of a map in an unfamiliar location while keeping track of it. In DR methods, after determining the initial position via the calibration process, the current position of the user can be iteratively calculated by knowing the last calculated position and current measured kinematic parameters.

Environmental factors [20], user motion [21], and knowledge of the indoor structure [22] pose serious challenges to the performance and reliability of IPS. IPS utilised in indoor firefighting scenarios is a typical case afore described. Firefighters often encounter dangerous missions of rescuing trapped people from burning buildings [23]. The power outage and high temperature in the burning building will impede the regular functioning of the transmitter nodes in WSN which poses significant challenges to the WSN based approach for localisation [24]. Considering the characteristics of the DR method, it has great advantages utilised in the firefighting scenario [25]. Compared with building dependent methods, DR methods work independently without external hardware pre-installed in the buildings, which reduces the setup time. This advantage enables firefighters to rescue in any building with no WSN deployment installed. Compared with SLAM which also belongs to building independent methods, DR methods are less susceptible to environmental conditions where the imaging quality of SLAM is easily affected by rapid motion, ionising radiation and weather conditions [26]. Consequently, DR methods outperform SLAM based methods with usage flexibility. Benefiting from these particularities, DR methods are identified as the most promising approach for firefighting scenarios.

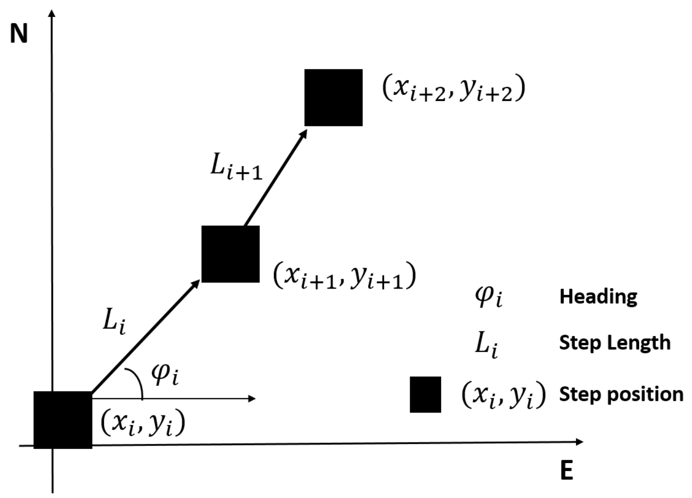

Figure 1.1: *Schematic of DR calculation with three continual steps (No. i to No. $i+2$).*

DR based navigation method has been one of the major research focus of IPS for over decades. The term DR is a process of computing the current position of a moving object by using a last calculated position with the incorporation of estimating step length, heading, and elapsed time [16] as visualised in Fig. 1.1. Specifically, the DR methods comprise of two major implementations: pedestrian dead reckoning (PDR) and inertial navigation system (INS) as visualised in Fig. 1.2. In PDR, the sampling rate is followed by the frequency of the step rate. The heading value and step length value for each detected step are the direct factors that affect the positioning accuracy. Another implementation INS, however, updates the positioning results following the sampling rate of the sensors which could achieve a higher rate than PDR. An optimisation approach is adopted to reduce the positioning bias and cumulative error. Both PDR and INS require accurate step detection for determining the optimal instant of positioning and optimisation. The heading estimation accuracy of PDR, optimisation performance of INS and precision of DR methods are the most significant research objectives in this field. In improving these, the cumulative error of DR would be decreased while the positioning accuracy at each time instant is improved.

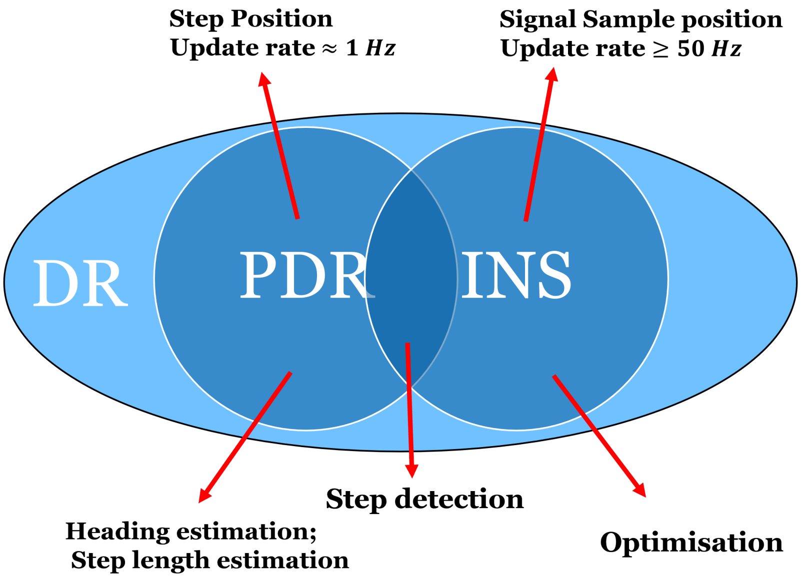

Figure 1.2: *The relationship diagram of DR, PDR, and INS.*

To narrow down the research objectives, this thesis focuses on the DR method using inertia data. The inertial measurement unit (IMU) [27] is one of the most commonly used sensors to measure inertia data. As illustrated in Fig. 1.3 [21], there are many options for the IMU placement for DR methods implementations. Specifically, foot-mount DR shows the lowest average positioning error compared with others. To achieve better positioning performance, DR methods with foot-mounted sensors for data collection will be mainly focused on in this thesis.

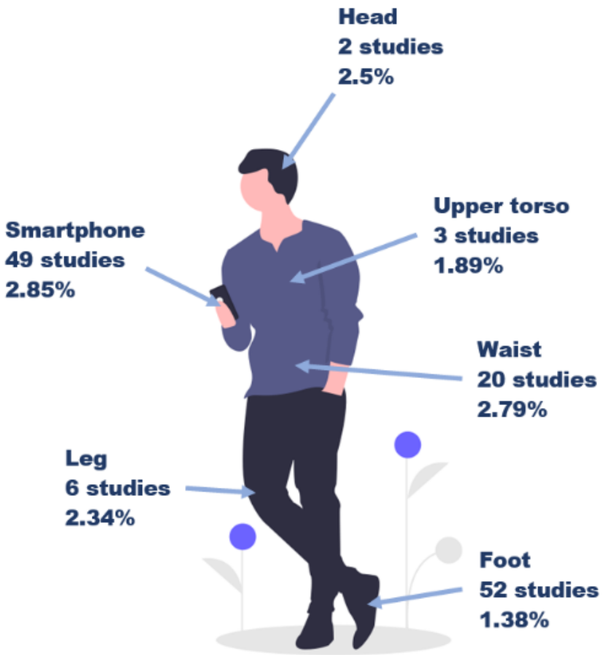

Figure 1.3: *Average positioning error of DR methods with different sensor placement [21].*

In light of the prospective firefighting applications of the DR method, three significant research gaps are identified. First, the firefighters' gait type changes due to the unpredictable and dangerous rescuing conditions, which hampers the accuracy of positioning utilising classic DR methods that rely on fixed thresholds [28] in motion estimation. Second, given the urgent need to rescue people, firefighters do not have the time to familiarise themselves with the structure of buildings beforehand, thereby heightening the likelihood of being disoriented. Being disoriented in such dangerous scenarios poses an immense peril that significantly jeopardises the safety of firefighters [29]. Finally, firefighters typically employ a collaborative approach [30] including multiple individuals to enhance support and promote collaboration among team members [31]. Existing literature indicates that few complete and specific DR methods address the enhancement of positioning accuracy, the reconstruction of layout and multi-person positioning.

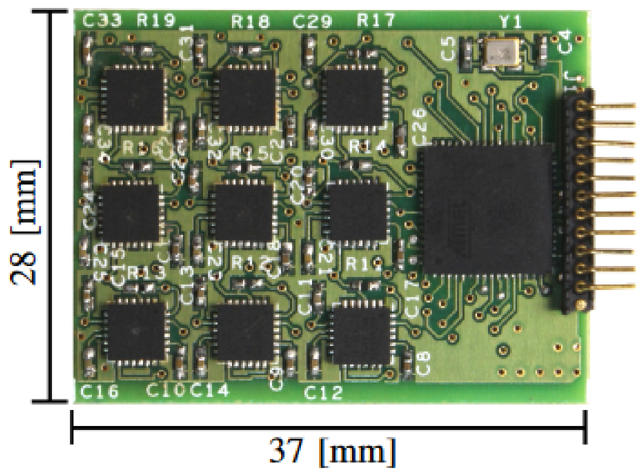

Figure 1.4: *An embedded sensor array platform holding 18 IMUs (9 on the top side and 9 on the bottom side) [32].*

Existing DR researches considered utilising sensor fusion methods to solve some of the presented problems. Building sensor array [32] for accuracy improvement is a typical solution. This design (refer to Fig. 1.4) enables multiple associated inertia data collection at the same time. By doing this, the measurement error over a short period is decreased. However, not only does the sensor array measurement provide difficulty in data fusion and global calibration because of the placement and the tiny differences in specifications of each sensor unit, but also causes implementation problems in the heavy onboard data processing load and difficulty in data transmission. Therefore, this design is impractical in real-world applications. Utilising high-quality IMU such as Xsens inertial motion capture module [33] can also achieve improved positioning accuracy. However, this module requires expensive module prices with high computing resources for motion calculation, which is not affordable and practical in pervasive application scenarios

Other sensor fusion based methods combine data readings from different sensors such as "IMU+UWB" [34], "IMU+WLAN" [35] and "IMU+BLE"

[36]. Though these methods improve positioning accuracy and reduce error cumulation, these improvements are beneficial from the WSN based positioning while not suitable to the assumed firefighting scenario that requires applying IPS without sensor pre-installation in the building. This thesis presents studies that aim to develop an advanced multi-person DR system with improved accuracy and surrounding map reconstruction, which is anticipated to fill the research gaps presented above, provide a practical system suitable for firefighting scenarios and facilitate the development of IPS for firefighters.

It is worth declaring that due to the challenges associated with environmental setups and the beyond-the-scope technology, such as wearable design, waterproof and heat resistant housing and wireless data transmission in real fire-rescuing scenarios, this thesis mainly focuses on enhancing the DR method under assumed conditions in burning buildings, such as low visibility, WSN and SLAM unavailability and gait variety [37, 38]. Consequently, the research questions and presented studies are carried out to fulfil the demands within these limited factors. The techniques employed in each study are also assessed under simulated experimental settings.

1.2 Research Questions

Having established the focus of applying the sensor fusion method in the DR system to perform improved indoor multi-person DR localisation, the scientific research questions presented in this thesis are listed below.

RQ1: What practical techniques can mitigate the cumulative errors in inertial based DR methods?

RQ2: What techniques can be utilised to reconstruct the layout of the surroundings in the DR method?
RQ3: What techniques can DR methods adopt to effectively update positioning results via common attributes from multiple persons?

To investigate and answer the research questions presented above, this thesis conducts specific studies.

To answer **RQ1**, this thesis explores three novel studies for DR system positioning accuracy improvement from different perspectives. Specifically, **Study 1** presents a gait analysis (GA) algorithm in heading estimation. By doing this, the heading value in DR calculation is enhanced which contributes to more accurate positioning results. The gait analysis-aided pedestrian dead reckoning (GA-PDR) is implemented for algorithm evaluation. **Study 2** focuses on the quality of step detection, another gait characteristic in DR systems. A dual foot synergistic method is investigated by analysing dual foot generalised likelihood ratio test (GLRT) [39] sequences. The objective is to establish the optimal timing for transitioning to the zero velocity phase, resulting in enhanced positioning accuracy. **Study 3** concentrates on the limited performance of dual foot optimisation when employing a fixed threshold in the dual foot stride length model. By detecting minimum stride length parameters in each gait using ultrasonic sensors, the dual foot optimisation performance is improved, which results in improved positioning accuracy. These studies concentrate on the disparity and distinctive characteristics of gait. The utilisation of adaptive methods throughout various stages of DR calculation yields superior positioning results compared with conventional methods.

To answer **RQ2**, **Study 4** explores the integration of the IMU and ultrasonic sensors through geometry calculation. The idea of this method is inspired by the occupancy grid map [40] where the coordinates of map points are calculated based on the estimated position and pose of the people with the measured distance data. Similarly, **Study 4** adopts this mechanism by exploring a polar projection based geometry algorithm for coordinate calculation. By doing this, the coordinates of map points are updated with positioning updates. It is worth noticing that the **Study 3** and **Study 4** are conducted together which implements inertial odometry and mapping (IOAM) system where the outcome of **Study 3** contributes to the inertial odometry and the one of **Study 4** contributes to the mapping.

In the final exploration study, **Study 5** explores the use of the magnetic field at the calculated positioning spot for detecting the timing of positioning updating relying on either self or others' original positional data. The implemented system in this study is called a multi-person inertial navigation system (Multi-INS). It is implemented through the sensor fusion method between IMUs and magnetometers from individuals and others. Multi-INS introduces a novel technique for calculating the trajectory of several individuals. It utilises an online process of comparing magnetic fingerprints (MF) to update the inertial state. Building upon an offline localisation technique that relies on magnetic fields, a new online method for organising magnetic field data is implemented to replace the current offline determination strategy. In addition, it proposes a method for selecting a region of interest in target MF data to improve the performance of MF matching by concentrating on the most relevant MF. **Study 5** develops two positional update mechanisms based on MF: individual self-update and multi-person cross-update which divides the position update into two cases where the individual's location is updated at certain reference points by utilising target MF data from the individual or another participant. The calculation result of **Study 5** is a single map which demonstrates updated locations from multiple users in a shared canvas. This means every user can identify the position of themselves and others in one fused map.

Table 1.1: Description of the Main Studies in the Thesis.

Research Questions	Study	Sensors	Frameworks	Methods
RQ1	1. GA-PDR	IMU	PDR	GA for heading estimation drift constraint;
RQ1	2. Dual foot synergistic method	IMUs	INS	Dual foot synergistic method in zero velocity detection;
RQ1	3. IOAM - Inertial Odometry	IMUs; ultrasonic sensors (stride length measuring)	INS	Dynamic minimum stride length based constraint for dual foot trajectory optimisation;
RQ2	4. IOAM - Ultrasonic Mapping	IMUs; ultrasonic sensors (surrounding range finer)	INS	Polar projection based map point modelling;
RQ3	5. Multi-INS	IMUs; Magnetometers	INS	Online magnetic fingerprint matching for multi-trajectory integration;

Within the majority of the work this thesis presents as shown in Table 1.1, an advanced DR system built upon the existing DR frameworks is developed. Experimental results indicate that the proposed DR system outperforms the state-of-the-art in terms of positioning accuracy and practical capabilities. The contributions this research work achieved in associated sensor fusion algorithms would facilitate the research of DR based methods and inspire new interests in IPS developments.

1.3 Thesis Outline

An overview of how the contents of this thesis is presented below.

Chapter2: literature Review The literature review chapter provides a wide overview of typical approaches to IPS. This chapter provides a comprehensive description of the advantages and disadvantages of each method, highlighting the technical description for considering the DR method. The limitations of the DR method using sensor fusion are also discussed.

Chapter 3: Methodology This chapter provides a detailed methodology descriptions of presented from **Study 1** to **Study 5**. Specifically, the system overview, notation definition and derivation of formulas including the detailed calculation process are comprehensively presented. In addition, this chapter provides a detailed description of the experimental setup section including sensor specifications, experimental situations, participant details and the design of the experiment, for evaluating the performance of the methods presented above.

Chapter 4: Results and Discussion This chapter examines the results of the proposed systems in terms of positioning and mapping, utilising error evaluation metrics and visualisation. The subjective and objective views are both considered while discussing the performance of the trajectory and map.

Chapter 5: Conclusion In this chapter, a comprehensive summary of contributions derived from the presented research is described. The limitations of this research work are discussed thoroughly. And future work section describes how the new ideas might be applied in the design, development and evaluation of multi-person localisation research.

Appendix A provides a comprehensive list of the abbreviations presented in this thesis. **Appendix B** presents a preliminary investigation of the progress and mapping capabilities of INS. The content of Appendix B consists of information extracted from a peer-reviewed study, which serves to better elucidate the advancements made in the research.

Chapter 2

Literature Review

This chapter presents the state-of-the-art in the research field of IPS. IPS approaches are classified into two categories: building dependent and building independent. The limitations of applying WSN and SLAM technologies in simulated environments are explored. Subsequently, this thesis presents a thorough investigation of DR methods utilising sensor fusion techniques.

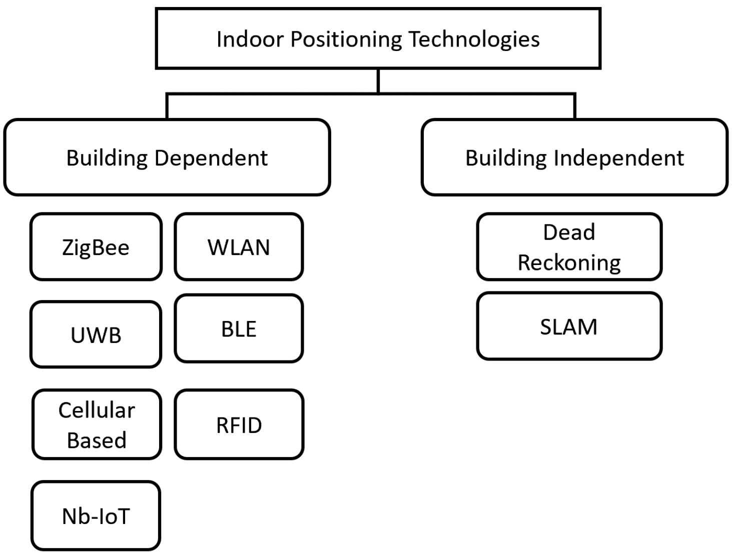

Figure 2.1: *Classification of IPS Technologies.*

2.1 WSN based IPS

RF navigation systems are widely used for localisation, making them one of the most popular methods in this field [41]. Wireless transmission protocols employing distinct RF possess varying capacities in terms of transmission range, resistance to interference and capacity to penetrate obstacles. WSN [42] is a common building dependent approach of IPS, in which multiple routers (referred to as nodes in WSN) communicate inside a given WSN using a shared protocol to exchange data. The position of moving nodes in a WSN is typically determined using the triangulation approach, as described in the study by Kuriakose *et al.* [43]. Before the calculation, the positions of static reference nodes are measured as prior information. Triangulation is conducted to ascertain the location by creating triangles using both the mobile nodes and the nodes with known positions. Typical RF in WSN methods include WLAN [44], BLE [45], Zigbee [46], Nb-IoT [12], UWB [10], 5G [47], RFID [48] which function positioning in different using cases.

WSN based IPS methods hold well-developed technology that achieves high accuracy and stability in ideal scenarios. However, WSN approaches need to pre-install the transmitters or access tags before use. This operation usually has high labour cost which requires the initial mapping of the building with optical calculations to find the best placement positions. This issue makes the WSN method hard to cover all the buildings such as massive residential buildings. Additionally, some WSN transmitters necessitate a continuous power supply, which might be inconvenient in specific scenarios e.g. firefighting where the power is cut.

2.2 SLAM based IPS

SLAM has emerged as a highly promising option for indoor positioning in service areas[49]. This technique utilises the detection of sequential features to gather surrounding data and simultaneously determine the trajectory and surrounding map. SLAM utilises a comprehensive system structure that involves extracting features, modelling geography, reconstructing space and optimising the system to build a map and track people or objects. SLAM aims to tackle the mapping problem in the absence of any prior knowledge about the environment. SLAM has found extensive applications in various fields, including the sweeping robot [50], autonomous vehicles [51], augmented reality (AR) [52], minimally invasive surgery (MIS) [53] and Unmanned Aerial Vehicle (UAV) [54].

Visual simultaneous localisation and mapping (vSLAM) [55] plays an important role in the SLAM area. Visual imaging from a digital camera provides informative data in an ideal environment to estimate position and mapping. However, limited by the characteristics of cameras, the vSLAM method is highly affected by dynamic changes in the environment [26] where images with mass blur provide less valuable feature information. Thermal-infrared SLAM [56] uses thermal infrared imaging from a thermographic camera to track the user and reconstruct the surrounding structure. However, in firefighting scenarios, the temperature of the object's surface is dynamic and the flow and heat radiation in the environment adversely affect the imaging quality and SLAM performance. Alternatively, Lidar-based SLAM constructs the trajectory and surrounding layout [57] from the pose graph and occupancy grid map via a 360-degree laser ranging strategy. However, this method is vulnerable to interference from external light sources and the measuring range is short. These disadvantages affect the reliability of Lidar SLAM in firefighting scenarios. Radar SLAM [58] benefits from millimeter-wave radar ranging, having fewer environmental conditions than visual cameras and Lidar. However, the enormous radar node rendering and low measurement resolution limit its widespread usage.

In summary, in firefighting scenarios with harsh environmental conditions, it is quite hard for SLAM to collect high quality data for tracking and mapping. Also, in the cases where firefighters move fast, the motion blur makes the SLAM system very difficult to calculate the accuracy position. Therefore, the SLAM system is not suitable for the presented scenario and it is consequently not considered in this thesis.

2.3 DR based IPS

DR methods analysis utilises the characteristics of body inertia to iteratively compute the individual position over time. Inertia data provides information on the force vector and angular rate of an object, revealing its current motion state. The IMU is a commonly used sensor for measuring inertia data. This sensor utilises a MEMS construction to convert the physical deformation of micromechanics into an electronic signal. An IMU typically comprises an accelerometer and a gyroscope, which is used to monitor 3-axis acceleration and 3-axis angular rate data. This section will introduce the inertial DR based method with its application.

2.3.1 Development and Improvements of DR

Heading Estimation

The DR system employs data from IMUs to anticipate the trajectory of user movements. This technique consists of three components: step detection, step-length estimate and heading estimation [21]. PDR is a traditional implementation of DR methods. The effectiveness of PDR relies heavily on the precision of the heading estimation [59, 60]. An approach to determine the heading involves utilising magnetometer data to compute the user's direction in relation to magnetic north [61]. Nevertheless, the calculation of magnetic heading is susceptible to distortion caused by irregular magnetic fields due to external magnetic interferences [62]. Other techniques for estimating headings using gyroscopic data have also been found to be problematic, mostly because of significant biases and drift errors [63]. Several methodologies have been suggested for achieving reliable heading predictions. Sensor filtering is a widely used method for combining data from several sources in order to minimise estimation mistakes. Fan *et al.* [61] introduced a novel approach that enhances the precision of heading estimation by integrating an adaptive KF with a complementary filter. Qiu *et al.* [64] introduced a PDR technique that relies on inertial and magnetic sensors. The algorithm utilises an EKF and a clustering-based method for detecting stance phases to estimate heading. Ashkar *et al.* [65] conducted an analysis on the performance of a fusion system that combines a magnetometer and inertial sensor using unscented Kalman filters (UKFs), EKFs and error-state EKFs (EEKFs). They demonstrated the efficacy of UKFs and EEKFs in this context. Wu *et al.* [66] proposed a method that utilises a KF and a maximum-likelihood-type estimator to detect outliers and enhance the accuracy of heading estimation. Zhang *et al.* [67] introduced a dual foot-range restriction to facilitate the calculation of adaptive step length and correction of heading. While these sensor fusion methods enhanced the precision of the heading estimation, gait errors arose due to misalignment between the foot's heading direction and the body's heading direction. Some studies have explored the use of machine learning techniques to achieve precise estimations of heading with great accuracy. In their study, Wang *et al.* [68] introduced a convolutional neural network to identify walking patterns and match magnetic finger trajectories for direction correction. Wang *et al.*[69] employed a support vector machine (SVM) for motion identification and a decision tree method for reducing localisation error. In their study, Wu *et al.* [70] introduced an adaptive approach that utilises human action to adjust the heading direction. An alternative optimisation strategy, based on non-steady-heading operations, was developed to reduce the accumulation error in PDR. While the findings of these studies enhanced the precision of heading calculations, machine learning-based methods are not feasible due to the time-sensitive nature of fire rescue scenarios.

In addition to employing filtering and machine learning techniques, certain research has included RF and RSSI-related technologies to enhance the accuracy of heading calculations. Zhang *et al.* [67] introduced a technique for estimating headings using anchor points that has predetermined position coordinates. The anchor points were employed for the initial calibration and subsequent correction of the heading at corners. Tateno *et al.* [71] introduced a technique that utilised WLAN signals and a RSSI algorithm to enhance the accuracy of heading estimation. Chen *et al.* [72] introduced a method that uses UWB technology to address the issue of error accumulation in PDR. The precision of the direction was enhanced by the use of external sensors, although the practicality of deploying these beacons is hindered in smoke-filled buildings during fire rescue operations.

To mitigate the adverse consequences of heading drift, scholars have suggested employing the corridor direction within buildings as a limit on the trajectory. The heading direction will be adjusted to the nearest dominating direction established in advance to minimise the mistake caused by drift in the IMU data. Borenstein and Ojeda [73] proposed a heuristic drift elimination (HDE) method to rectify bias drift and other gradual errors originating from gyroscopes and accelerometers. Nevertheless, the precision of the method diminished after a certain duration of prolonged walking due to excessive correction. To address the issue of misalignment of HDE in the dominant direction, Jiménez *et al.* [74] presented an enhanced version of HDE known as iHDE (improved HDE). The iHDE utilises movement analysis and a confidence estimator to minimise heading mistakes. Nevertheless, this approach is not feasible due to the prevalent usage of predetermined thresholds for movement analysis. Muhammad *et al.* [75] introduced a HDE technique that incorporates a zero-velocity update turn detector and heading correction for pelvic rotation. While the direction drifting inaccuracy was mitigated, some walking patterns, including those that involve turning around (a frequently employed firefighting move to minimise risk by retracing a previously investigated route), were not taken into account when utilising this approach. Wu *et al.* [76] employed a heuristic approach. A method for correcting heading using heading reduction and a cardinal heading-aided inertial navigation technique was proposed. However, the implementation of this strategy was limited in emergent rescue scenarios due to the requirement of a complicated multilayer perception network and an EKF for pre-processing.

Step Detection

Foot-mounted inertial navigation system (FT-INS) is another implementation of DR methods [77] to track users' walking movement. Different from PDR which updates position for each step, FT-INS analyses foot motion characteristics from continual inertia samples which achieve higher positioning resolution. Compared to widely used passive indoor localisation methods [78–82], INS offers superior performance as it calculates trajectories without relying on external transmission nodes or initialisation operations. Dual foot INS (DF-INS) is an enhanced version that leverages data from both feet for more robust and accurate localisation [29, 83]. The gait cycle in DF-INS is identified through zero-velocity detection [84], distinguishing the stance and swing phases [85]. During the stance phase, INS optimises the error in users' states using zero-velocity update and dual foot fusion calculations. The motion states, including velocity, pose and location, are then determined during the swing phase. However, accurately classifying these phases is challenging due to variations and dynamics in user motion.

Conventional methods like Acceleration-Moving Variance (AMV) [86], Acceleration Magnitude (AM) [87] and Angular Rate Energy (ARE) [88] heavily rely on raw inertia data, which leads to issues such as cumulative error and motion dynamics. To overcome these limitations, Skog *et al.* [89] proposed an improved GLRT method that incorporates prior knowledge of AMV, AM and ARE. This method effectively mitigates false detection by integrating acceleration and gyroscope data to calculate the likelihood of the stance and swing phases. However, the existing zero-velocity detection still relies on a fixed threshold, limiting its adaptability to different users.

Positioning Optimisation

The positioning accuracy of the inertial based DR is susceptible to drift due to the short-term drift of the IMU [90]. Various methodologies have been employed to mitigate deviations or prolong the standard measurement duration. The KF is widely regarded as one of the most common methods in this field [91]. The KF is widely utilised in various technological domains such as navigation, vehicle control and system optimisation. The fundamental premise of the KF is to construct a predictive model of the linear system state using the system's dynamic model and measurements from external sensors. The prediction model serves as an optimal state estimator with the minimal mean-square-error (MSE) [92]. In general, the standard KF method consists of two phases: prediction and update. During the prediction phase, the object state is updated by taking into account significant state transitions, such as the physical laws governing the velocity of automobiles or the walking pattern of individuals. During the prediction phase, an external sensor will be utilised to observe the condition of the object. The KF is employed to determine the impact of both major concerns and external observation on state dynamics by calculating weights. This is necessary due to the varying measurement covariance, which leads to uncertain state estimation. Following the KF calculation, the two measurements are combined using a tight coupling approach.

Because of the nonlinearity of the parameters and the instability of the mechanical specifications of the IMU, the linear KF is incapable of addressing the estimate of nonlinear parameters. The EKF is a more sophisticated iteration of the KF that enables state estimation on a nonlinear system [93]. In the context of single-foot mounted INS calculation using EKF, the objective is to periodically update the IMU state by incorporating external pseudo-measurements derived from specific features. These features include zero speed during the stance phase using ZUPT [94], zero angular rate during the stance phase using ZARU [95] and other manually configured methods [96]. The dual foot motion in FT-INS is represented by the sphere [97] and ellipsoid geometries [98]. The threshold for this representation can be either set, as proposed by Prateek [99], or dynamically measured using the range finder method, as proposed by Wu [29]. This approach combines the dual foot INS results, resulting in enhanced positioning accuracy and error refinement performance. This thesis exclusively focuses on studies about DF-INS. Therefore, this study does not cover certain KF platforms that incorporate sensor fusion and navigation optimisation techniques, such as the UKF [100], adaptive Kalman filter (AKF) [101] and multiplicative extended Kalman filter (MEKF) [102].

"Openshoe" [103, 104] is one of the embedded DF-INS utilising ZUPT in its implementation. Norrdine A *et al.*[105] utilised a magnetometer to update the altitude estimation by KF. Li *et al.*[106] proposed a UKF for initial alignment and fuse ZUPT, ZARU and magnetometer readings to correct the estimation error. However, the tracking performance of these methods with a single IMU or attitude and heading reference system (AHRS) sensor used is easily affected by mechanical and measurement errors of electronic components.

Other studies research on dual foot mounted INS for positioning optimisation. Prateek *et al.* [99] proposed a sphere limit algorithm built upon the "Openshoe" model to merge the two-foot INS data. Zhao *et al.* [97] proposed a dual gait analysis approach to optimise step length estimation. Wang *et al.* [107] proposed an adaptive inequality constraint in KF for sensor fusion of dual foot. A. A. Abdallah *et al.* [108] presented a Deep Neural Network (DNN) based synthetic aperture navigation (SAN) to suppress multipath error of ZUPT based INS platform. These dual foot-mounted DR systems improve the tracking performance, but they take the surrounding structure as a priori by default to navigate people which may be unavailable in some special cases like indoor firefighting and cave exploration. A single trajectory without surrounding geography information loses the semantics to understand.

In addition, dual-foot sensor data fusion lacks trajectory fusion, which renders these systems unsuitable for real-world applications. The mass-separated trajectories from the left and right feet increase the difficulty of position estimation. Thus, one body-level trajectory creates more differences in the context of the IPS. However, the INS area has no suitable solution for fusing the dual trajectory. The centre body of mass (CBoM) [109] is a commonly used model that determines body movement based on biomechanical concepts [110]. However, most CBoM methods utilise force platforms [111], visual motion capture systems [112] and magneto-inertial measurement units (MIMUs) based motion analysis approaches [113] which are impractical for long-term localisation.

2.3.2 Multi-person Localisation

Apart from the limited accuracy of DR methods, multi-person localisation is a challenging problem in the field of DR, enabling the simultaneous localisation of multiple users. Traditional methods merely extend individual localisation functionality. Zhang *et al.* [114] proposed a WLAN-based multi-person localisation system using intelligent reflecting surfaces (IRS). Qian *et al.* [115] implemented a multi-tracking platform based on path-loss-based adaptive joint probabilistic data association (PLA-JPDA) using impulse-radio UWB (IR-UWB) radar. These methods utilise different wireless transmission protocols and tracking algorithms to localise multiple individuals. However, such passive localisation methods are still constrained by the initial setup of transmission devices and prior knowledge of indoor infrastructures, limiting their practicality in real-world applications.

Other research explores device-free methods for multi-person localisation, allowing localisation without individuals carrying devices. These methods simplify tracking operations and expand application scenarios. Wu *et al.* [116] adopted millimetre wave radio (MWR) for multi-person localisation. A multi-target detection approach was proposed to estimate the positions of individuals and generate trajectories based on continuous tracking operations. This method offers high accuracy in small spaces but is limited in normal indoor buildings due to the maximum range of MWR. Yang *et al.* [117] introduced a multi-person localisation method using pyroelectric infrared (PIR) sensors. A deep learning model with domain knowledge was applied to count individuals and estimate their locations. However, PIR sensors require line-of-sight for sensing, limiting their practicality in indoor scenarios with frequent structural obstructions.

Landmark Recognition Method

The accuracy of INS was prone to accumulating errors from dead reckoning calculations [118]. While ZUPT and ZARU periodically updated the INS state and suppressed estimation errors [119], spatial errors in the trajectory accumulated over time. Several methods have been developed to mitigate these errors by periodically updating the system state based on specific reference landmark matching. A successful match of landmarks indicated the detection of a familiar location for loop closure. Following a loop closure operation, the estimated position was corrected to a previously visited location, where the cumulative error was minimised [120].

Landmarks were typically categorised as artificial or natural. Artificial landmarks included self-defined [120, 121] or pre-determined [11, 122] features with regular or distinctive environmental and spatial characteristics, such as elevators, doors, columns, stairs, and other predefined locations. Determining these landmarks usually required an initial survey to obtain their positional information, and the matching process often required manual activation [123], increasing the complexity and risk. Conversely, natural landmarks consisted of inherent environmental factors with regular dynamics or long-term stability, such as light density [124, 125] and magnetic field distribution [126, 127]. The characteristics of natural landmarks made them more convenient for online usage, enhancing timeliness [127]. Compared to artificial landmarks, natural landmarks were easier to employ in various environments but might have required external landmark feature detection and calibration operations. Among natural landmarks, magnetic fields were particularly suitable for multi-person INS due to their long-term and short-term stability. Additionally, the directional nature of magnetic values increased the uniqueness of MFs, enhancing their performance in loop closure.

MF Mapping and Matching

Geomagnetism and indoor infrastructure influence the magnetic field distribution within a building [128]. Magnetic fields exhibit high stability in the presence of long-term and dynamic environmental factors [129, 130], making them suitable for indoor positioning through magnetic field analysis [131]. Magnetic field data typically consists of a 3-D vector obtained from a 3-axis magnetometer. The magnetic field intensity (MFI) [132] is often normalised based on the 3-D magnetic vector. Both the 3-D magnetic vector and MFI contribute to the determination of MFs. Many approaches collect spatial fingerprints to create fingerprint maps using space projection [133] and interpolation [134]. Fingerprint maps can serve as references for indoor localisation and they can be categorised into offline and online modes.

Offline MF matching involves the separation of magnetic field collection and matching operations in a temporal manner [135, 136]. Existing research primarily collects and constructs MF maps prior to localisation. These maps serve as prior knowledge for the localisation process. In contrast, online fingerprinting combines fingerprint detection and location calculation simultaneously [126]. This approach requires no prior initialisation before position calculation, enhancing efficiency in scenarios requiring high timeliness and in unknown environments. However, online fingerprint maps typically have lower resolution than offline maps, as they lack signal post-processing and enhancement operations.

Dynamic time wrapping (DTW) [137] is a typical method for signal pattern matching which is suitable for applying in MF matching. DTW compresses and stretches two input sequences to align them, calculating the DTW value based on the distance between these aligned sequences. This value represents the similarity between the two sequences. Magnetic field sequences differ from audio signals processed using DTW, as magnetic sequences include amplitude and direction, increasing the complexity of calculations. Researchers have proposed various techniques to address these challenges. Wang *et al.* [138] introduced a backwards magnetic trajectory detection method that broadens the range of applications for MF matching. Chen *et al.* [139] presented a magnetic sequence segmentation algorithm and a magnetic feature classification method to address distortion and shifting issues in original MF sequences. Chen *et al.* [140] proposed a 3-D DTW (3DDTW) method to enhance magnetic sequence matching accuracy by extending the dimensionality of the matching sequences. Guo *et al.* [141] introduced a semantic trajectory segmentation and hybrid DTW matching method to improve magnetic sequence matching in spatial contexts.

2.4 Summary

Table 2.1: Summary of DR Related Study

Research Topic	Sub-topic	Typical Approaches	Limitations	References
Development and improvement of DR method	Heading Estimation	Calculate and optimise heading from magnetic and inertia measurements	Accuracy is affected by magnetic interference	[61, 64–67]
		Walking pattern recognition for heading correction	Time-consuming model training	[68–70]
		UWB and WLAN for heading estimation enhancement	External device installation, not convenient	[67, 71, 72]
		Make assumption for corridors' direction and eliminate drift accordingly	Walking patterns are not considered	[73–76]
	Step Detection	AMV, AM, ARE, and GLRT	GLRT utilises a fixed threshold. There is no dual foot synergistic method	[84–89]
	Positioning Optimisation	ZUPT, ZARU; EKF, UKF, AKF, MEKF.	KF requires accurate parameter for fusion and optimisation	[93–95, 100–102]
		Fuse dual foot motion for tracking using sphere and ellipsoid constrains.	The stride length constraint is based on fixed threshold	[97, 98, 107, 108]
Multi-person Localisation	Existing Multi-person localisation	WLAN, UWB, MWR, and PIR	External device installation, not convenient	[114–117]
	Landmark Recognition	lifts, doors, columns, stairs, other specified locations and pre-determined marks	Hard to measure the coordinates; need manually recording	[142]
		Intensity of light; magnetic fields	Need to encode the magnetic fields data	[124–127]
	MF Mapping and Matching	Magnetic field intensity transformation; DTW	No online magnetic fingerprint for multi-trajectory fusion	[128–141]

This chapter provides a comprehensive discussion of the state-of-the-art IPS methods. The advantages and disadvantages of WSN, SLAM and DR methods are introduced. It is worth noticing that in emergency scenarios such as firefighting, DR methods present better performance for deployment due to their minimal hardware pre-installation requirements and strong resilience to interference from environmental and human factors.

Though DR methods exhibit promising potential, their limitations can not be overlooked as shown in Table 2.1. Existing research proposes many sensor fusion approaches to improve positioning accuracy by reducing the IMU drifting issues. However, few studies considered gait analysis to reduce cumulative error. In addition, the lack of mapping and multi-person localisation limits its application opportunity in emergency services.

To overcome the limitations presented above, the research work of this thesis conducts specific studies to answer three research questions presented in Chapter 1. **Study 1**, **Study 2** and **Study 3** investigate different gait analysis techniques in DR systems to mitigate heading estimation bias, attain more precise step recognition and accomplish correct dual foot trajectory optimisation, respectively. **Study 4** researches a DR based mapping approach to reconstruct the surroundings together with positioning calculation. Finally, the implementation of online magnetic fingerprint based Multi-INS is explored by **Study 5** which presents a novel approach for multiple person's trajectory integrations. The comprehensive descriptions of these studies are presented in the following chapters.

Chapter 3

Methodology

This chapter introduces five studies throughout the course of PhD study as shown in Fig. 3.1, where the first three studies focus on the accuracy of the DR method, Study 4 aims to reconstruct the surrounding map and Study 5 explores the multi-person positioning method. To control variables such as human and environmental factors in each study performance evaluation, this chapter also introduces the specific experimental setup for each study.

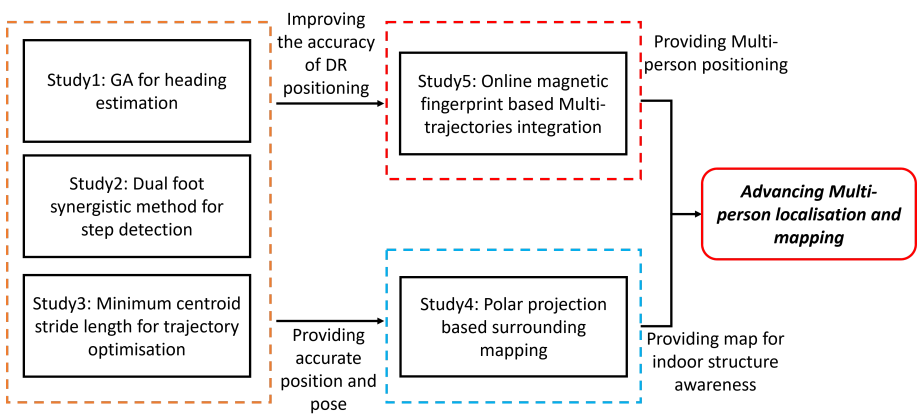

Figure 3.1: *The Overview structure of the studies presented in this thesis.*

It is worth declaring that all experiments adhered to ethical guidelines and were approved by the university's research ethics committee. Participants received information sheets and signed consent forms before the commencement of the experiments. They were informed of their right to terminate their participation at any time if they so requested.

3.1 GA-PDR

To address inaccurate heading estimation impacted by the walking patterns of different users, **Study 1** proposes a gait analysis–aided PDR (GA-PDR) system based on the principle of HDE for locating users in smoke-filled environments by analysing an individual's gait. A motion sensor is placed on protective footwear during data collection. The gait analysis (GA) is presented in two parts using a gait detection (GD) algorithm for step pattern determination and a redundant turn elimination (RTE) method for correcting misclassified step patterns. The results indicate the effectiveness of GA-PDR in the gait adaptation for different users and accuracy within both ideal and smoke-filled environments.

Typical DR method PDR [21, 143] is a popular technique for computing a pedestrian's position by measuring their gait information, which includes step detection, step length and heading direction. This technique can overcome the limitations of vision-based methods, in which gait measurements are less frequently affected by environmental factors e.g. smoke. The performance of PDR can be affected by several factors, including the drifting problem in the case of motion sensors [144] and distinct individual gait [66]. Their stable wireless transmission and efficient computation are more practical in emergencies e.g., fire rescuing. The walking pattern of firefighters is different from that of a typical civilian. Firefighters will typically walk with their bodies leaning forward on the ground and at a slower pace than a typical civilian due to the low visibility of smoke-filled environments and the heavy equipment they carry. Therefore, it is important to consider non-standard walking types when studying and developing solutions for various users, such as firefighters.

3.1.1 System Overview

One general notation model of PDR footprint is presented for problem description. Fig. 3.2 demonstrates the impact of this difference in walking style on PDR performance. The included angle, i.e., Δ_Ψ, between the actual walking direction, i.e., Ψ_{gt} and the footing direction, i.e., Ψ_{foot}, is dynamic within a consecutive gait cycle. The preliminary work [145] showed that PDR heading estimation, when not considering gait, can be inaccurate. The proposed GA-PDR system is presented in Fig. 3.3. The

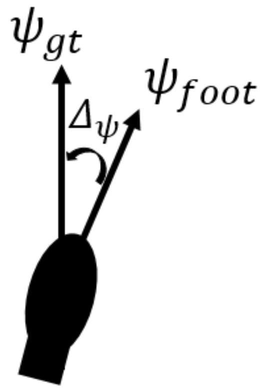

Figure 3.2: *A schematic clamping angle is shown between the real direction, i.e., Ψ_{gt} and the heading angle of the foot.*

normalised acceleration, $a_{norm,raw)}$, angular velocity, $\omega_{z,raw}$ and unwrapped heading angle yaw, Ψ_{raw} information from the IMU data was first passed through a low-pass filter to eliminate high-frequency noise. Filtered acceleration, a_{norm}, was then applied to detect steps [146] and to estimate the step-length [147]. The heading, estimated using GA, comprised a sequence of processes, GD and RTE. GD detected the peaks and valleys of ω_z with the assistance of the deviance of Ψ to determine the step pattern (SP).

The RTE corrected the SP based on the time-domain analysis for Ψ to reduce the bias caused by redundant small turns during a complete physical turn. Finally, the heading direction of each step, i.e., Ψ', was computed according to the corrected SP. The position of each step was calculated by a PDR formula based on the step detection, step length (L) and Ψ'. The calculated step points were connected along the timestamp to generate a trajectory which was projected to the (x,y)-Cartesian coordinate system. The details of the GA method will be discussed further in the following sections.

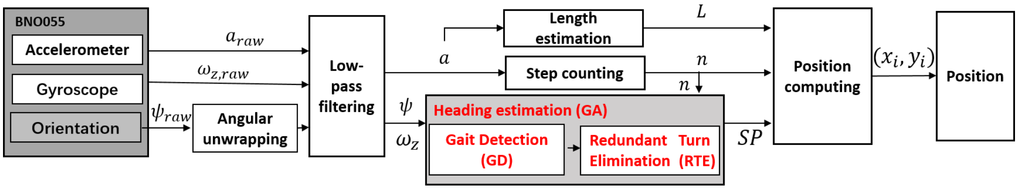

Figure 3.3: *A system overview of GA-PDR with GA comprising GD and RTE for heading estimation.*

3.1.2 Gait Detection (GD)

GD is the initial stage of GA and determines the SP candidates. This study assumed that the rooms and corridors in a building were structured according to the research proposed by [73], where the movements of a user mainly comprise four dominant directions, i.e., heading forward, left and right, with 90-degree intervals. The SPs associated with the directions defined in this study are 90-degree turn-left and turn-right 180-degree turn-around from the left and from the right and no turn (forward heading). To identify the SP, first, the raw angular velocity of the z-axis, i.e., $\omega_{z,raw}$ and Ψ_{raw} data are smoothed using a low-pass filter to reduce the noise generated from the sensors and electronic circuits. An angle unwrapping method is also introduced to maintain the continuity of the angle signal as follows:

$$\omega_z = LP\left(\omega_{z,raw}, t_\omega\right) \tag{3.1}$$

$$\psi = \mathrm{UW}\left(\mathrm{LP}\left(\psi_{raw},\mathrm{t}_{yaw}\right)\right) \tag{3.2}$$

where LP is a low-pass Butterworth filter [148] with a fixed minimum height threshold, i.e., $t_\omega$and t_Ψ for $\omega_{z,raw}$ and $\Psi_{z,raw}$, respectively; UW (unwrapping) [149] is a method for solving the angular shifting problem at a 0-degree to 360-degree junction to guarantee the signal continuity as follows:

$$psi_{i:m} = \begin{cases} \psi_{i:m}+2\pi, |\psi_i - \psi_{\mathrm{i+1}}| > \pi \\ \psi_{i:m}, otherwise \end{cases} \tag{3.3}$$

where i is the index of the signal sample and $\psi_{i:m}$ is the signal segment indexed from the current instant i to the total length (m) of this signal.

Second, the turn action has a significantly higher angular rate than that of normal forward motion which shows a pulse in the ω_z signal. These pulses, which have the highest absolute value compared with their neighbouring pulses, could potentially be detected as a turn. Peak and valley detectors are utilised to define these turns from the left and right sides, respectively.

$$peak_{\omega,L} = \begin{cases} 1, \quad \omega_{z,k-1} < \omega_{z,k} \ \omega_{z,k} > \omega_{z,k+1} \ \Delta_{\omega,L} > th_{fs} \ \ |\omega_z| > th_{\omega,L} \\ 0, \quad otherwise \end{cases} \tag{3.4}$$

$$valley_{\omega,R} = \begin{cases} 1, \quad \omega_{z,k-1} > \omega_{z,k} \ \omega_{z,k} < \omega_{z,k+1} \ \Delta_{\omega,R} > th_{fs} \ \ |\omega_z| > th_{\omega,R} \\ 0, \quad otherwise \end{cases} \tag{3.5}$$

In the above equations, k is the index number of each sample, Δ is the required minimum horizontal distance between neighbouring peaks or valleys, th_{fs} is the fixed threshold for $\Delta_{\omega,L}$ and $\Delta_{\omega,R}$ and $th_{\omega,L}$ and $th_{\omega,R}$ are the absolute value thresholds for peak and valley detection, respectively. Then, P_i is utilised to calculate the variation in Ψ between two continuous steps to distinguish an invalid turn, a 90-degree turn and a 180-degree turn-around as follows:

$$P_i = std\left(\psi_{T(i)} : \psi_{T(i+1)}\right) \tag{3.6}$$

where T is a function used to convert the step index number into a timestamp. Finally, the value of the SP is defined, based on (3.7). Each step is tagged with SP_i to enable heading estimation. The SP with a value greater than 0 is labelled a "positive SP," which indicates that the corresponding step is a turning action, as shown below.

$$P_i = \begin{cases} 1, \quad \exists T\left(Peak_{\omega,L}\right) \in [T(i), T(i+1)]\, P_i \in [LT, HT] \\ 2, \quad \exists T\left(Valley_{\omega,R}\right) \in [T(i), T(i+1)]\, P_i \in [LT, HT] \\ 3, \quad \exists T\left(Peak_{\omega,L}\right) \in [T(i), T(i+1)]\, P_i > HT \\ 4, \quad \exists T\left(Valley_{\omega,R}\right) \in [T(i), T(i+1)]\, P_i > HT \\ 0, otherwise \end{cases} \tag{3.7}$$

where the SP_i values of 1, 2, 3, 4 and 0 represent a 90-degree turn-left and turn-right, a 180-degree turn-around from the left and the right and no turn (forward motion), respectively. Moreover, LT and HT are the low threshold and high threshold for the P_i turning judgment. A P_i lower than the LT value indicates no turning; a P_i greater than the LT value but less than the HT indicates a potential 90-degree turn, while a P_i greater than the HT indicates a potential 180-degree turn.

As shown in (3.8), the heading estimation, Ψ_i', for each step can be calculated based on SP_i, as follows:

$$\psi_i{}' = \begin{cases} \psi_{i-1}{}', SP_i = 0 \\ \left|\left(\psi_{i-1}{}' + 90\right)\%360\right|, SP_i = 1 \\ \left|\left(\psi_{i-1}{}' - 90\right)\%360\right|, SP_i = 2 \\ \left|\left(\psi_{i-1}{}' + 180\right)\%360\right|, SP_i = 3 \\ \left|\left(\psi_{i-1}{}' - 180\right)\%360\right|, SP_i = 4 \end{cases} \tag{3.8}$$

3.1.3 Redundant Turn Elimination (RTE)

Commonly, a complete turning action requires multiple continuous small turns, which causes one turn with multiple positive SPs via GD. An example of this problem is shown in Fig. 3.4.

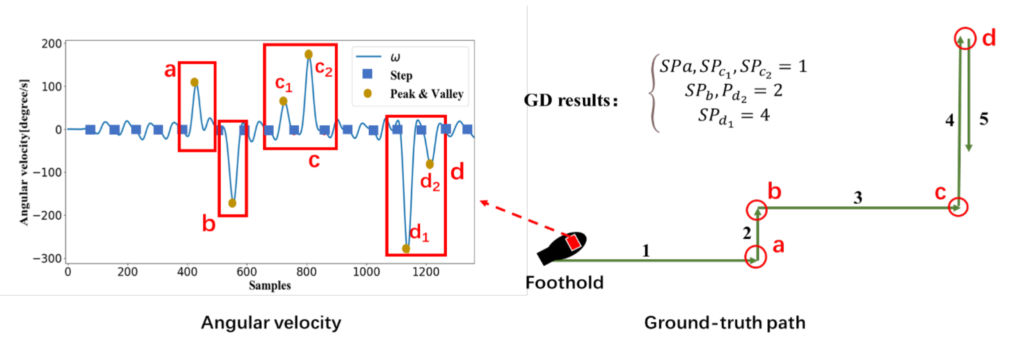

Figure 3.4: *An experiment segment in which a redundant turn problem occurred.*

The SP_i calculated by GD is denoted as the peaks and valleys plotted in the angular velocity series that are demonstrated in Fig. 3.4, where the green lines serve as a sample of the walking trajectory. Each turn labelled by a red circle with a lowercase letter is associated with the red box and corresponding lowercase letter in the angular velocity plot. Left-turning can be seen at the a and c positions, which are associated with peaks a and c, respectively, in the angular velocity data series. Similarly, right-turning can be identified at position b with the associated valley b from the data series. However, the left-turning located at position c is associated with multiple peaks, i.e., c_1 and c_2; the 180-degree turning located at position d is associated with multiple valleys, i.e., d_1 and d_2, during continued steps. A single turn with multiple peaks or valleys interferes with the normal heading estimation. To address this problem, the RTE method can be utilised to verify these redundant SPs.

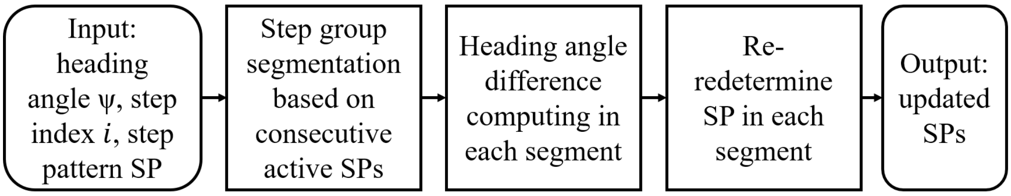

Figure 3.5: *The flowchart of RTE method.*

Fig. 3.5 illustrates the flowchart of the RTE method. The algorithm inputs the GA-PDR data array, which includes i, Ψ and SP_i derived from the GD and outputs the corrected SP_i. First, RTE detects the consecutive steps with positive SPs and defines these step segments as step groups. Second, it calculates the absolute heading difference between the starting step and the ending step in each group. Finally, the method updates the SPs of the steps in the step groups according to the heading value difference within groups. Thus, one turn including multiple steps with positive SPs will be verified to determine the actual SP of each step. Multiple potential turns computed by GD at one corner will be eliminated into a single turn that matches the real cases.

3.1.4 Experimental Setup

To evaluate the GA-PDR performance, the experiment preparation section introduces the hardware setup and layout of the experimental scenario.

Table 3.1: The IMU (BNO055) Parameters

Parameter	Value
Sampling rate	100 Hz
Acceleration	3-axis ± 4 g
Gyroscope	3-axis ± 2000 dps
Orientation, Yaw	0°–360°

The proposed GA-PDR comprises a BNO055 IMU and a Seeeduino XIAO micro-computing unit, as shown in Fig. 3.6. The IMU was calibrated utilising an internal calibration module in hardware. The sensor components were assembled and placed on the upper side of a firefighter's protective boot and the sensor data were transmitted to a terminal via long-range radio communication (Lora). The data analysis was performed using a desktop terminal equipped with Windows 10, an Intel(R) Core (TM) I5-8250U @1.60G Hz processor and 8 GB RAM. Table 3.1 summarises the specifications of the IMU sensor that was used in this study. The raw yaw readings of this IMU were filtered through the inner calculator [150] to reduce drifts. The update rate of GA-PDR was 100Hz, following the sampling rate of IMU.

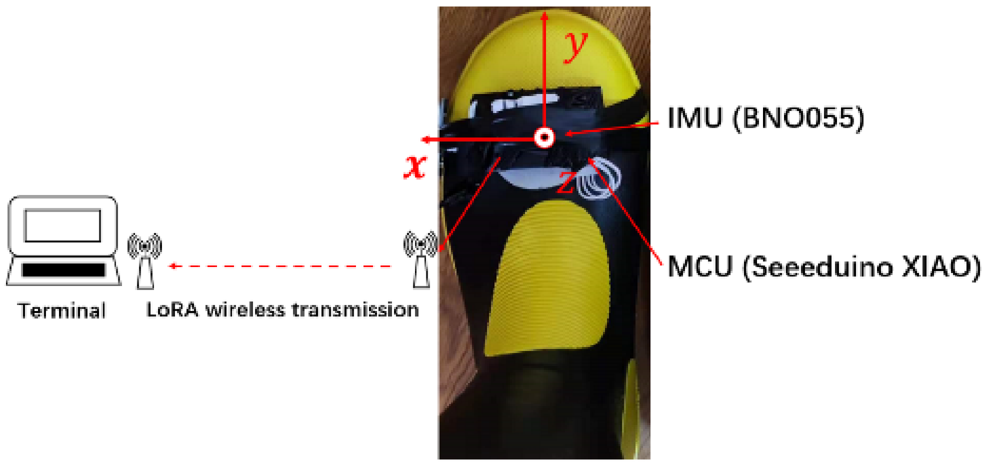

Figure 3.6: *The design and hardware placing of the GA-PDR data collector.*

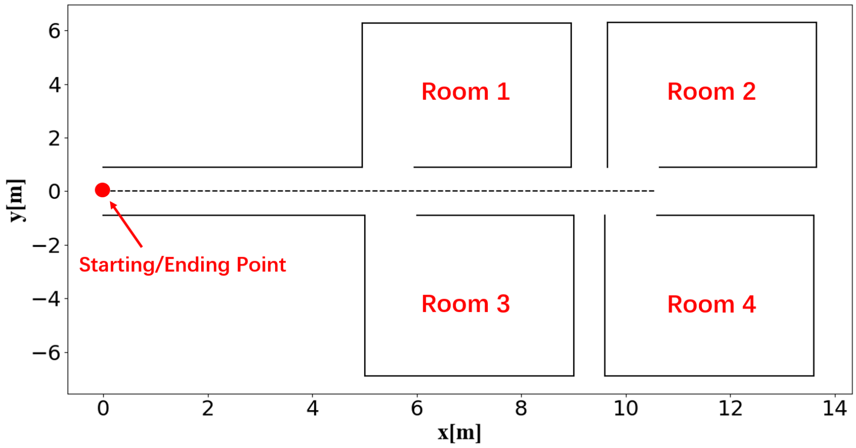

(a)

(b)

Figure 3.7: *The schematics of the experimental site: (a) Layout information and (b) photo of smoky scenario.*

The experiments were examined inside a building comprising multiple structured rooms on a single floor. A schematic of the indoor structure used for the experiment is shown in Fig. 3.7a, which comprised 4 rooms of similar size. The size of the rooms was measured with a laser range finder; rooms 1, 2, 3 and 4 were 24, 21.64, 24 and 24 m^2, respectively.

Two male firefighters voluntarily participated in the study for data collection. Firefighter 1 (173 cm tall and weighing 82 kg) was instructed to complete the walking trajectory as shown in Fig. 3.8a (Scenario 1). Firefighter 2 (180 cm tall and weighing 85 kg) was asked to complete two scenarios (see Figs. 3.8b and 3.8c) in a smoke-filled environment with a visibility range below 1 m, as shown in Fig. 3.7b, the smoke was produced by a smoke generator. All the walking plans were made under the guidance of professional firefighting teams which consist of all the walking patterns: forward, left- and right-turn and around-turn from left or right-side movements referred to HDE. There was no restriction on the walking pattern that participants could adopt. Every experiment was conducted three times in order to avoid subjective issues from human factors.

3.2 Dual Foot Synergistic Method

Dual foot INS (DF-INS) is an enhanced version that leverages data from both feet for more robust and accurate localisation [29, 83]. Achieving accurate zero-velocity detection is crucial for optimal performance in zero-velocity updating and trajectory calculation in DF-INS. However, conventional techniques rely on fixed thresholds to identify the zero-velocity (stance) phase, which is not suitable for dynamic scenarios and diverse users. Moreover, the step detection of DF-INS regards two-foot as separated systems where there was no synergistic pattern recognition considered in dual foot motion analysis in DF-INS. This design will decrease the accuracy of DF-INS when the dual foot gait cycle is irregular. To address this problem, **Study 2** introduces a dual foot synergistic method to determine dynamic thresholds for zero-velocity detection in a two-foot system. Initially, the GLRT sequences from both feet are smoothed using a moving average filter. The points of equality within these sequences are then identified as transition points between the stance phase and the swing phase.

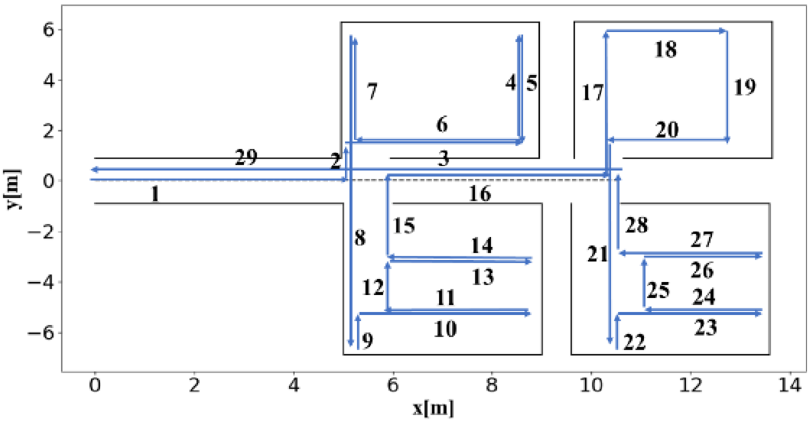

(a)

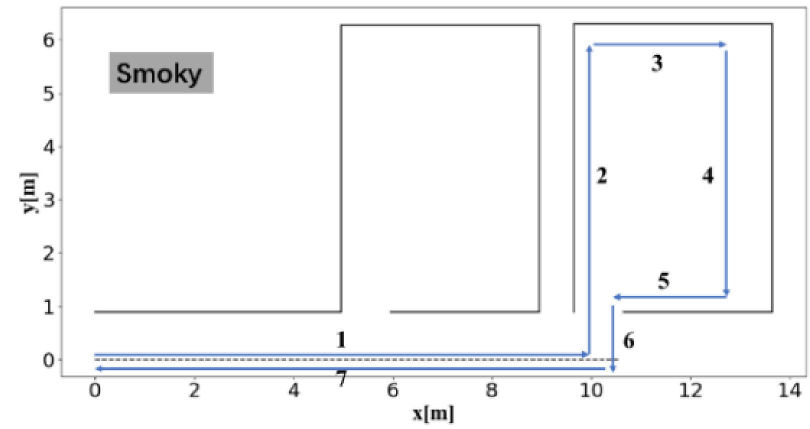

(b)

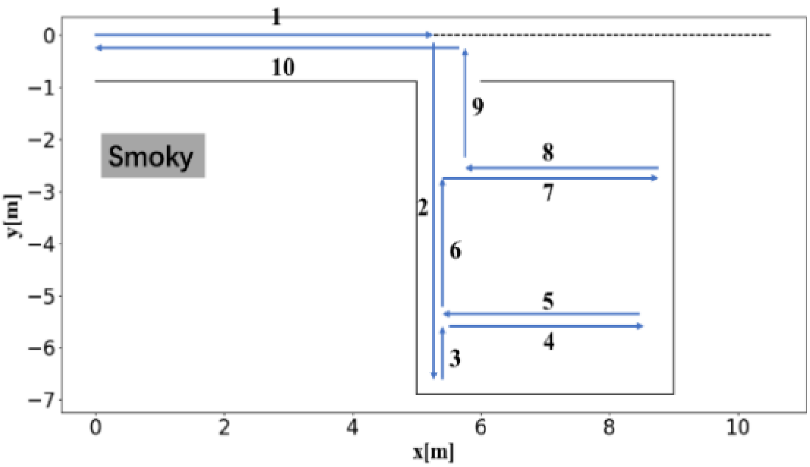

(c)

Figure 3.8: *Walking plan routes in ideal and smoky environments: (a) a complicated trajectory and (b) a moderate (c) a turning around–oriented trajectory in smoke-filled environments.*

3.2.1 Dual Foot GLRT (DF-GLRT)

In the context of DF-INS, the sensor measurements captured by a dual foot mounted IMU system can be denoted as $y_{s,k} \in \mathbb{R}^6$, as demonstrated in Eq. 3.9,

$$y_{s,k} = \begin{bmatrix} y^a_{s,k} \\ y^\omega_{s,k} \end{bmatrix}, s \in [L, R] \tag{3.9}$$

where $y^a_{s,k}$ signifies the three-axis acceleration vector and $y^\omega_{s,k}$ represents the three-axis gyroscope vector in a three-dimensional Cartesian coordinate system at timestamp k, as well as s denotes the index of the IMU placed on the left (L) or right (R) foot.

In order to assess the likelihood of the measurement sequence $z_{s,n}$ (see Eq. 3.10) being stationary, a moving detection window with a size of N is employed. Within the context of dual foot zero-velocity detection, two hypotheses, $\mathcal{H}_{s,0}$ and $\mathcal{H}_{s,1}$, are formulated, as expressed in Eq. 3.11.

$$z_{s,n} \triangleq \left\{ y_{s,k} \right\}_{k=n}^{n+N-1} \tag{3.10}$$

$$\begin{aligned} &\mathcal{H}_{s,0} : The foot mounted \text{IMU } s \text{ is in a moving state.} \\ &\mathcal{H}_{s,1} : The foot mounted \text{IMU } s \text{ is in a stationary state.} \end{aligned} \tag{3.11}$$

The GLRT method [89] is employed to compute the probability rate of the hypotheses $L_{s,G}$ which is essential for determining the states of $z_{s,n}$, as indicated in Eq. 3.12,

$$L_{s,G} = \frac{p(z_{s,n};\theta^1,\mathcal{H}_{s,1})}{p(z_{s,n};\theta^0,\mathcal{H}_{s,0})} > \gamma \tag{3.12}$$

where $p(\cdot)$ represents the probability density function (PDF) [151], θ^0 and θ^1 denote the maximum likelihood estimates (MLE) [152] of the unknown parameters in the IMU system for $\mathcal{H}_{s,0}$ and $\mathcal{H}_{s,1}$ and γ is a fixed threshold value used to discern between the moving and stationary states.

To overcome the computational challenges arising from the logarithmic nature of Eq. 3.12, the variable $L_{s,G}$ is redefined as $T(z_{s,n})$ in Eq. 3.13,

$$\begin{aligned} T(z_{s,n}) &= -\frac{2}{N} ln(L_{s,G}) \\ &= \frac{1}{N}\sum_{k\in\Omega_n}\left(\frac{1}{\sigma_a^2}\left\| y^a_{s,k} - g\frac{\bar{y}^a_{s,n}}{\left\|\bar{y}^a_{s,n}\right\|}\right\|^2 + \frac{1}{\sigma_\omega^2}\left\| y^\omega_{s,k}\right\|^2\right) < \gamma^{'} \end{aligned} \tag{3.13}$$

where $\Omega_n = \tau \in \mathbb{N}, n \leq \tau < N-1$ represents a moving window with a size of N, $\gamma^{'} = -\frac{2}{N}\ln\gamma$ is a fixed threshold in logarithmic form, g represents the local gravity acceleration parameter, $\bar{y}^a_{s,n}$ denotes the average value of $y^a_{s,k}$, σ_a and σ_ω indicate the standard deviations of the accelerometer and gyroscope measurement noises respectively. Zero-velocity detection is computed independently for each foot.

3.2.2 Dual Foot Synergistic Method

In order to improve the computational smoothness of the sequence $T(z_{s,n})$ in Eq. 3.13, a moving average filter [153] with a window size of M is utilised where $\hat{T}_i(z_{s,n})$ (see Eq. 3.14) is the smoothed signal at time i.

$$\hat{T}_i(z_{s,n}) = \frac{1}{M}\sum_{i-M+1}^{i} T_i(z_{s,n}) \tag{3.14}$$

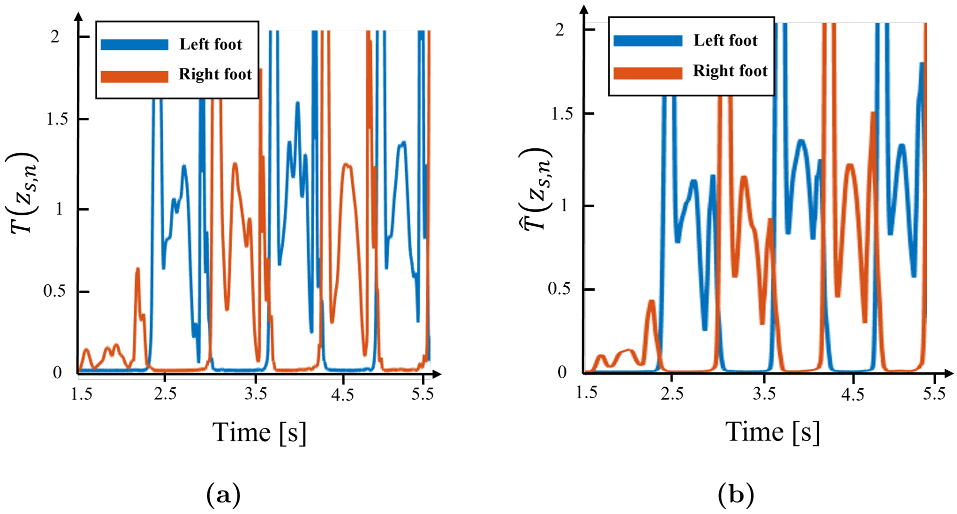

Figure 3.9: *Comparison of (a) raw signal $T_i(z_{s,n})$ and (b) filtered signal $\hat{T}_i(z_{s,n})$, using a moving average filter.*

Figure 3.9 presents the comparison between $T_i(z_{s,n})$ and $\hat{T}_i(z_{s,n})$, demonstrating a significant reduction in high-frequency noise achieved by the filtered signal.

The gait cycle, as depicted in Fig. 3.10, encompasses various phases such as heel-off (HO), heel-strike (HS), foot-flat (FF) and toe-off (TO). Mid-stance represents the point at which the foot bearing weight functions as a stabilising support for standing, whereas mid-swing pertains to the intervals during which the foot without weight undergoes a swinging motion. The transition from the swing phase to the stance phase occurs when both heel-off (HO) and heel-strike (HS) events are detected in the dual foot system. Conventional methods of identifying the stance phase commonly rely on predetermined thresholds, which may be affected by the dynamics of the GLRT sequence. This could result in the erroneous rejection of hypothesis $H_{s,1}$, leading to false rejections and consequently impacting the performance of the INS. In this study, the condition $\hat{T}(zL, k) = \hat{T}(zR, k)$ signifies that the dual foot GLRT sequences are employed synergistically to facilitate gait switching. This approach considers the dual foot measurements as an integrated system, accounting for the interrelationship between the feet. The equality of $\hat{T}(z_{s,n})$ represents the maximum likelihood when the gait of both feet reaches the demarcation point.

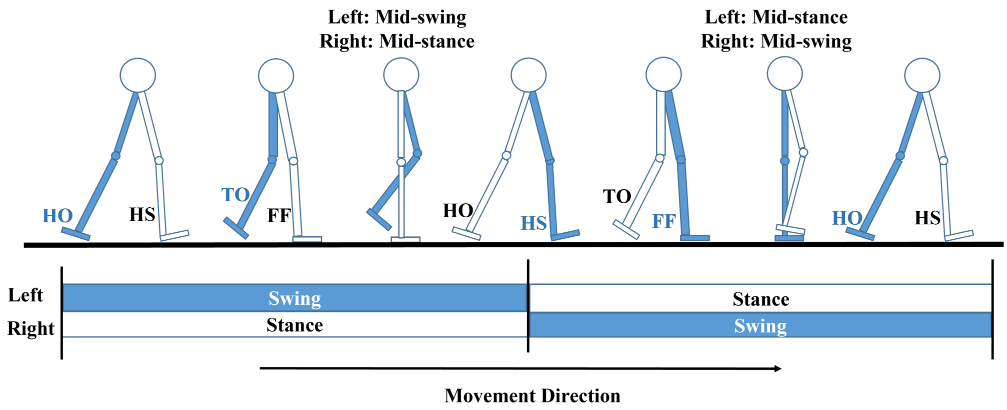

Figure 3.10: *Schematic representation of the gait cycle for the dual foot.*

Finally, the stationary hypotheses $H_{s,1}$ functioning as the primary determination of the synergistic method are evaluated based on the Eq. 3.15,

$$\begin{aligned} &\mathcal{H}^{i}_{L,1} \text{ is true if } \hat{T}_i(z_{L,n}) \leq \hat{T}_i(z_{R,n}) \text{ or } \hat{T}_i(z_{L,n}) < \gamma^{'}_{min} \\ &\mathcal{H}^{i}_{R,1} \text{ is true if } \hat{T}_i(z_{L,n}) \geq \hat{T}_i(z_{R,n}) \text{ or } \hat{T}_i(z_{R,n}) < \gamma^{'}_{min} \end{aligned} \tag{3.15}$$

where $i \in \Omega_n, \gamma^{'}_{min}$ represents the minimum threshold for detecting zero-velocity in the dual foot system at the beginning and end of the gait cycle.

3.2.3 Experimental Setup

The proposed wearable for foot mounting utilises a MPU9250 (200Hz) and a Seeeduino ESP32 dual-core micro-computing unit for each foot. The sensors were integrated and securely attached to the front of each shoe using a Velcro strap. The IMU was calibrated utilising an internal calibration module in hardware. The transmission of inertia data was collected wirelessly through Wi-Fi, utilising the On-The-Go (OTG) protocol, from the sensors to a handheld ESP32 Wi-Fi kit, which was connected to a smartphone (refer to Fig. 3.11). The algorithm responsible for processing the data was implemented in MATLAB 2022a and executed on a laptop with an Intel i7-10510U 1.8 GHz processor and 16 GB RAM. The update rate of DF-INS was 200Hz, following the sampling rate of IMU.

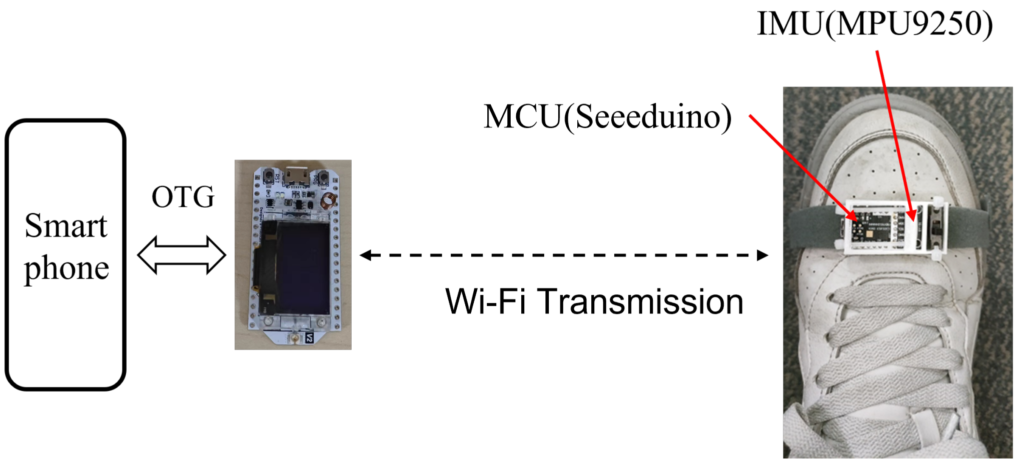

Figure 3.11: *System design for data collection*

To evaluate how well the system performed, a set of indoor tests was carried out in a building shaped like a square, which included a central courtyard. The path for walking spanned around 160 meters and started and finished at the same spot, as illustrated in Figure 3.12. Four volunteers took part in the experiment and the researcher analysed recorded videos to determine the step count of both the left foot (SC_L) and the right foot (SC_R) for each participant.

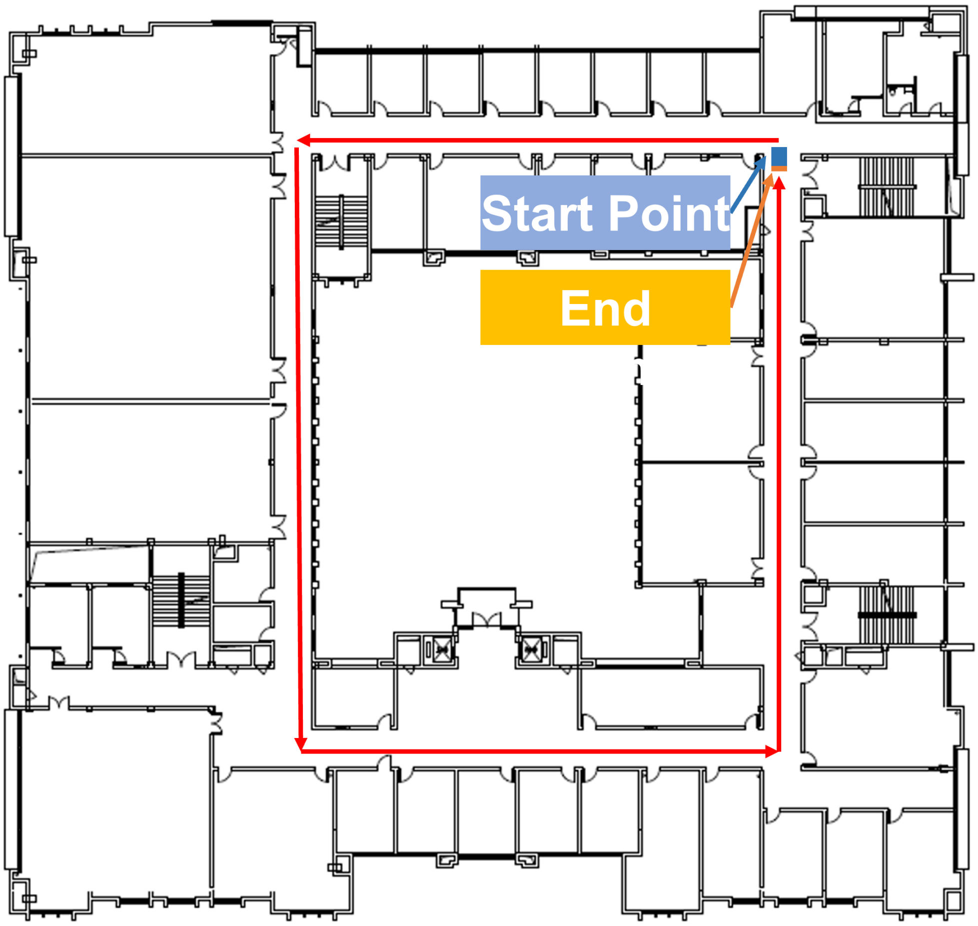

Figure 3.12: *Layout of experimental scenario.*

3.3 IOAM

With the development of IPS, the DF-INS has been extensively used in many fields involving monitoring and direction-finding. It is a widespread IPS implementation with considerable application potential in various areas such as firefighting and home care. However, the existing DF-INS is limited by a high inaccuracy rate due to the highly dynamic and non-stable stride length thresholds. The system also provides less clear and significant information visualisation of a person's position and the surrounding map. To address the aforementioned issues, **Study 3** and **Study 4** propose a novel wearable inertial odometry and mapping (IOAM).

It is worth noticing that, the methods of **Study 3** and **Study 4** are implemented in the same INS framework to perform IOAM, for calculation and visualisation. To ensure good coherence of the method presenting, the notation definition, experiment and results discussion of **Study 3** and **Study 4** are presented in the same section.

3.3.1 System Overview

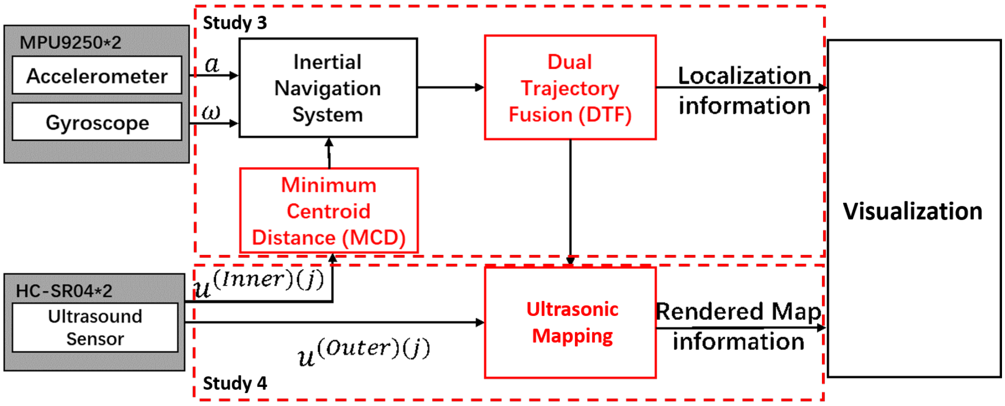

Figure 3.13: *System overveiw of IOAM.*

This part provides a technical overview (Fig.3.13) of the proposed IOAM implementation. First, IOAM introduces a minimum centroid distance (MCD) method that calculates the stride length ultrasonic distance measuring data specifications and determines the dynamic threshold for centroid-method-based dual-foot fusion in INS. In doing so, the dynamic threshold with an accurate stride length constraint improves the tracking estimation performance. Second, IOAM proposes a dual trajectory fusion (DTF) method to fuse the two separated trajectories from the two feet and combine them into one body-level localisation information. DTF analyses the centre body of mass (CBoM) specifications during movement to determine the weight for left and right trajectory fusion. Finally, a 2D-plane map is projected through outer ultrasonic distance measuring using the polar projection theory. The map area is obtained via a surrounding occupancy grid map (S-OGM) [40] to calculate the occupancy status of every pixel (clearing/irrelevant). The localisation and mapping information is then visualised using a uniform canvas.

3.3.2 MCD Aided INS for Dual Foot Fusion

EKF Initialisation

Owing to the physical transmission properties of sound and electronic limitations [154], the sampling rate of the ultrasonic sensor is lower than that of the IMU. The nearest interpolation method [155] was adopted to align the range data and IMU data, as follows:

$$u^{(i)(j)} = \mathrm{interp}\left(\hat{u}^{(i)(j)}, \frac{Ts\left(imu^{(j)}\right)}{Ts\left(\hat{u}^{(i)(j)}\right)}\right) \tag{3.16}$$

where $\hat{u}^{(i)(j)}$ and $u^{(i)(j)}$ represent the original and interpolated ultrasonic sensor measurement signals, respectively. $i \in \{\text{Inner, Outer}\}$ represents the placement, that is, the inner and outer sides of the ultrasonic sensors attached to one foot. $j \in \{R,\ L\}$ represents sensors mounted on the right or left foot. Ts indicates the sampling rate of the sensor data. Two data sequences from the sensors on each foot were synchronised. The IMU data $D_k^{(i)} \in R^6$ is defined as:

$$D_k^{(j)} \triangleq \left[a_k^{(j)} \ \ \omega_k^{(j)}\right]^T \tag{3.17}$$

where $a_k^{(j)} \in R^3$ and $\omega_k^{(j)} \in R^3$ represent 3-axis acceleration (m/s^2) and angular rate (rad/s^2), respectively. $k \in N^+$ indicates the time stamp of the data sequence.

The initial coordinate of the CBoM trajectory from the DTF calculation (p_{COM}) is defined as:

$$p_{COM} = \begin{bmatrix} 0 & 0 & 0 \end{bmatrix}^T \tag{3.18}$$

To separate the dual-foot coordinate calculation, the two-foot initial position coordinates $p_1^{(j)}$ are defined as posteriori by inner ultrasonic sensor distance measuring. The coordinates of $p_1^{(L)}$ and $p_1^{(R)}$ is defined as:

$$p_1^{(L)} = \begin{bmatrix} -\frac{\mu}{2} & 0 & 0 \end{bmatrix}^{-1}, p_1^{(R)} = \begin{bmatrix} \frac{\mu}{2} & 0 & 0 \end{bmatrix}^{-1} \tag{3.19}$$

where μ determines the initial x-axis direction stride-length parameter. A priori IMU state $\hat{x}_k^{(j)}$ in the navigation system is defined as [156] :

$$\hat{x}_k^{(j)} \triangleq \begin{bmatrix} \hat{p}_k^{(j)} & \hat{\mathrm{v}}_k^{(j)} & \hat{\theta}_k^{(j)} \end{bmatrix} \tag{3.20}$$

where $\hat{p}_k^{(j)} \in R^3$, $\hat{v}_k^{(j)} \in R^3$ and $\hat{\theta}_k^{(j)} \in R^3$ represent a priori position, velocity and pose estimation on the 3-axis coordinate system [99, 131]. A step detector [157] classifies each $D_k^{(i)}$ sample according to its motion state as either moving or stationary. When a stationary phase is detected, the INS sets pseudo-measurements in the EKF to compute the posteriori of the $\hat{x}_k^{(j)}$ [158–161].

MCD

The centroid method defines the relative range between the two feet. In a typical dual-foot INS, the distance between two feet has a maximum range constrained by a sphere or ellipsoid model. The distance constraint [156] is described as:

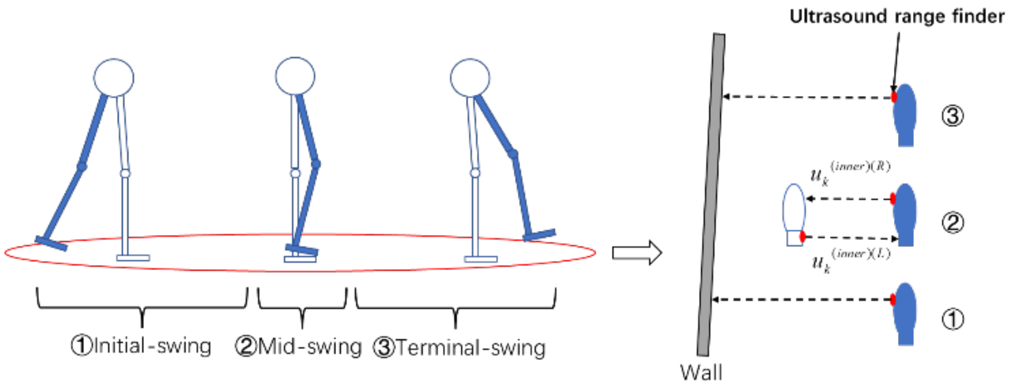

Figure 3.14: *Schematic of right foot swing and inner ultrasonic sensor scanning process.*

$$\left\|\hat{p}_k^{(R)} - \hat{p}_k^{(L)}\right\|_2 \leq \gamma_k, \ \forall k \in N^+ \tag{3.21}$$

where $\|\|_2$ denotes the two-norm calculator and γ is a fixed range threshold. The Lagrange function [162] solution for position pseudo-measurement $p_k^{(j)}$ under the constrained least squares (CLS) [156, 163, 164] framework is defined as:

$$\begin{aligned} p_k^{(R)} &= \frac{\left(\left\|\hat{p}_k^{(R)} - \hat{p}_k^{(L)}\right\|_2 + \gamma\right)\hat{p}_k^{(R)} + \left(\left\|\hat{p}_k^{(R)} - \hat{p}_k^{(L)}\right\|_2 - \gamma\right)\hat{p}_k^{(L)}}{2\left\|\hat{p}_k^{(R)} - \hat{p}_k^{(L)}\right\|_2}, \\ p_k^{(L)} &= \frac{\left(\left\|\hat{p}_k^{(R)} - \hat{p}_k^{(L)}\right\|_2 + \gamma\right)\hat{p}_k^{(L)} + \left(\left\|\hat{p}_k^{(R)} - \hat{p}_k^{(L)}\right\|_2 - \gamma\right)\hat{p}_k^{(R)}}{2\left\|\hat{p}_k^{(R)} - \hat{p}_k^{(L)}\right\|_2} \end{aligned} \tag{3.22}$$

Then, the predefined maximum range pseudo-measurement is applied to optimise the foot's position using the EKF. The maximum range constraint can only address out-of-range drifting problems due to the dynamic stride length during movement and unpredictable gaits from different users. The bias error from position and altitude estimation would also cause trajectory coinciding and crossing problems, reducing the tracking accuracy. A

MCD method is proposed to determine the dynamic stride length constraint threshold via inner ultrasonic distance measuring during the mid-swing phase in the gait cycle. The gait cycle during the swing phase of the moving state can be categorised into three continual sub-statuses: initial swing, mid-swing and terminal swing [165] based on the position of the swinging leg relative to the stationary leg (Fig.3.14). It is assumed that the normal gait cycle did not involve leg cross-swinging.

In MCD, the mid-swing phase detection can be determined as:

$$S_k^{(j)} = \begin{cases} 1, \; \kappa_{min} < u_k^{(inner)(j)} < \kappa_{max} \\ 0, \; others \end{cases} \tag{3.23}$$

where κ is the stride length parameter.

To reduce inaccurate measurements during the swinging phase, the inner stride length range is designed to operate in the stance phase of the opposite foot. The DTF algorithm first detects the zero-speed states using the GLRT [155] which is defined as:

$$ZUPT_k^{(j)} = \begin{cases} 1, \; zero\ velocity\ detected \\ 0, \; others \end{cases} \tag{3.24}$$

Each IMU sample is indicated with either one or zero markers representing the current motion state. The minimum internal sampling strategy (Eq. 3.25) is utilised in this method to reduce the over-optimisation of dual-foot data fusion.

$$t_k - t_{LO} < \sigma \tag{3.25}$$

where t is the sample timestamp conversion function, LO represents the last operation of the MCD method and σ is the parameter of the timestamp interval. The flow chart of the proposed MCD method is shown in Fig.3.15.

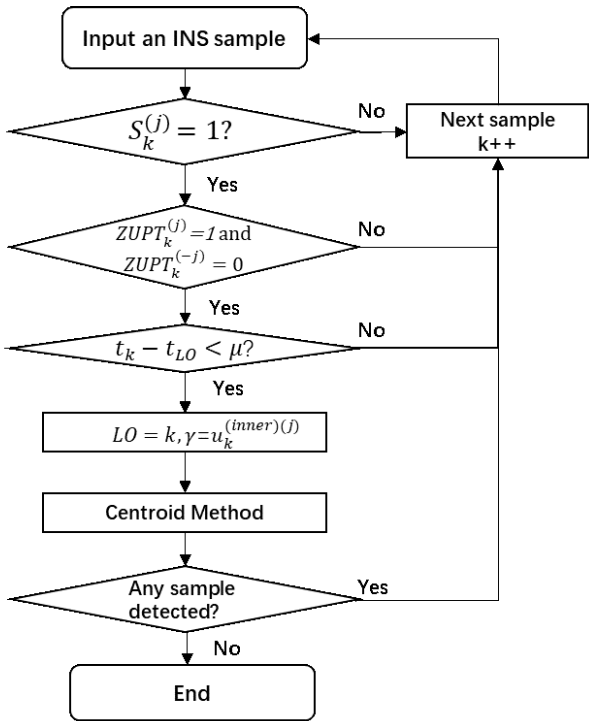

Figure 3.15: *Process of MCD algorithm.*

In MCD, the x- and y-axis data for pseudo-measurements PM are utilised in the EKF, whereas the z-axis data (height) are not considered in the ultrasonic sensor scanning in the 2D plane, as follows:

$$PM_k^{(j)} = \begin{bmatrix} PM_{k,x}^{(j)} \\ PM_{k,y}^{(j)} \\ p_{k,z}^{(j)} \end{bmatrix} \tag{3.26}$$

where PM_k indicates the calculated posteriori centroid distance of the pseudo-measurement in the EKF and $p_{k,z}^{(j)}$ represents the original z-axis height information in the INS. Finally, using these pseudo-measurements in the Kalman filter platform, the formulas are described as follows [156] :

$$K_k^{(j)} = P_k^{(j)} (H_p)^T \left[H_p P_k^{(j)} (H_p)^T + R_p \right]^{-1} \tag{3.27}$$

$$\hat{x}_k^{(j)} = \hat{x}_k^{(j)} + K_k^{(j)} \left[PM_k^{(j)} - H_p \hat{x}_k^{(j)} \right] \tag{3.28}$$

$$H_p = [I_{3\times3}\ 0_{3\times3}\ 0_{3\times3}\ 0_{3\times3}\ 0_{3\times3}] \tag{3.29}$$

$$P_k^{(i)} = [I_{15\times9} - K_k H_p]\, P_k^{(j)} \tag{3.30}$$

where $K_k^{(j)}$ denotes the Kalman gain and H_p the observation transition matrix with pseudo-measurement. $I_{3\times3}$ denotes the identity matrix and $0_{3\times3}$ denotes the zero matrix. R_p denotes the noise-covariance matrix of H_p.

Projection of CBoM for DTF

In this study, the dual-foot structure is defined as a rigid body to simplify the tracking visualisation and transform the footpath to the user's trajectory [166, 167]. The CBoM is calculated by merging the dual-foot estimated position using the weight fusion [168] method:

$$p_{COM} = g\left[p^{(R)}\quad p^{(L)}\right] = \alpha p^{(R)} + \beta p^{(L)},\ \alpha + \beta = 1 \tag{3.31}$$

where $p_{COM} \in R^3$ indicates the position of the hypothetical CBoM of the body of the sensor carrier. α and β are the weight parameters for the right- and left-foot INS, respectively.

During the swing phase (Fig.3.14), the heading direction is in the sagittal plane (Fig.3.16). The CBoM swings at the frontal plane of the body during the alternating movement of the two legs during walking, which can be defined as a pendulum model [170, 171]. The pendulum range can represent the fusion weight, which is defined by a sine function [172–174]. The ZUPT clustering method used to calculate the weight is shown in Fig. 3.17, where $ZUPT - j_m^n$ denotes the ZUPT cluster containing continual zero-speed samples ($ZUPT = 1$), m indicates the order number of ZUPT

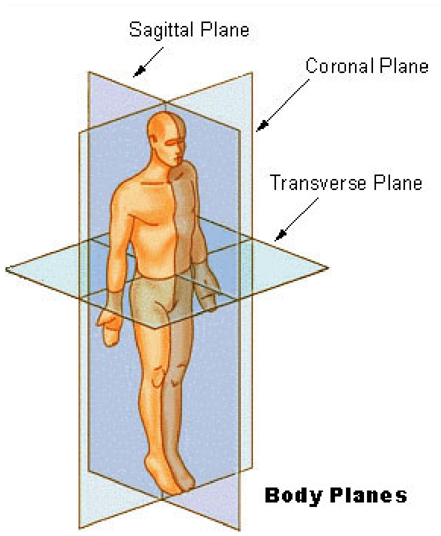

Figure 3.16: *Determination of the CBoM [169].*

clusters in all input samples, n indicates the order number in a specific ZUPT cluster.

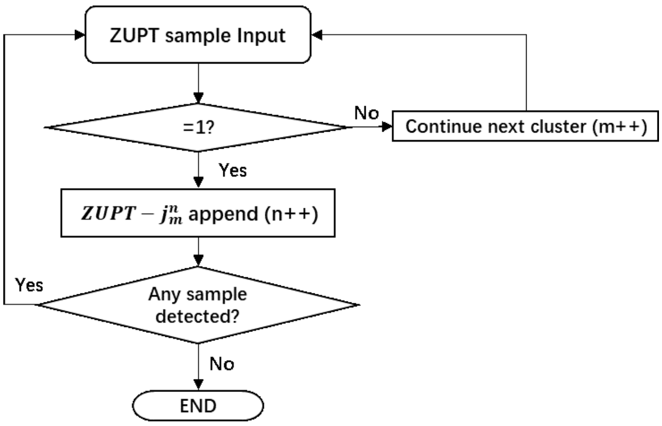

Figure 3.17: *Calculation of ZUPT clustering.*

Then, the weight of the DTF is defined as:

$$weight = \begin{cases} 0.5 + 0.25 * sin\left(\frac{n}{length(ZUPT - L_m^n)}\right), & ZUPT^{(L)} = 1 \\ 0.5 & , ZUPT^{(L)} \oplus ZUPT^{(R)} = 1 \\ 0.5 + 0.25 * sin\left(\frac{n}{length(ZUPT - R_m^n)}\right), & ZUPT^{(R)} = 1 \end{cases} \tag{3.32}$$

Thus, the p_{COM} calculation according to Eq.3.31 would be defined as:

$$p_{COM} = weight * p^{(R)} + (1 - weight)\, p^{(L)} \tag{3.33}$$

The fused trajectory is then filtered through a $\left(1 \times \frac{Ts}{2}\right)$ mean filter [175] for small drifting in the motion integral calculation, as follows:

$$\hat{p}_{COM,k} = \frac{2 * \sum p_{COM,k}}{Ts} \tag{3.34}$$

3.3.3 Ultrasonic Mapping

Polar projection mechanism

The coordinates of the ultrasonic mapping points are calculated based on the step position and the pose estimated by the INS. The range direction of the ultrasonic sensor is parallel to the x-axis of the IMU in each foot. To project the 3D scanning onto the 2D XOY coordinate, a polar transform method is described as follows [168, 176, 177]:

$$M\left(r_k^{(i)(j)}\right) = \begin{bmatrix} \cos\theta\cos\varphi \\ \cos\theta\sin\varphi \end{bmatrix} \tag{3.35}$$

where θ and φ denote the pitch and yaw angles in pose estimation, respectively. The coordinates of the ultrasonic mapping point $Up_k^{(i)(j)}$ under the maximum covering principle are calculated as follows:

$$Up_k^{(i)(j)} = \left[Ux_k^{(i)(j)}\ Uy_k^{(i)(j)}\ \right]^T = \begin{cases} \left[p_k^{(j)} + u_k^{(i)(j)} diag(1,1) M\left(r_k^{(i)(j)}\right)\right]^T \\ \quad , i, j = inner, L || outer, R \\ \left[p_k^{(j)} - u_k^{(i)(j)} diag(1,1) M\left(r_k^{(i)(j)}\right)\right]^T \\ \quad , i, j = inner, R || outer, L \end{cases} \tag{3.36}$$

For the ultrasonic range measuring, it should satisfy the condition:

$$R_{min} < u_k^{(i)(j)} < R_{max} \tag{3.37}$$

where R_{min} and R_{max} are the ultrasonic sensors' minimum and maximum available measurement ranges (Table 3.3), respectively. The inner ultrasonic mapping points should also be calculated at the initial swinging and terminal swinging phrases (Fig.3.14) and satisfy the $u_k^{(inner)(j)} > \kappa_{max}$ condition.

S-OGM calculation

Compared with the laser range finder, the ultrasonic sensor has a lower cost and wider detection angle, making it more practical for wearable applications [178]. In addition, ultrasonic sensors are stable under smoke- and vapour-filled environments with lower energy consumption among different range measurement methods [154, 178]. According to ultrasonic specifications, each ranging process is modelled as a rectangular zone (white arrow in Fig. 3.18) in the occupancy grid map (OGM) [40] follows:

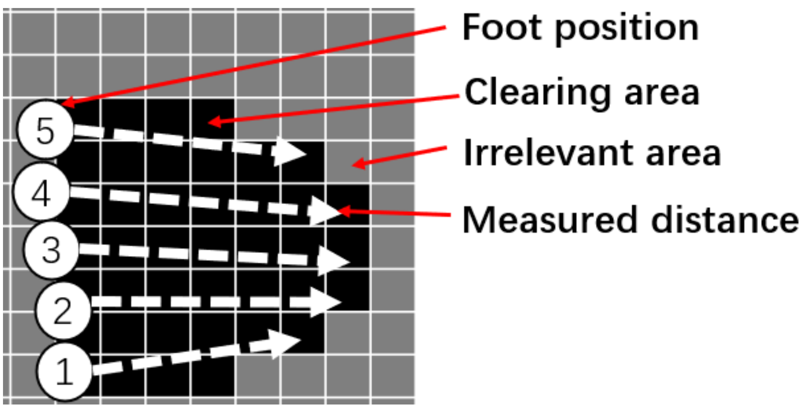

Figure 3.18: *Schematic of ultrasonic S-OGM process with five footsteps.*

The single grid cells of the map are categorised as empty (black) or irrelevant (gray) areas. The S-OGM algorithm is defined as:

$$B\left(p_k^{(j)}, Up_k^{(i)(j)}\right) \tag{3.38}$$

where B denotes the Bresenham algorithm [179], $p_k^{(j)}$ and $Up_k^{(i)(j)}$ indicate the ultrasonic sensor placement position coinciding with the foot position and position of the pixel at the clearing area boundary, respectively.

3.3.4 Experimental Setup

A pair of wearable sensor modules was designed for the data collection. The proposed wearable module is shown in Fig. 3.19a and consists of a MPU9250 IMU (see Table 3.3), two HC-SR04 ultrasonic sensors (see Table 3.2) and an ESP32 dual-core micro computing unit.

Table 3.2: Specifications of HC-SR04 ultrasonic sensor

Specifications	Values
Operating Voltage	DC 5V
Operating Current	15 mA
Operating Frequency	40 kHz
Range	2cm – 5m
Ranging Accuracy	3 mm
Measuring Angle	15 degrees
Trigger Input Signal	10 µS TTL Pulse
Sampling rate	15 Hz

The module was mounted on the front side of each shoe using a hook and loop tape. The placement of ultrasonic sensors are improved based on the original design from [168]. Two ultrasonic sensors are mounted in one shoe for inner and outer side range measurement where the inner ultrasonic sensor are able to make compensation for more accurate map generation. The inner ultrasonic sensors are staggered and placed separately at the back and front sides of the two feet to avoid potential ultrasound-emitting interference. The IMU was calibrated utilising an internal calibration module

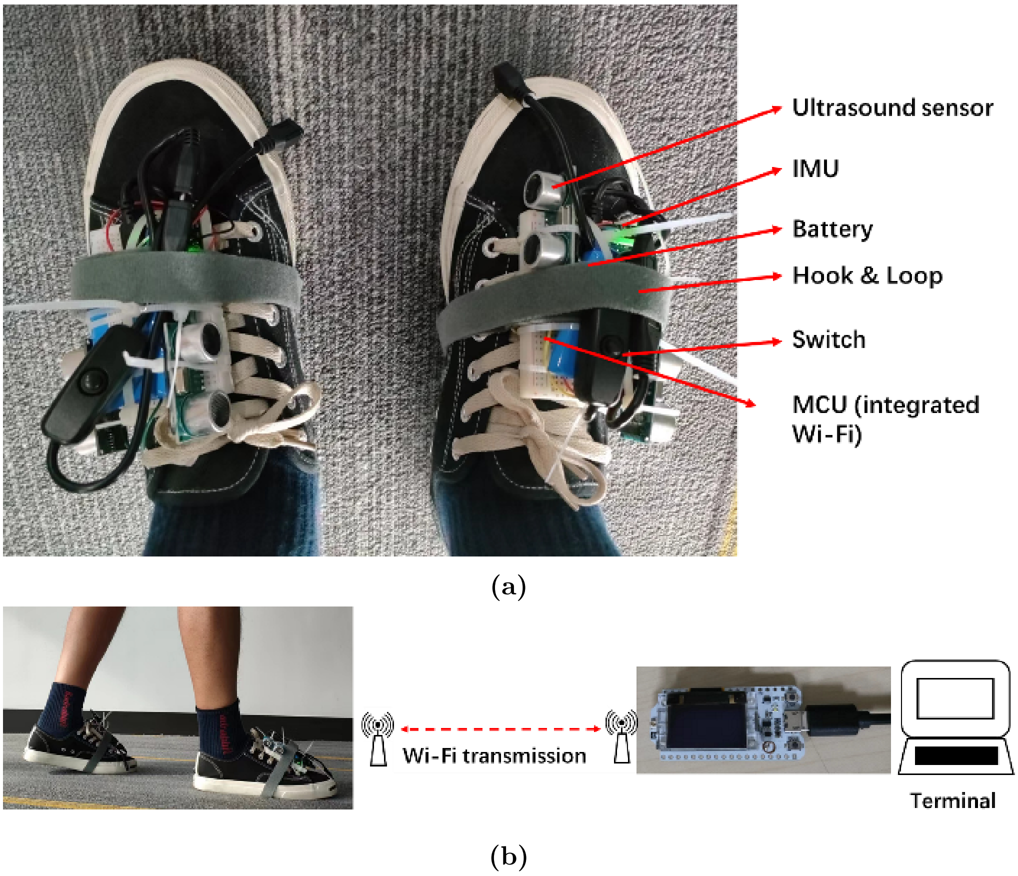

Figure 3.19: *Component layout of IOAM wearable devices (a) and data transmission schematic during the experiment (b).*

in hardware. A 900 mAh battery with an estimated 2-h power supply was attached to the shoe. Sensor data were transmitted via Wi-Fi to a nearby terminal, as shown in Fig. 3.19b. The data receiver application at the terminal was implemented in MATLAB 2022a using an Intel i7-10510U 1.8 GHz, 16GB RAM laptop. The update rate of inertial odometry and ultrasonic mapping were 200 Hz, following the sampling rate of IMU.

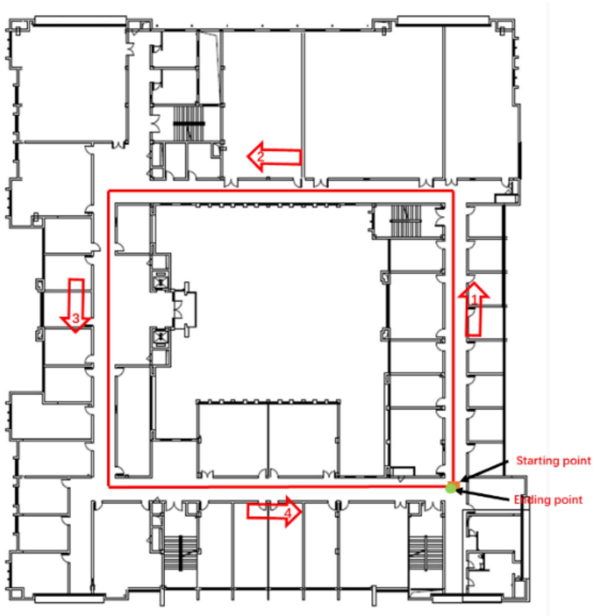

(a)

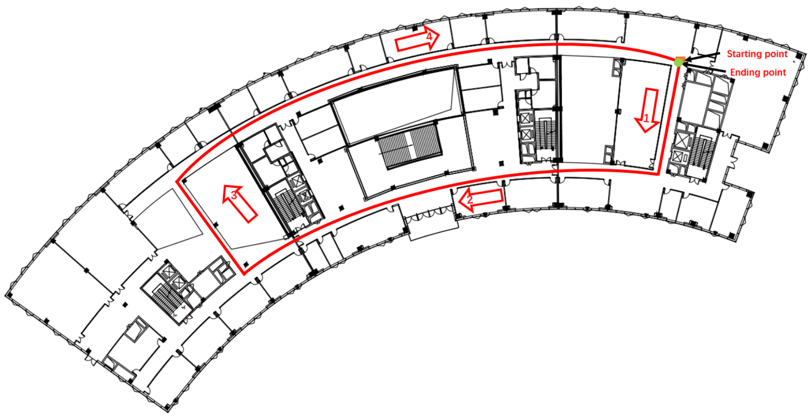

(b)

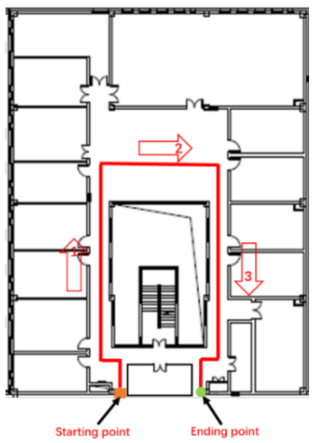

(c)

Figure 3.20: *Layout of data collection locations for scenarios 1 (a), 2 (b) and 3 (c).*

Table 3.3: Specifications of MPU9250 IMU

Specifications	Values
Operating Voltage	DC 5 V
Accelerometer Scale Range	±16g
Gyroscope Scale Range	±2000°/s
Communication Interface	I^2C
Sampling Rate	200 Hz

Table 3.4: Height and Weight Information of Volunteers

Participants	Gender	Height [cm]	Weight [kg]
a	male	175	65
b	male	185	85
c	female	163	50
d	female	163	50
e	male	175	70
f	male	172	53
g	male	170	55
h	female	170	47

Eight volunteers were recruited to participate in the experiment, as listed in Table 3.4. Volunteers provided informed consent and the study was approved by the faculty ethics review board. Three scenarios were designed and set up at three different office-like buildings with solid red line reference routes (see Fig. 3.20): a rectangular route (Scenario 1, 161.23 m), a fan-shaped route (Scenario 2, 198.55 m) and a bottle-shaped route (Scenario 3, 53.06 m). Volunteers were requested to wear the designed modules and walk along the pre-arranged route. There were no gait or gesture limitations during walking. Each volunteer walked in all three scenarios.

3.4 Multi-INS

Achieving precise individual loop closure and global multi-person position fusion is crucial for mitigating accumulative errors and accurately determining the positions of multiple individuals. Existing FT-INS lack the reference information needed for loop closure and multi-person trajectory fusion, limiting their applicability in scenarios involving numerous users. To address this challenge, **Study 5** presents the Multi-INS, which employs an online MF matching approach for inertial state updates.

3.4.1 System Overview

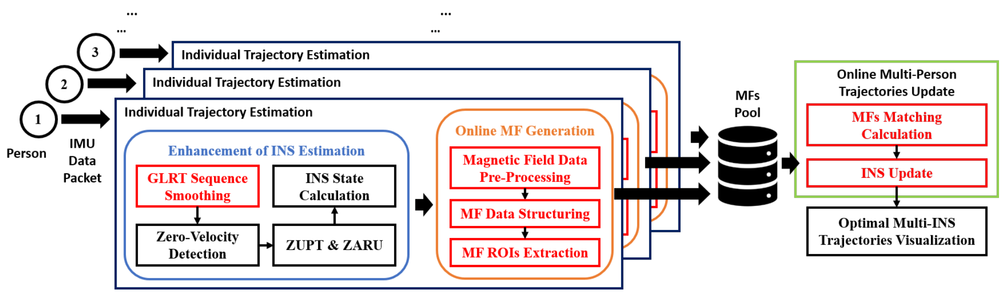

Figure 3.21: *System overview of the proposed Multi-INS.*

Figure 3.21 presents a comprehensive depiction of the proposed Multi-INS system, which is divided into individual trajectory estimation (see Section 3.4.2) and online multi-person trajectories update (see Section 3.4.6). Initially, individual trajectories are estimated using collected IMU data packets, containing 3-axis acceleration, 3-axis angular rate, and 3-axis magnetic field data. GLRT sequences are initially generated using the GLRT model and then smoothed, which is subsequently utilised for zero velocity (ZV) detection. Then, the ZUPT and ZARU algorithms are employed to calculate the individual INS states, including 3-axis position, 3-axis velocity, and 3-axis attitude. Gait cycles are identified and segmented from the detected ZV sequences to derive individual MF data sequences. A proposed selection algorithm is employed to extract the target MF data sequences from each individual's MF data sequences, forming the multi-person MF pool. It is important to note that the INS estimation and MF generation phases are carried out online, departing from the traditional offline approach.

In the phase of updating multi-person trajectories, MF key points are extracted by identifying the local peaks in the MF data, indicating turning points (refer to Section 3.1.2). Subsequently, a conditional similarity-based MF is introduced to facilitate cross-updating of INS states among individuals, aligning their trajectories within a shared space. This innovative framework significantly reduces computational time and effectively resolves trajectory mismatch issues among individuals in the shared space. Potentially, the proposed MF cross-update model possesses the capability to simultaneously match the trajectories of an unlimited number of individuals sharing the same space, effectively reducing positional errors among them. To further validate the practicality of the proposed work, this study conducts experimental testing, involving five users simultaneously walking in an indoor environment.

3.4.2 Individual Trajectory Estimation

This section covers the process of estimating individual trajectories, focusing on improving INS estimation and generating MF data online.

3.4.3 INS State Model

The IMU data packet of the right foot, denoted as $D_i^{(n)} \in R^{(9)}$ for multi-person configurations, can be defined as:

$$D_i^{(n)} \triangleq \begin{bmatrix} a_i^{(n)} \\ \omega_i^{(n)} \\ m_i^{(n)} \end{bmatrix} \tag{3.39}$$

where n represents the person's index, and $a_i^{(n)} \in R^{(3)}$, $\omega_i^{(n)} \in R^{(3)}$, and $m_i^{(n)} \in R^{(3)}$ indicates the 3-axis measurements of acceleration (m/s^2), angular rate (rad/s^2) and magnetic field (μT) within the IMU data, respectively. Additionally, $i \in N^+$ signifies the time instant of the data sequences. The initial coordinate $l^{(n)}$ for each individual's position is defined as:

$$l^{(n)} = \begin{bmatrix} x^{(n)} \\ y^{(n)} \\ z^{(n)} \end{bmatrix} \tag{3.40}$$

where $x^{(n)}$, $y^{(n)}$ and $z^{(n)}$ denote the positional coordinates for each individual after EKF was applied. The prior individual INS state $\hat{x}_i^{(n)}$ is defined as:

$$\hat{x}_i^{(n)} \triangleq \begin{bmatrix} \hat{l}_i^{(n)} \\ \hat{v}_i^{(n)} \\ \hat{\theta}_i^{(n)} \end{bmatrix} \tag{3.41}$$

where $\hat{l}_i^{(n)} \in R^{(3)}$, $\hat{v}_i^{(n)} \in R^{(3)}$ and $\hat{\theta}_i^{(n)} \in R^{(3)}$ represent the prior estimated position, velocity, and pose of each individual, respectively, based on the 3-axis coordinate system.

3.4.4 Enhancement of INS Estimation

GLRT Sequence Smoothing

During this phase, the GLRT model [39] is employed to generate GLRT sequences for the n-th person, denoted as $T^{(n)}(z_i)$, using the $a^{(n)}$ and $\omega^{(n)}$ from $D^{(n)}$, where z indicates the likelihood measurement. Initial observation [180] indicates that the generated GLRT sequences contain noise, potentially leading to incorrect ZV detection (see Section 3.4.4). This inaccuracy primarily resulted from motion differences due to variations in gait movements among users, such as body tremors. To address this issue, a moving average filtering method [181] is introduced to generate smoothed

GLRT sequences, as shown in Eq. (3.42):

$$\hat{T}_i^{(n)}(z_i) = \frac{1}{M} \sum_{i-M+1}^{I} T_i^{(n)}(z_i) \tag{3.42}$$

where M denotes the window size of the filter, and $\hat{T}^{(n)}(z_i)$ represents the smoothed GLRT sequences of the n-th person. This approach significantly decreases the likelihood of false ZV detection.

Detection of Zero-Velocity

Subsequently, the ZV sequences of the i-th person, denoted as $ZV_i^{(n)}$, are determined based on the smoothed $\hat{T}^{(n)}(z_i)$. The state $ZV_i^{(n)}$ at time instant i is classified as either a stance state of 1 or a swing state of 0 (see Fig. 3.22), as described in Eq. (3.43):

$$ZV_i^{(n)} = \begin{cases} 1, \, \hat{T}_i^{(n)}(z_i) \leq \tau \\ 0, \, \hat{T}_i^{(n)}(z_i) > \tau \end{cases} \tag{3.43}$$

where τ represents the predefined threshold.

Calculation of INS State

If $ZV_i^{(n)}$ is classified as the stance state, the EKF method is applied to compute the posterior state of $\hat{x}_i^{(n)}$, utilising ZUPT and ZARU algorithms to optimise the $\hat{v}_i^{(n)}$ and $\hat{\theta}_i^{(n)}$, as shown below:

$$\hat{x}_i^{(n)} = \hat{x}_i^{(n)} + K_i^{(n)} \left[v, \theta_i^{(n)} - H\hat{x}_i^{(n)} \right] \tag{3.44}$$

$$K_i^{(n)} = P_i^{(n)} H^T \left[H P_i^{(n)} H^T + R_H \right]^{\text{-1}} \tag{3.45}$$

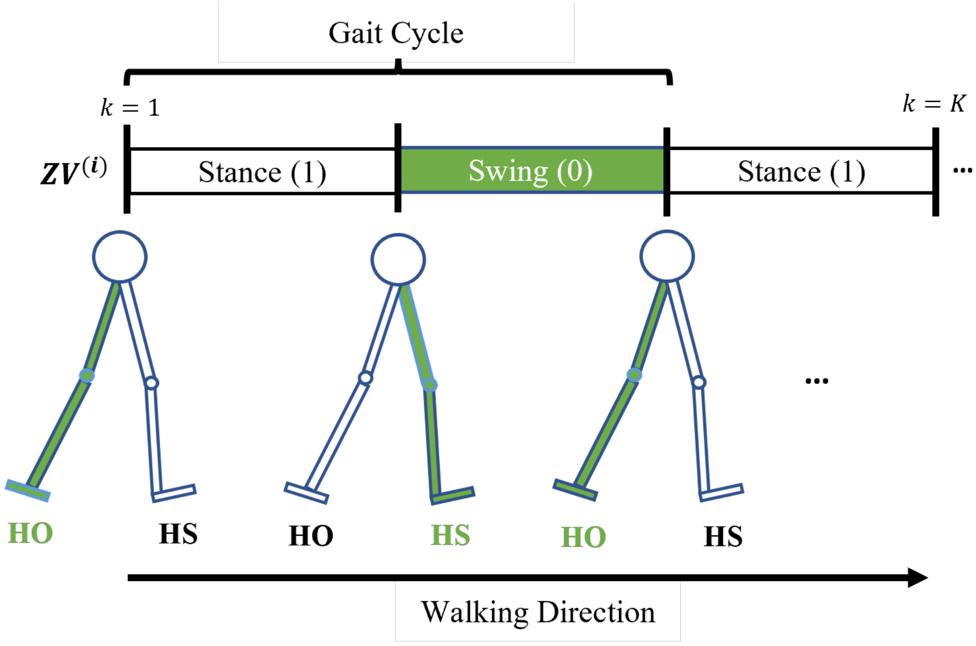

Figure 3.22: *Overview of the ZV detection.*

$$H = H_{v,\theta} = \begin{bmatrix} I_{3\times3} & 0_{3\times3} & 0_{3\times3} \\ 0_{3\times3} & 0_{3\times3} & I_{3\times3} \end{bmatrix} \tag{3.46}$$

$$P_i^{(n)} = [I_{9\times9} - K_i H]\, P_i^{(n)} \tag{3.47}$$

where $K_i^{(n)}$ represents the Kalman gain matrix for the i-th person, $H_{v,\theta}$ is the velocity and angular rate observation transition matrix of the pseudo-measurement, $I_{3\times3}$ is the identity matrix, $0_{3\times3}$ is the zero matrix, R_H denotes the noise covariance matrix of H and $P_i^{(n)}$ indicates the predicted state of prior covariance matrix.

3.4.5 Online Generation of MF Data

The section starts with an overview of gait data processing, including the generation and calibration of MF data. It then introduces a new technique for identifying target MF data by utilising a turning-points detection approach to extract regions of interest (ROIs). These ROIs, containing the target MF data, formed the MF pool dataset, which is subsequently employed to update the INS states of multiple individuals.

Magnetic Field Data Calibration

Each footstep in a person's gait cycle consists of stance and swing phases, determined based on the results from $ZV_i^{(n)}$ at time instant i. The IMU's magnetic field readings yield spatial magnetic intensity. Given the relatively stable environmental conditions and consistent facility placement, this magnetic field data distribution is well-suited for navigation-based fingerprinting [129, 130]. The raw vector of magnetic field data for a person is defined as follows:

$$m^{(n)} \triangleq \begin{bmatrix} m_x^{(n)} \\ m_y^{(n)} \\ m_z^{(n)} \end{bmatrix} \tag{3.48}$$

where m_x^n,m_y^n and m_z^n represent magnetic field data in three-axis Cartesian coordinates. However, due to magnetic interference from the surroundings, magnetic field data is prone to distortion. Calibration of each IMU sensor is required by introducing an offset matrix [182], denoted as $O^{(n)}$, to the raw magnetic field data:

$$O^{(n)} = \begin{bmatrix} O_x^{(n)} \\ O_y^{(n)} \\ O_z^{(n)} \end{bmatrix} \tag{3.49}$$

where $O_x^{(n)}$, $O_y^{(n)}$ and $O_z^{(n)}$ represent the three-axis offset values associated with the n-th person's IMU, respectively. The calibrated magnetic field vector data $\hat{m}^{(n)}$ is calculated by compensating for $O^{(n)}$ as follows:

$$\hat{m}^{(n)} = m^{(n)} + O^{(n)} \triangleq \begin{bmatrix} \hat{m}_x^{(n)} \\ \hat{m}_y^{(n)} \\ \hat{m}_z^{(n)} \end{bmatrix} \tag{3.50}$$

where $\hat{m}_x^{(n)}$, $\hat{m}_y^{(n)}$ and $\hat{m}_z^{(n)}$ represent the three-axis calibrated magnetic field data in the x, y and z-coordinates, respectively. Following the calibration of magnetic field data, dynamic movement sequence data, contingent upon variations in the spatial magnetic distribution of the surroundings, are acquired during the swing state.

Structuring of MF Data

The MF data structure at time instant i consists of seven elements, including:

- *ID*: Indicates the identifier of a MF, assigned with the order number of the timestamp.
- *TS*: Indicates the timestamp of a MF.
- *SO*: Indicates the step order of a MF.
- *POS*: Denotes the three-axis position of the foot.
- *ATT*: Denotes the attitude (pose) of the foot.
- *GoH*: The Gradient-of-Heading indicates the changes of the motion heading between step at t_i and step at t_{i-1} which is used to determine the moving pattern (forwarding or turning).
- $\hat{m}^{(n)}$: The calibrated three-axis magnetic field data.

The overview of the MF data structure of magnetic fingerprinting is depicted in Table 3.5.

Extraction of MF ROIs

Fingerprint matching tasks are often time-consuming, with a time complexity of $O(mn)$, as shown in [183]. The general matching algorithm costs $O(n^2)$ for traversal matching, introducing high complexity to the study. To

Table 3.5: Overview of data structure of MF

No.	Element	Format & Unit	State
1	ID	Character	Stance
2	TS	[DD:HH:SS]	Stance
3	SO	Number	Stance
4	POS	$\hat{p}_i^{(n)} = [\hat{p}_{x,i}^{(n)}, \hat{p}_{y,i}^{(n)}, \hat{p}_{z,i}^{(n)}]$	Stance
5	ATT	$\hat{\theta}_i^{(n)} = [\hat{\theta}_{x,i}^{(n)}, \hat{\theta}_{y,i}^{(n)}, \hat{\theta}_{z,i}^{(n)}]$	Stance
6	GoH	$\Delta\theta$	Stance
7	$\hat{m}^{(n)}$	$\hat{m}_i^{(n)} = [\hat{p}_{x,i}^{(n)}, \hat{p}_{y,i}^{(n)}, \hat{p}_{z,i}^{(n)}]$	Swing

address this issue, the initial study [180] showed that magnetic field data obtained at each corner of the indoor environment provided higher significant signatures compared to the corridors. Therefore, in this study, the region of MF data at each turning point was selected to serve as indicators for position estimation. Each turning point is detected by finding the local peaks in the GoH sequences where the movement headings indicate a significant change in orientation between time frames, as shown in Fig. 3.23. The region-of-interest of MF (ROI-MF) in each gait cycle is selected based on the conditions described below:

1. $[\mathrm{MF}_{i+1}^p, \mathrm{MF}_{i+2}^p, \mathrm{MF}_{i+3}^p]$ if $p = 0$
2. $[\mathrm{MF}_{i-2}^p, \mathrm{MF}_{i-1}^p, \mathrm{MF}_{i}^p, \mathrm{MF}_{i+1}^p, \mathrm{MF}_{i+2}^p]$ if $0 < p < SO$
3. $[\mathrm{MF}_{SO-2}, \mathrm{MF}_{SO-1}, \mathrm{MF}_{SO}]$

where p is the index of the detected peak at time instant i. The selected ROI-MFs are then formed into a MFs pool, subsequently utilised for updating multi-person trajectories.

3.4.6 Online Update of Multi-Person Trajectories

This section outlines the approach for updating the multi-person INS state using the MF matching method. The process involves two phases: individual position update and multi-person position update.

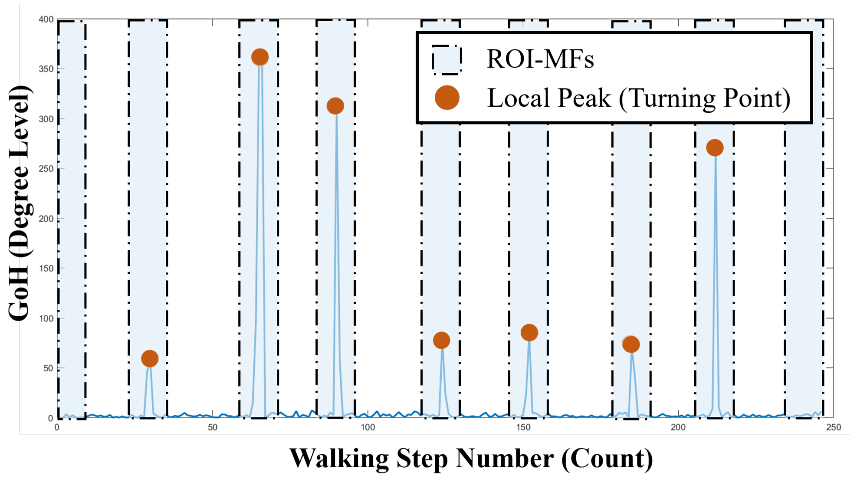

Figure 3.23: *Illustration of ROI-MFs, which is denoted as the light blue regions, based on the detected local peaks from GoH.*

MF Matching for Updating Individual Position

Previous studies [184] attempted to decrease computation time in MF matching by employing various dimension reduction techniques, often resulting in information loss. To maintain the accuracy of MF matching, the tri-axis DTW method [140] is utilised in this study to assess the similarity between MFs of different durations. The cost of MF matching using DTW (referred to as DTW cost), represented as $D(\hat{m}^{(n)}X, \hat{m}^{(n)}Y)$ for the n-th individual at two time sequences, $X = x_i, ..., x_I$ and $Y = y_j, ..., y_J$, is calculated as follows:

$$D(i, j) = d(x_i, y_j) + min \begin{Bmatrix} D(i-1, j) \\ D(i, j-1) \\ D(i-1, j-1) \end{Bmatrix} \tag{3.51}$$

where the $d(x_i, y_j)$ is defined as:

$$d(x_i, y_j) = \|x_i - y_j\| \tag{3.52}$$

where $d(x_i, y_j)$ denotes the Euclidean distance between two MF data points at different time sequences.

INS State Updating for Multi-Person Position

The selected MF with the shortest distance is then utilised to update the tri-axis position pseudo-measurement, defined as follows:

$$p_{i|1:3}^{(n)} - p_{\zeta}^{(n)} = [I_{3\times3} \quad I_{3\times6}\ ]\hat{x}_i^{(n)} + \epsilon_{\zeta} \tag{3.53}$$

where $p_{i|1:3}^{(n)}$ represents the estimated 3-axis position state, $p_{\zeta}^{(n)}$ denotes the pseudo-measurement of position from the selected MF, and ζ signifies the noise covariance matrix of the pseudo-measurement. The initial MF data for each individual's prior INS state is collected and chosen for the MF matching used in individual INS state updates, as initial MF data typically has the lowest position error. The INS state update proceeds as follows:

$$K_i^{(n)} = P_i^{(n)} H^T \left[H P_i^{(n)} H^T + R_H \right]^{-1} \tag{3.54}$$

$$\hat{x}_i^{(n)} = \hat{x}_i^{(n)} + K_i^{(n)} \left[p_{\zeta}^{(n)} - H\hat{x}_i^{(n)} \right] \tag{3.55}$$

$$H = [0_{3\times3}\ I_{3\times3}\ 0_{3\times3}] \tag{3.56}$$

where $K_i^{(n)}$ represents the Kalman gain, H is the position observation transition matrix with pseudo-measurement, $I_{3\times3}$ is the identity matrix, $0_{3\times3}$ denotes the zero matrix and R_H is the noise-covariance matrix of H.

Figure 3.24 depicts a scenario where the walking trajectory of Person 1 at round $k+1$, shown by the blue line, displays significant positioning errors compared to the ground truth trajectory (black line), resulting in cumulative errors in subsequent trajectories. The individual MF matching approach is employed by updating the closing point of the walking trajectory at round $k+1$ using the closing point's position at round k (shown by the red line). This approach significantly reduces the cumulative position-

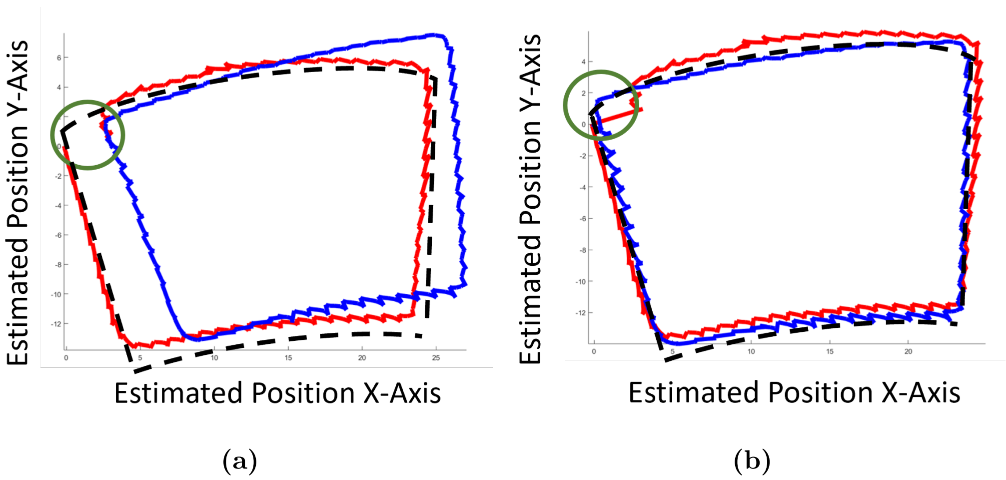

Figure 3.24: *Visualisation of (a) walking trajectories of Person 1 for rounds k (red line) and $k+1$ (blue line), with the trajectory of round $k+1$ exhibiting significant positioning errors compared to the ground truth trajectory (black line), and (b) the trajectory errors of round $k+1$ are minimised through an individual MF matching approach, which involves updating the closing point of round $k+1$ based on the closing point of round k.*

ing errors, as demonstrated in Fig. 3.24b. Conversely, Fig. 3.25 illustrates a scenario where the walking trajectory of Person 2 at round k (indicated by the red line) exhibits significant positioning errors. These errors are mitigated by utilising the cross-update MF matching approach, which updates Person 2's closing point at round k using the closing point of Person 1 at the same round (indicated by the red line), as depicted in Fig. 3.25b.

Similarly, Fig. 3.25 illustrates the position update of an individual's closing point during two rounds of walking trajectories, albeit based on another person's MF matching.

3.4.7 Experimental Setup

The proposed system, adopting Internet-of-things (IoT) principles, integrates an IoT-based wearable module that incorporates a MPU9250 IMU and a Seeed Studio XIAO ESP32C3 dual-core micro-computing unit (MCU) for data collection. The module is designed using a custom-designed printed

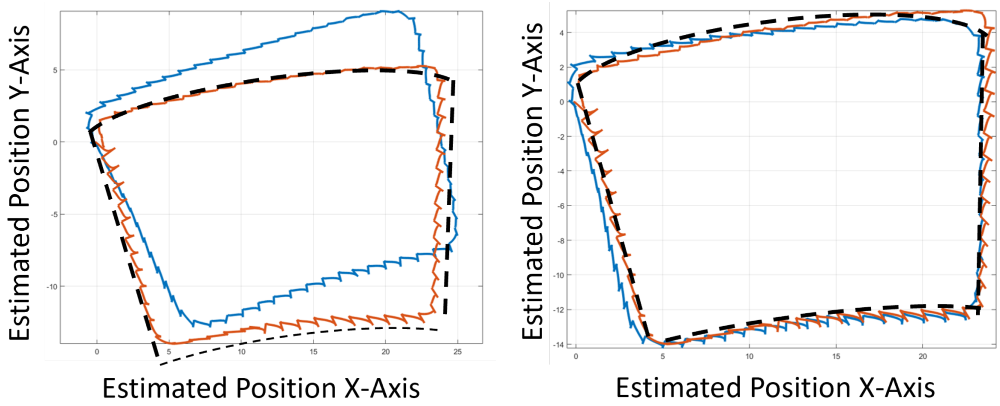

(a) (b)

Figure 3.25: *Example visualisation of (a) walking trajectories of Person 1 (red line) and Person 2 (blue line) for rounds k, with the trajectory of Person 2 exhibiting significant positioning errors compared to the ground truth trajectory (black line), and (b) the trajectory errors of Person 2 is minimised through a cross-update MF matching approach, which involved updating the closing point of Person 2's trajectory based on the closing point of Person 1's trajectory.*

circuit board (PCB) encased within a 3D printed housing to ensure stability as depicted in Fig. 3.26a. A flexible antenna is attached externally to improve signal transmission quality, with the entire module enveloped in a grey insulation sheath to protect its electronic components. Each subject's shoe securely holds the wearable module using zip ties. Additionally, a 1300 mAh battery with an estimated 5-hour power supply capability is integrated. Sensor data are transmitted via Wi-Fi to a handheld cellphone (OnePlus 5T), which connects to an ESP32 Wi-Fi module using the OTG protocol (as illustrated in Fig. 3.26b). Subsequently, data are stored and computed on a laptop equipped with an Intel i7-10510U 1.8 GHz processor and 16 GB of RAM. The IMU was calibrated utilising an internal calibration module in hardware.

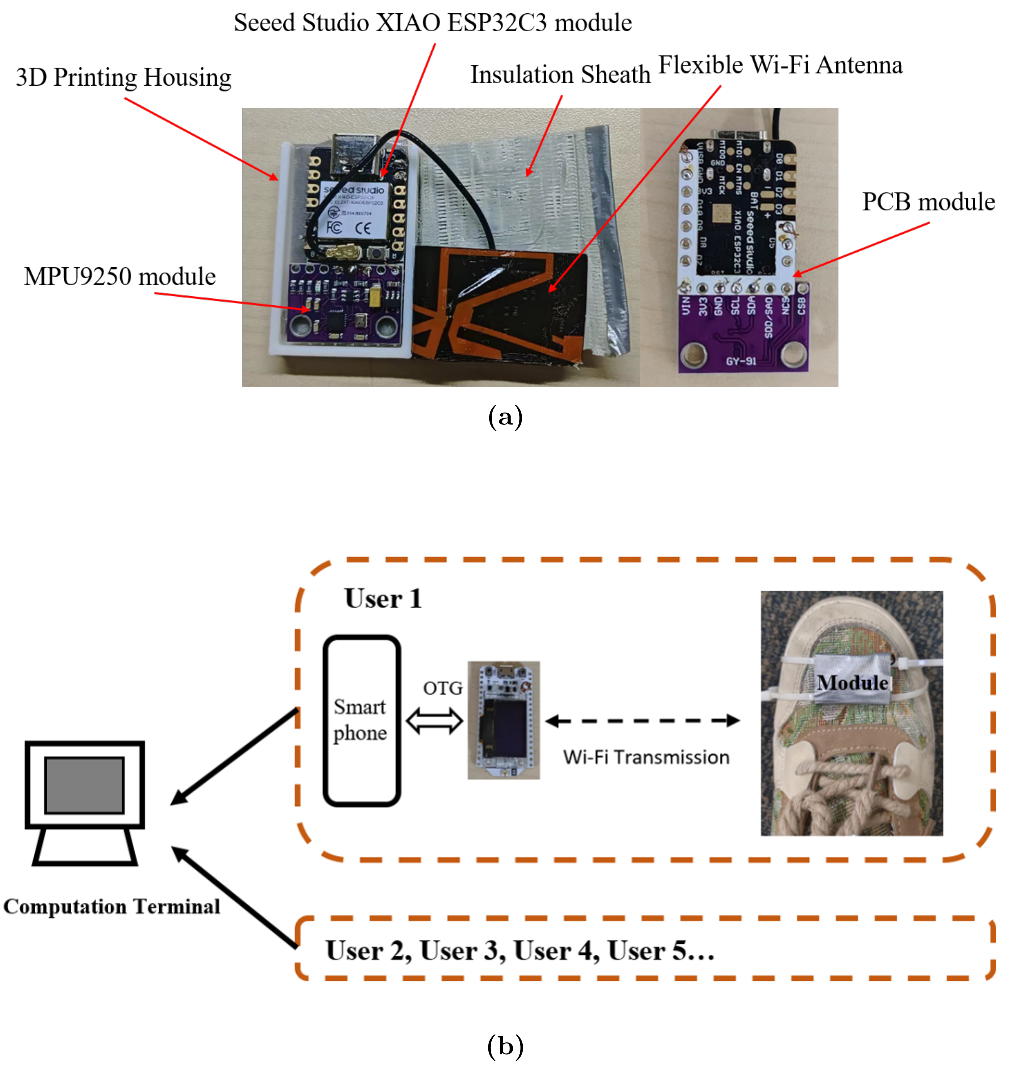

Figure 3.26: *The hardware components: (a) PCB housing module and (b) wireless transmission module of the proposed system.*

This wearable module, illustrated in Fig. 3.26a, was constructed using a custom-designed Printed Circuit Board (PCB) enclosed within a 3D printed housing to ensure stable placement. To enhance signal transmission quality, a flexible antenna was affixed to the exterior of the housing. The entire module was encased in a grey insulation sheath to safeguard its electronic components. The wearable module was securely fastened to the front of each subject's shoe using zip ties. A 1300 mAh battery with an estimated 5-h power supply capability was integrated into the module. The sensor data was transmitted via Wi-Fi to a handheld cellphone (OnePlus 5T), which was connected to an ESP32 Wi-Fi module using the OTG protocol (as shown in Fig. 3.26b). Furthermore, data were subsequently stored and computed on a laptop with an Intel i7-10510U 1.8 GHz processor and 16 GB of RAM. The update rate of Multi-INS was 200Hz, following the sampling rate of IMU.

Table 3.6: Basic Profiles of Participants

Group	Participant ID	Gender	Height [cm]	Weight [kg]
1	1	Female	163	50
	2	Male	185	85
	3	Male	170	65
	4	Female	164	45
2	5	Female	163	50
	6	Male	173	72
	7	Male	180	76
	8	Female	168	52

The experiments involved eight participants, with their basic profiles outlined in Table 3.6. The study received approval from the university's faculty research ethics committee which complies with the ethical guidelines. Prior to starting the experiments, participants were provided with information sheets and consent forms, which they signed to indicate their agreement to proceed. They were also informed of their right to withdraw from the experiments at any time.

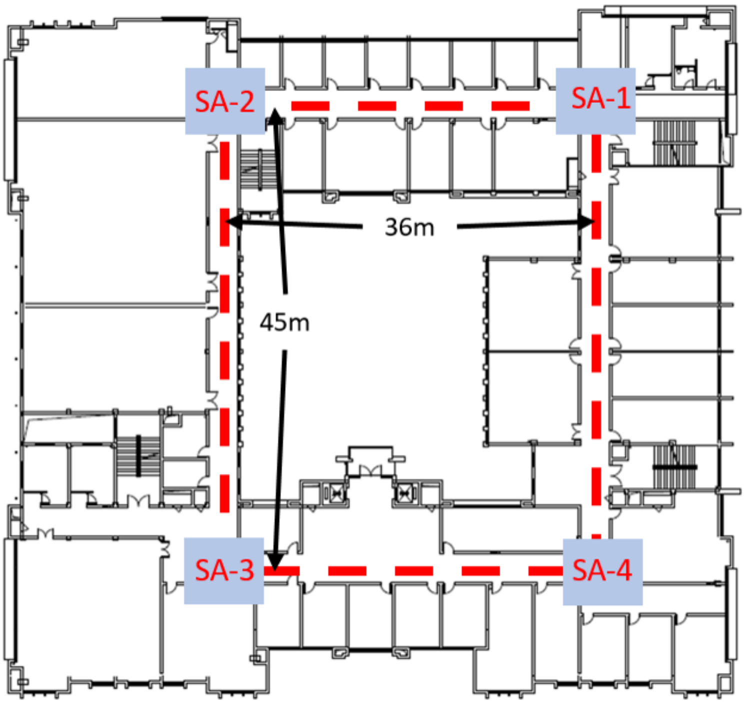

(a)

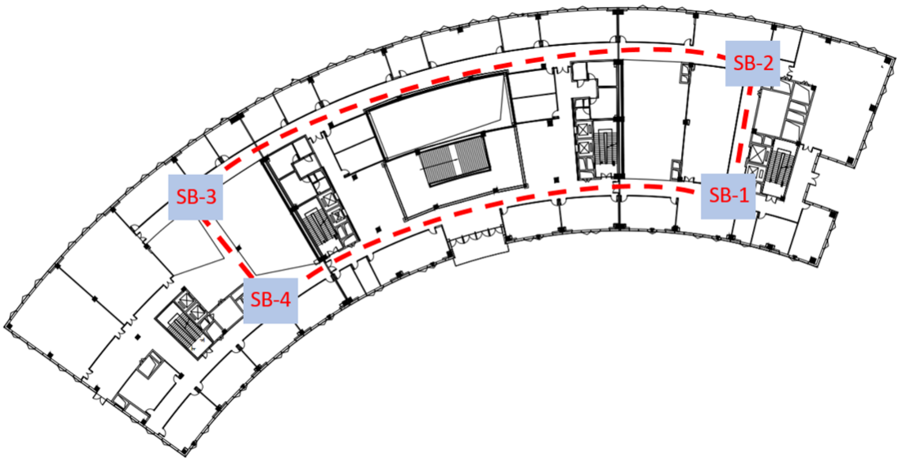

(b)

Figure 3.27: *Visualisation of the experiment settings in two distinct walking scenarios: (a) SA constituted a rectangular walking route with total walking distance of approximately 162 meters while (b) SB featured an annular sector walking route with total walking distance of approximately 199 meters.*

The experiment involved participants wearing shoes equipped with an IoT-based wearable module and walking predefined routes within two different office buildings. These buildings presented two distinct walking scenarios: scenario A (SA) constituted a rectangular route with a total walking distance of approximately 162 meters (depicted in Fig. 3.27a) while scenario

B (SB) featured an annular sector route with a total walking distance of approximately 199 meters (shown in Fig. 3.27b). Participants were divided into two groups, with the second group (G2) conducting their experiments ten days after the first group (G1) to avoid potential environmental fluctuations, such as variations in geomagnetic data.

Throughout the experiments, all participants were allowed to walk at their own pace for two consecutive rounds, without any restrictions on their walking speed. However, they were requested to pass through four designated corner points (landmarks) labelled as “S-1”, “S-2”, “S-3”, and “S-4” (refer to Fig. 3.27). Completion of a single round was defined as passing through all the landmarks in sequential order, starting from their designated positions and returning to those starting positions (e.g., starting from “S-3”, passing through “S-4”, then “S-1”, then “S-2”, and returning to “S-3”). These landmarks served as reference positions (ground truth positions) where their coordinates were determined by measuring the distances between each consecutive landmark using a laser range finder. Table 3.7 presents the starting positions of each participant at one of these designated landmarks for both SA and SB.

Table 3.7: Starting Positions for Participants in SA and SB

G1	G2	Starting Position (SA)	Starting Position (SB)
1	5	SA-2	SB-2
2	6	SA-3	SB-3
3	7	SA-4	SB-4
4	8	SA-1	SB-1

The quantitative assessment of positioning accuracy involved the calculation of the root mean square error (RMSE, ϵ) at four designated landmarks

[185] where ϵ was defined as:

$$\epsilon = \sqrt{(l^s_{est_x} - l^s_{ref_x})^2 + (l^s_{est_y} - l^s_{ref_y})^2} \tag{3.57}$$

where $l^s_{est_x}$ and $l^s_{est_y}$ represent the estimated position of the x- and y-coordinates at landmark $s = 1, ...4$, while $l^s_{ref_x}$ and $l^s_{ref_y}$ denote the corresponding reference position of the x- and y-coordinates. The performance of the estimated positions using the proposed method was compared with that of the existing ZUPT-aided INS method [186], which is referred to as ZA-INS throughout this study.

3.5 Summary

This Chapter introduces the methods and experimental setups for each study presented in this thesis. Specifically, **Study 1**, **Study 2** and **Study 3** aim to answer **RQ1**. These studies are developed to provide GA based approaches to improve the accuracy of positioning by advancing three essential bodies of the DR, which are heading estimation, step detection and positioning optimisation. To answer **RQ2**, **Study 4** considers designing a polar projection based map point coordinate calculation algorithm, for surrounding reconstruction. Consequently, based on the outcomes the first four studies achieved, **Study 5**, aiming to answer **RQ3**, researches on multi-trajectories integration via online magnetic fingerprint matching. In addition, this chapter introduces the specific experimental setup for each study including hardware design, scenarios and experiment activities.

Chapter 4

Results and Discussion

This chapter demonstrates the trajectory and map calculated from each proposed study. Evaluation metrics are used to assess the performance and effectiveness of the positioning system. The mapping results are also visualised for subjective evaluation. An associated discussion for each study is presented at the end of each section.

4.1 GA-PDR

4.1.1 Evaluation of Localisation Performances

The positioning performance for the proposed GA-PDR approach was evaluated against existing PDR methods using raw inner filtered heading data obtained from the BNO055 IMU [145]. This study evaluated GA-PDR and PDR under the three scenarios presented in Section 3.1.4. The trajectory prediction performance was calculated using the RMSE [65], as shown in (4.1).

$$RMSE = \sqrt{(x_{start} - x_{end})^2 + (y_{start} - y_{end})^2} \tag{4.1}$$

where (x_{start}, y_{start}) and (x_{end}, y_{end}) indicate the starting and ending coordinates for the calculated trajectory of the positioning, respectively, of the path in each scenario. The coordinate of the starting point was usually set as $(0, 0)$ which simplified the RMSE calculation to $RMSE = \sqrt{(x_{end})^2 + (y_{end})^2}$ The RMSE results are shown in Table 4.1.

Table 4.1: The RMSE [m] Comparison Between GA-PDR and PDR [145].

	GA-PDR (Ours)	PDR
Scenario 1	**0.94**	7.54
Scenario 2	**2.65**	7.07
Scenario 3	**1.59**	3.67
Mean	**1.73**	6.09

As shown in Table 4.1, GA-PDR outperformed PDR in all of the experimental scenarios. The mean error of GA-PDR was reduced compared with that of PDR. The detailed heading and trajectory comparisons are discussed below. The GA improved the trajectory accuracy and heading stability in the three scenarios. The heading direction and trajectory computed by GA-PDR and PDR were plotted together for performance comparisons, as shown in Fig. 4.1, Fig. 4.2 and Fig. 4.3. The dots in the trajectory path represent the step points detected by each method.

Significant improvement could be observed for Scenario 1, where the GA-PDR (RMSE = 0.94 m) trajectory outperformed that of PDR (RMSE = 7.54 m). The trajectory calculated by GA-PDR was closer to the ground truth path in Fig. 3.8a compared with that calculated by PDR. Each direction of the trajectory matched with the ground truth consistently which eliminates the cumulative error from heading perspectives. Some paths were slightly outside the boundary, this was caused by an inaccurate length estimation but this aspect was beyond the scope of the present study. In contrast, the PDR trajectory showed a drifting error following the first forward movement where the heading and positioning results diverge from the intended route. The PDR error accumulated over time and most of the paths were outside of the boundary, which caused significant difficulty in terms of aligning them to the ground truth. In this experiment, GA-PDR demonstrates high consistency of heading estimation during the whole walking period which consequently achieves higher accuracy in positioning.

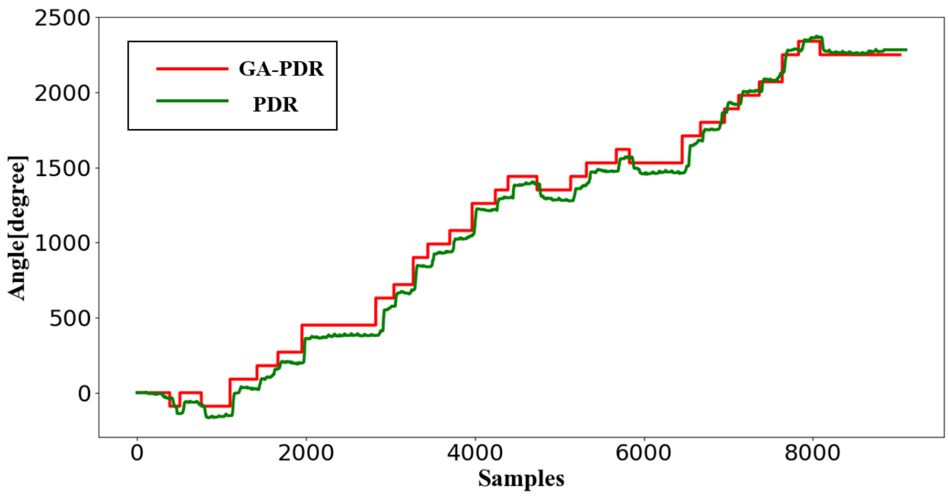

(a)

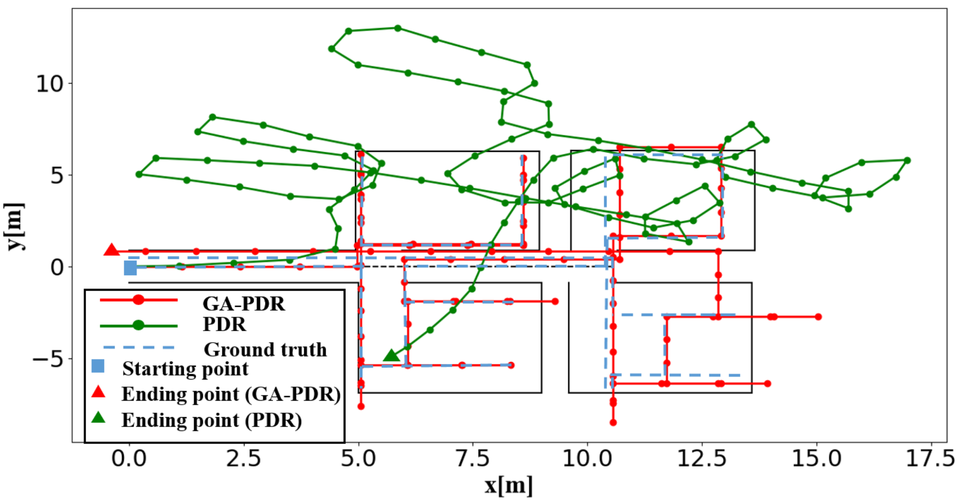

(b)

Figure 4.1: *Plotting the trajectory of Scenario 1 with their heading directions (a) and the trajectories (b) generated by GA-PDR (red line) and PDR (green line).*

Scenarios 2 and 3 were evaluated in a smoke-filled environment, in which the firefighters were more cautious about their movements due to low visibility. In Scenario 2, a 10 m forward movement was set at the start of the path. Compared with the ground truth shown in Fig. 3.8b, the PDR trajectory deviated from the dominant forward direction after moving three steps. The GA-PDR trajectory remained in the dominant direction until the subsequent turn. The heading direction in Fig. 4.2a shows that GA-PDR could smooth small fluctuations arising from sensor noise and reduce drifting by correcting the heading estimation to better fit the dominant direction. In Scenario 3, the degree of the first turn for PDR was smaller than 90 degrees, which caused deviation from the rest of the path (see Fig. 4.3b). Here GA-PDR (RMSE = 1.59 m) outperformed PDR (RMSE = 3.67 m), as its trajectory matched the ground truth path more closely compared with that of PDR in Fig. 3.8c. The final GA-PDR path crossed the boundary, indicating its relatively high deviation. A possible explanation for this issue may be caused by inaccurate step detection, which was beyond the scope of this study.

In summary, GA-PDR (mean RMSE = 1.73 m) outperformed PDR (mean RMSE = 6.09 m) in three test scenarios. It overcame the adverse effects of users with different gaits. Low visibility arising from the presence of smoke had a limited impact on it. The evaluation results indicated the effectiveness of using GA-PDR in a smoke-filled environment and the method was able to extend the use of the PDR technique to a firefighting context.
Table 4.2 shows the computation times for the GA-PDR and PDR methods that were tested in this evaluation. Each evaluation was performed three times in the same environment. The computational efficiency was comparable to PDR. GA-PDR introduced minimal overhead compared with PDR, resulting in an approximately 0.01 s difference among the three scenarios.

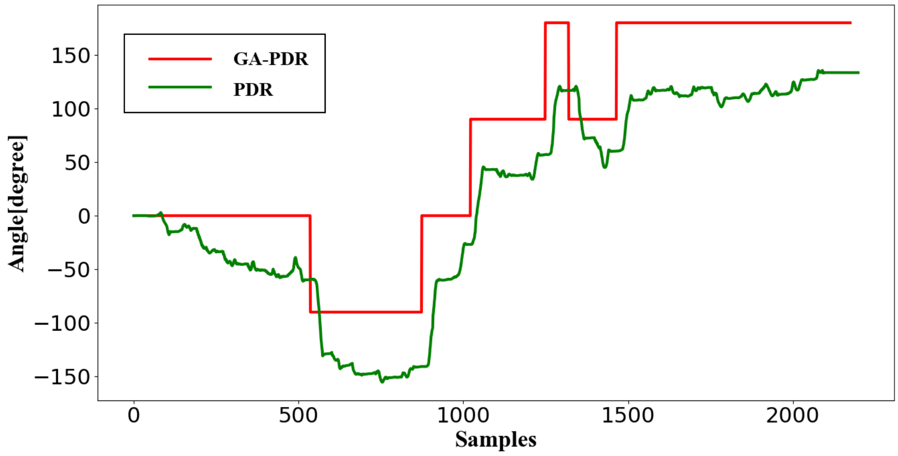

(a)

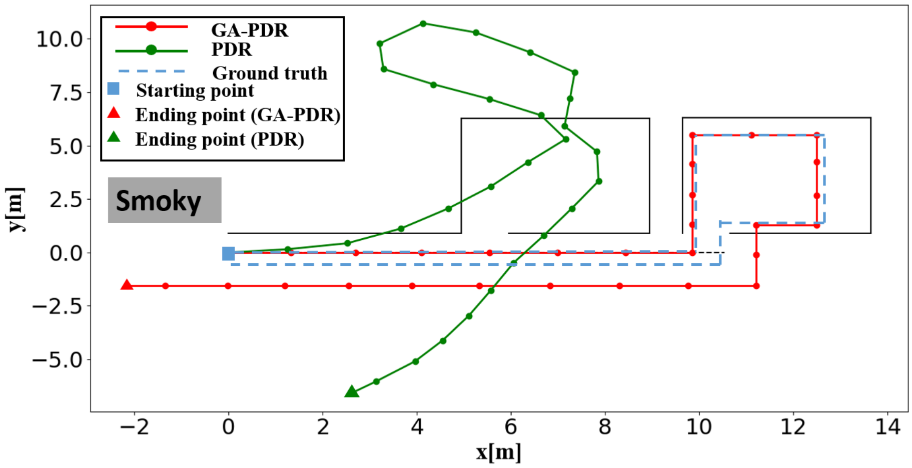

(b)

Figure 4.2: *Plotting the trajectory of Scenario 2 with its heading directions (a) and (b) the trajectory generated by GA-PDR (red line) and PDR (green line).*

4.1.2 Discussion

This study presents GA-PDR for improving the heading estimation of classical PDR. Due to the determination of DR theory, the cumulative error greatly affects the performance of PDR as shown in the experimental results. GA-PDR corrects the heading value by analysing the user's gait. In doing so, the heading estimation bias was greatly eliminated which performed improved the performance of positioning.

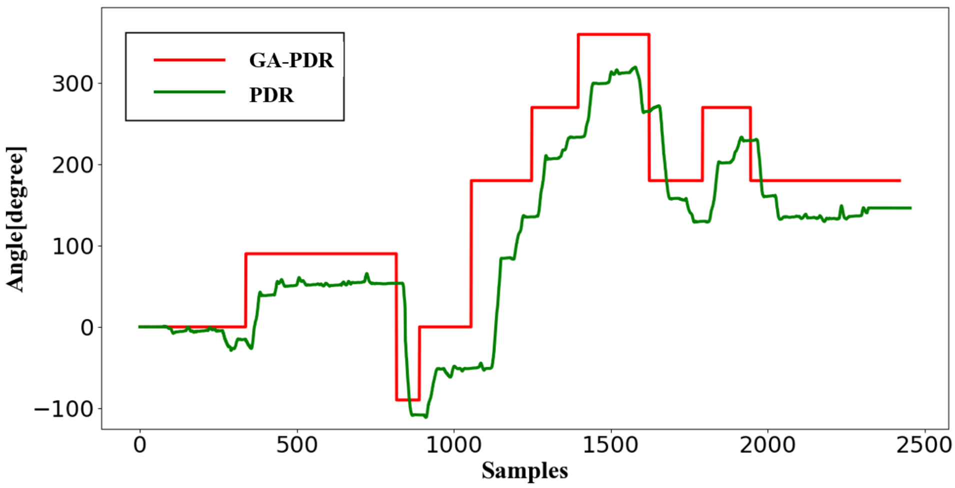

(a)

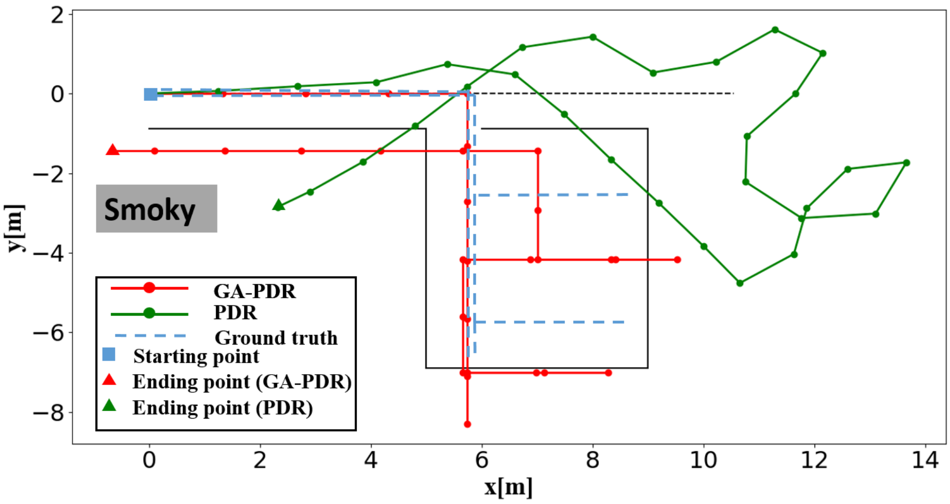

(b)

Figure 4.3: *Plotting the trajectory Scenario 3 with its heading directions (a) and (b) the trajectory generated by GA-PDR (red line) and PDR (green line).*

Three limitations are identified in the current study's implementation of GA-PDR. First, step detection and length estimation were beyond the scope of this study; accordingly, some generated trajectory paths in Scenario 1 (see Fig. 4.1b) and Scenario 3 (see Fig. 4.3b) were outside of the boundary. Second, there was no accurate ground truth measurement for pedestrians in a smoke-filled environment, which was inconvenient for the evaluation. Finally, the current GA-PDR hardware was an experimental prototype. In future studies, the placement, component integration and

Table 4.2: A Comparison of the Computation Time [s] in Each Test Between the Proposed GA-PDR and PDR[145] Methods.

Scenario	GA-PDR (ours)	PDR
Scenario 1	0.29	0.27
Scenario 2	0.09	0.07
Scenario 3	0.07	0.06

insulation should be specifically considered for real firefighting scenarios.

4.2 Dual Foot Synergistic Method

4.2.1 Evaluation of Zero-Velocity Detection Performances

Zero-velocity detection performance was evaluated based on the step number value. Four volunteers took part in the experiment and the researcher analysed recorded videos to determine the step number of both the left foot (SC_L) and the right foot (SC_R) for each participant. Where the minimum absolute differences between the references and the experimental results illustrate the best performance.

The zero-velocity detection outcomes indicate that the proposed method outperforms both ARE's and GLRT's methods in terms of detection rate. The detection achieves nearly 100% accuracy for the majority of participants involved as stated in Table 4.3. However, a few instances of detection errors were attributed to the measurement noise from the IMU. Additionally, the proposed method exhibits the highest consistency in detecting zero-velocity within a two-foot range compared to existing methods, further emphasising its suitability for zero-velocity detection tasks.

Table 4.3: Results of Zero-Velocity Performances

ID	SC_L / SC_R	ARE	GLRT	Ours
A	103 / 102	161 / 140	137/209	**104 / 103**
B	124 / 124	127 / 189	127/204	**124 / 124**
C	122 / 122	133 / 136	126/131	**125 / 125**
D	115 / 115	177 / 184	173/143	**116 / 116**

4.2.2 Evaluation of Localisation Performances

The study employed the RMSE as a metric to assess the performance of DF-INS [187] localisation, incorporating a fixed threshold and a dual foot synergistic approach-based zero-velocity detection. The results presented in Table 4.4 indicate that, compared to GLRT and ARE, the proposed method achieved the lowest RMSE across the trajectories of four volunteers. Figure 4.4 visually demonstrates that the trajectory generated by the method exhibits superior smoothness and accuracy compared to alternative approaches. Moreover, the approach excels at identifying more precise zero-velocity phases, thereby enhancing the performance of ZUPT and trajectory calculation in DF-INS.

Table 4.4: Comparison of RMSE (Left/Right) [m] of DF-INS using Different Zero-Velocity Methods

ID	ARE	GLRT	Ours
A	11.209 / 10.763	4.973 / 5.048	**3.689 / 3.423**
B	12.965 / 12.999	21.945 / 21.894	**2.961 / 1.948**
C	10.989 / 10.239	14.529 / 13.99	**4.996 / 4.935**
D	9.054 / 8.561	7.977 / 7.343	**4.657 / 4.071**

4.3 IOAM

4.3.1 Demonstration of Trajectory Fusion

The results of DTF are shown in Fig. 4.5. Two single-foot trajectories (blue and green lines) demonstrate serrated lines with estimated stride lengths larger than 1.5 m in the turning phase, showing a significant bias

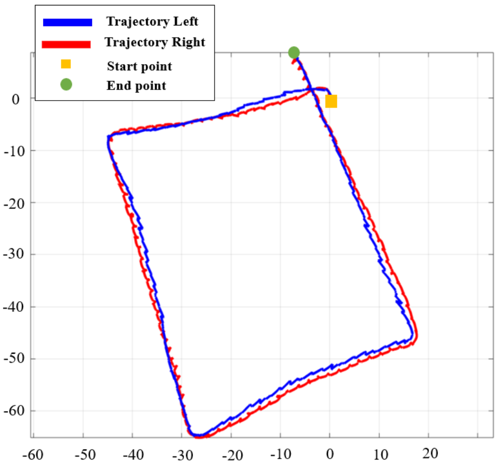

(a)

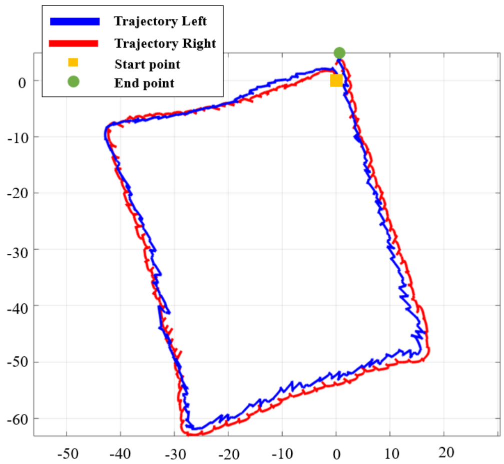

(b)

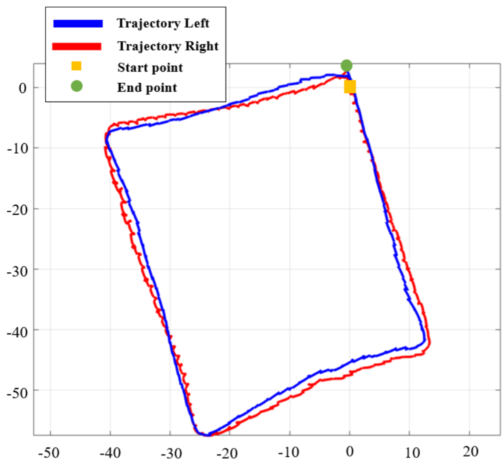

(c)

Figure 4.4: *Trajectory generated by DF-INS using data from participant A, using (a) ARE, (b) GLRT and (c) the proposed method, measured in meters.*

error. In this case, the individual's position is located at a 1.5-m possibility area, increasing the difficulty of the IPS visualisation. However, the fused trajectory (red line) illustrates one path of the CBoM, which is easy to track and evaluate. Section B's INS tracking performance evaluation was used to analyse the accuracy of the fused trajectory.

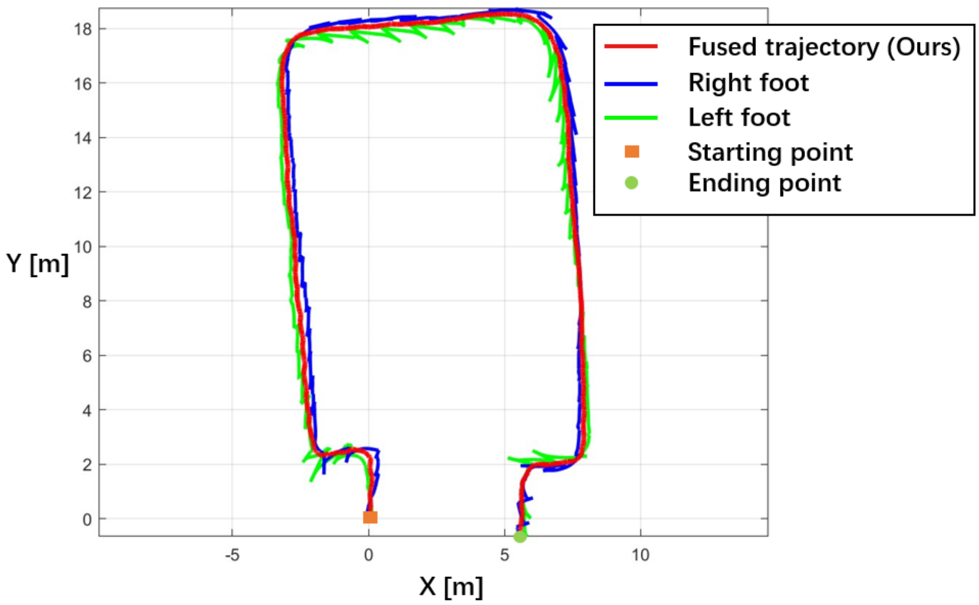

Figure 4.5: *2D plotting of the single foot and dual fused trajectory of Scenario 3 participant b.*

4.3.2 Evaluation of Tracking Performance

The RMSE [188] was used to evaluate the localisation accuracy of the fused trajectory (4.1). Scenario 1 and 2 are closed routes that were used to evaluate the RMSE of the x- and y-axes between the estimated starting and ending points. Scenario 3 contains an open route, which was evaluated by the RMSE of the x-axis (evaluating the ground truth horizontal distance) and the y-axis separately. The bold values indicate results with a relatively lower error. The error rate calculates the ratio of the RMSE error to the route length [189].

Scenario 1

Table 4.5: Comparison of RMSE [m] of INS Trajectory with and without MCD Constraint for Scenario 1

Subject	RMSE of INS w/ MCD (ours)	Error rate (%) w/ MCD (ours)	RMSE of INS w/o MCD	Error rate (%) w/o MCD
a	**0.538**	0.334	2.196	1.362
b	**0.353**	0.219	1.114	0.691
c	**2.725**	1.690	6.235	3.867
d	**0.892**	0.553	8.496	5.270
e	**2.760**	1.712	3.623	2.2470
f	**0.288**	0.179	1.256	0.779
g	**0.560**	0.348	1.019	0.632
h	**0.329**	0.204	0.566	0.351
Ave./std.	**1.06/1.06**	0.65/0.67	3.06/2.88	1.90/1.79

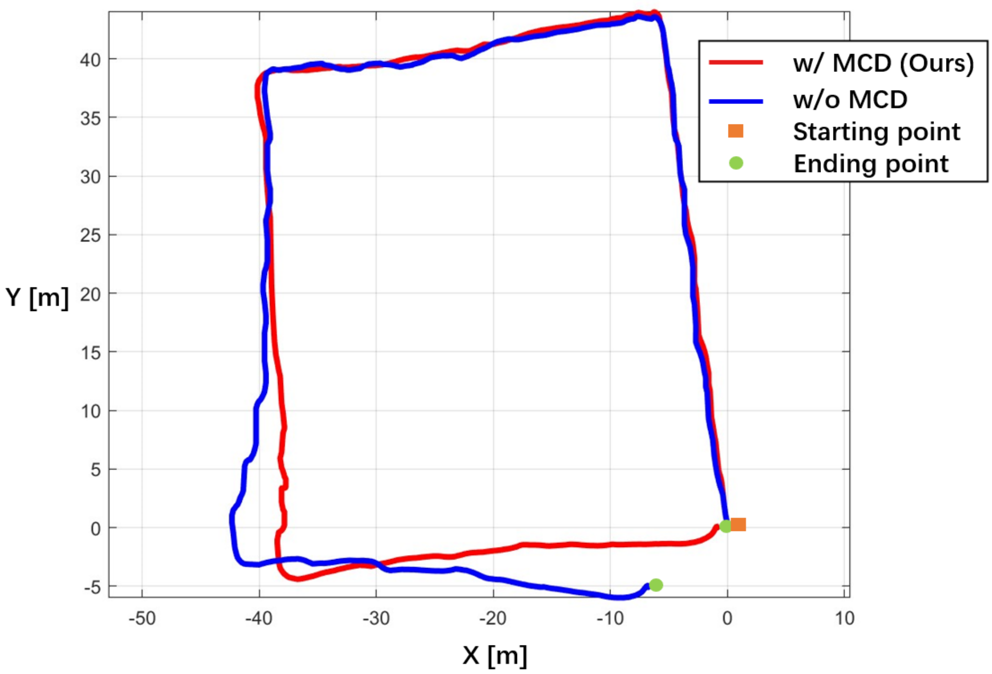

Figure 4.6: *2D plotting of the fused trajectory with MCD (red line) and without MCD (blue line) of Scenario1 participant d.*

Table 4.5 illustrates the RMSE and error rate of the Scenario 1 experiment. The proposed method had a lower average RMSE (1.06 m) than the method without MCD (3.06 m) for all participants. All participants with MCD had an error rate of less than 2 %, which is acceptable for localisation. Participant d (see Fig.4.6) showed the most significant error rate improvement. The starting and ending points of the trajectory this study proposed coincide more closely than those of the method without MCD. For the result without MCD (blue line), the drifting bias significantly increases from the coordinate position (-40,20), which causes a significant bias error at the ending point. The proposed MCD method further constrained the drift of foot position estimation. Thus, the RMSE of the fused trajectory is reduced. The same improvement was also observed in participant a (0.334/1.362) and participant c (1.69/3.867), which proves the versatility of the MCD.

Scenario 2

Table 4.6: Comparison of RMSE [m] of INS Trajectory with and without MCD Constraint for Scenario 2

Subject	RMSE of INS w/ MCD (ours)	Error rate (%) w/ MCD (ours)	RMSE of INS w/o MCD	Error rate (%) w/o MCD
a	**6.3940**	3.220	6.879	3.465
b	**0.3872**	0.195	2.224	1.120
c	**0.580**	0.292	1.115	0.562
d	**1.886**	0.950	4.994	2.515
e	**3.931**	1.980	12.830	6.462
f	**0.726**	0.366	4.578	2.306
g	**1.525**	0.768	2.672	1.346
h	**1.212**	0.611	3.417	1.721
Ave./std.	**2.08/1.94**	1.05/1.04	4.84/3.69	2.44/1.86

Scenario 2 comprises two long curved routes, as shown in Fig. 3.20b, which challenges the position estimation of the INS. The proposed method (shown in Table 4.6) has a lower error rate (Ave.= 1.05 m) and the RMSEs are less than 1 m in participants b, c and f, indicating that the method significantly outperforms the method without MCD. The standard variance of the method was also less than that of the others, indicating that the MCD method was efficient in reducing the bias error of different participant estimations. The trajectory of participant c (see Fig. 4.7) demonstrates that the proposed MCD method reduces the noise of pose estimation and increases the stability during the curing path walking phase, thereby achieving a lower error rate.

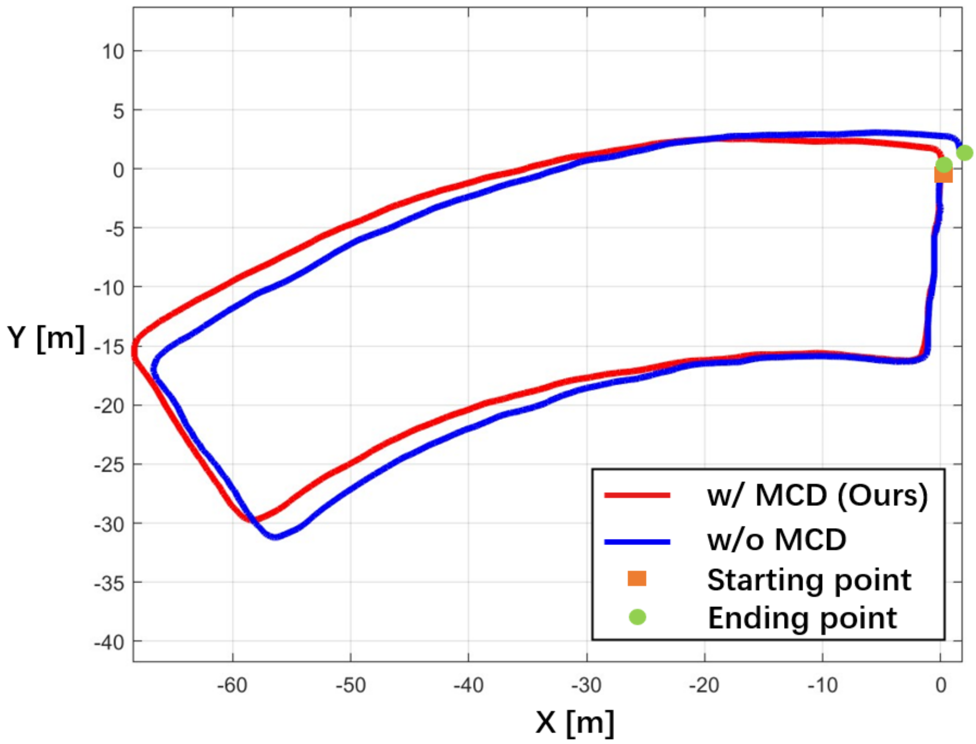

Figure 4.7: *2D plotting of the fused trajectory with MCD (red line) and without MCD (blue line) of Scenario2 participant c.*

Scenario 3

The separated x-axis and y-axis biases measure the distance between the estimated results and the ground truth. The evaluation of the open path needs to consider the horizontal and vertical bias errors. The results (shown in Table 4.7) indicate that the proposed method outperforms most of the samples, particularly for participants a, g and h. The average RMSE is less than without MCD both on the x-axis (ours = 0.45, w/o MCD = 0.85) and y-axis (ours = 0.40, w/o MCD = 0.53). For example, the estimated trajectory of participant a (see Fig. 4.8) was closer to the ground truth route.

Table 4.7: Comparison of RMSE [m] of INS Trajectory with and without MCD Constraint for Scenario 3

Subject	RMSE of INS w/ MCD x-axis (ours)	RMSE of INS w/o MCD x-axis	RMSE of INS w/ MCD (ours) y-axis	RMSE of INS w/o MCD y-axis
a	**0.268**	0.946	**0.249**	0.480
b	**0.056**	0.538	0.569	**0.467**
c	**0.109**	0.130	**0.108**	0.119
d	**0.601**	0.689	**0.164**	0.513
e	**0.914**	2.189	1.101	**0.846**
f	**0.838**	1.065	0.395	**0.284**
g	**0.707**	1.110	**0.110**	0.307
h	**0.086**	0.115	**0.544**	1.237
Ave./std.	**0.45/0.36**	0.85/0.67	**0.40/0.34**	0.53/0.36

In a few samples, such as participants b and e, the x- or y-axis error was higher than that of the participants without MCD. A possible explanation is the bias caused by the participants' subjective error between the preset ending (black dot) and the real foot landing place (green dots).

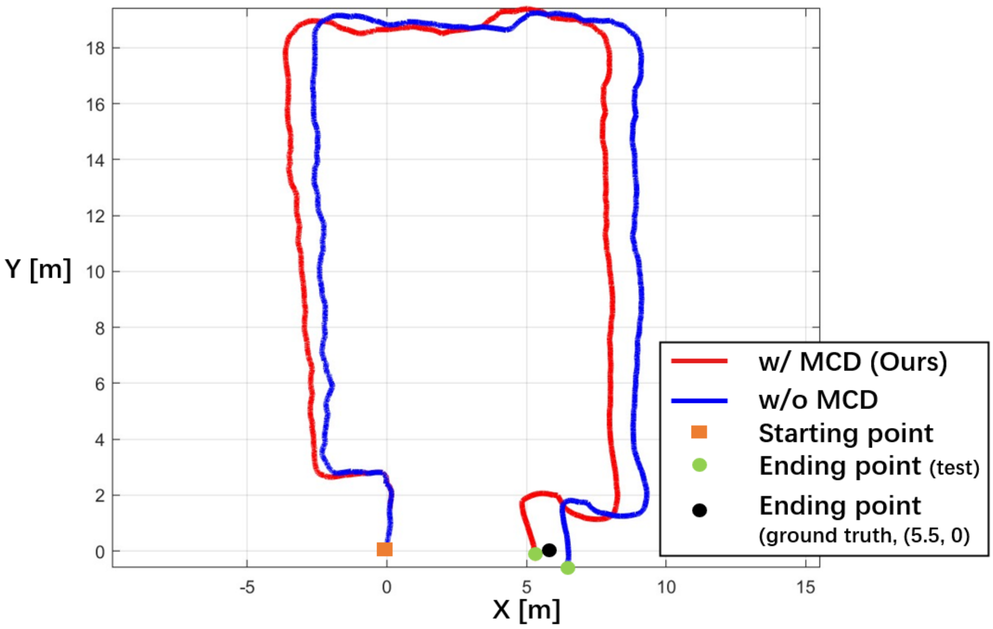

Figure 4.8: *2D plotting of the fused trajectory with MCD (red line) and without MCD (blue line) of Scenario3 participant a.*

In conclusion, the proposed DTF demonstrated a comprehensive individual trajectory which increases the efficiency of visualisation and evaluation. Under this advantage, the proposed method showed improved tracking performance with an error rate of approximately 1 % in localisation under different types of walking scenarios and good adaptability with approximately 0.7 % standard variance for different participants. The proposed MCD reduces the drifting rate of trajectory estimation and improves the localisation accuracy of the INS without the MCD method.

4.3.3 Mapping Estimation

Two mapping results are presented in this section. Fig. 4.9 shows a mapping for Scenario 1 collected from participant h. Most of the mapping area has good consistency with the ground truth; however, some areas at the corner or empty places show an abrupt cone mapping area because the ultrasonic sensors were out of range.
The mapping for Scenario 2 (see Fig. 4.10) was collected from participant f, which also showed a closed trajectory with a fully covered corridor area. These results showed clear and recognisable surrounding maps which provide significant references for localisation.

4.3.4 Discussion

To the author's knowledge, this is a novel IPS system to implement INS as the odometer, which enables non-vision based localisation. The use of inertia and ultrasonic ranging makes the system less affected by unpredictable environmental factors like weather and motion blur. The combination of INS and S-OGM further broadens the potential application areas for localisation under scenarios without prior map information, such as firefighting and elder caring. Additionally, the proposed DTF and MCD contribute

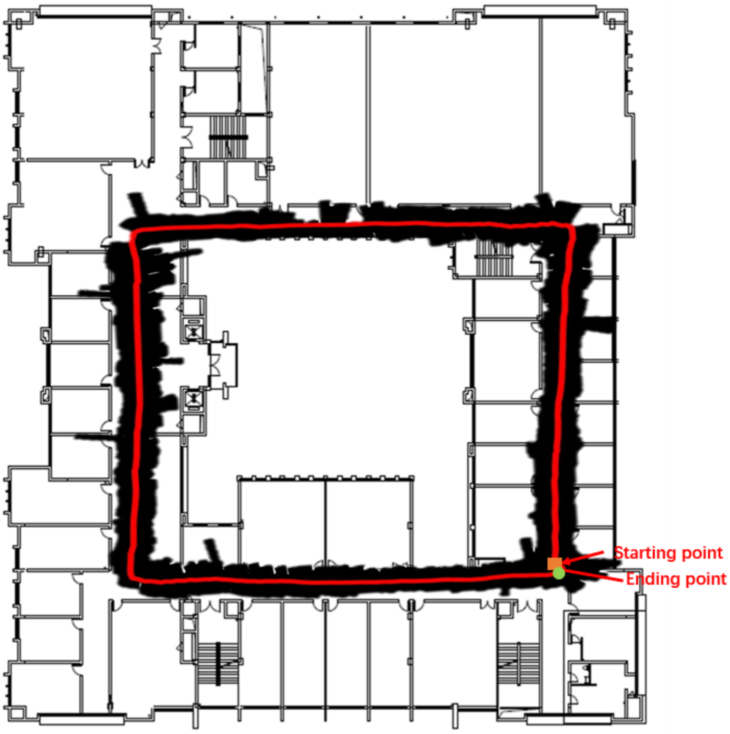

Figure 4.9: *Plotting the 2D mapping result of Scenario 1; the red line represents the individual's position and the black area represents the mapping results.*

valuable dual foot trajectory visualisation and error reduction ideas to the research community. Finally, the self-designed wearable costs significantly less than most of the existing approaches, which promotes the development of the corresponding industry.

The results are dependent on a number of factors, which makes it hard to compare them to existing works. Nevertheless, the experimental results are comparable to and in some cases superior to those reported in the literature by some state-of-the-art methods as shown in Table 4.8. The positioning error is lower in some studies with predefined landmarks [142] or with high-quality IMUs [190]. However, considering the application in commercial and industry cases, the hardware price IOAM system adopted was much lower than this study. The positioning error is also lower when external sensor assistance is used [191]. The proposed method outperforms

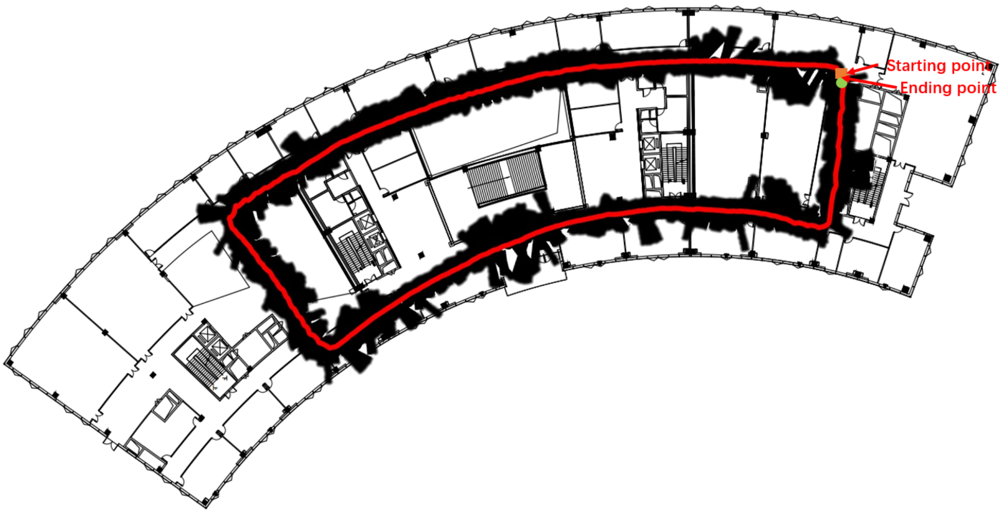

Figure 4.10: *Plotting of 2D mapping result of Scenario 2*

a study with similar quality IMU [99]. Also, the experiment had the most participants of any other study, which made the human factors, such as subjectivity, less of a factor.

Table 4.8: Comparison of Positioning Error with State-of-the-art Studies

Ref.	Sensor	Method	Scenario	Performance Metrics
[142]	IMU	INS with closing points and smoothing algorithm; trajectory matching algorithm	1500m repeated circular path	RMS = 0.5m
[191]	IMU, camera	Dynamic vision assisted zero velocity detector	160m indoor close-loop route	RMSE = 0.9m
[190]	IMU	Adaptive stance-phase detection	100m^2 in a close-loop area	RMSE = 0.85m
[192]	IMU, motion capture system	SVM, motion type classifier	1000m^2 hallway	MEPE = 2.68 m
[193]	IMU	DNN-based trajectory reconstruction	Office building on two separate floors (about 1650 and 2475m^2)	N/A
[99]	IMU	Spacial range constraint	indoor building	RMSE > 2m
[194]	IMU	Multi-sensor fusion for dual-gait analysis	100m straight route, 345m rectangle route	RMSE = 2.54m
[195]	IMU	Adaptive inequality constraints	87.2m straight route, 120m L-shaped route	PE = 2.5m
Ours	IMU	MCD	3 different indoor buildings	RMSE = 1.2m

However, limitations in the physical properties of low-cost ultrasonic sensors often led to inaccurate stride length measurements, which in turn affected the tracking performance. Several mappings were impacted due to noise in the data when the measurement was out of range, leading to incorrect boundary predictions. The accuracy of range measurements can also be affected by uneven ultrasonic reflective planes, which can affect mapping performance at the corners and empty areas. To overcome this limitation, a combination of ranging methods will be adopted in the future study.

4.4 Multi-INS

4.4.1 Scenario A

Test A - Individual Localisation

Each participant was requested to complete two consecutive rounds of walking along SA routes in separate experiments. Upon returning to the initial starting point, they were required to stand still for 5 seconds before resuming walking. This pause aimed to facilitate clearer segmentation of the route between rounds. Figure 4.11 displays the calibrated tri-axis magnetic field strength, $\hat{m}^4$, for participant 4 across two rounds of the SA walking route, showing high consistency of MFs data distribution over the same routes.

Table 4.9: Comparison of Individual Positioning Errors ($\bar{\epsilon}$ in Meter [m] Unit) for SA Walking Route

Participant ID	Total MF Data Points	$\bar{\epsilon}$ (ZA-INS)	$\bar{\epsilon}$ (Ours)
1	219	3.517	2.133
2	225	1.831	1.337
3	222	19.829	2.045
4	246	1.580	0.595
5	240	7.552	3.723
6	205	0.686	0.449
7	249	10.077	0.134
8	261	10.550	1.293

Table 4.9 summarises the total MF data points collected for each partici-

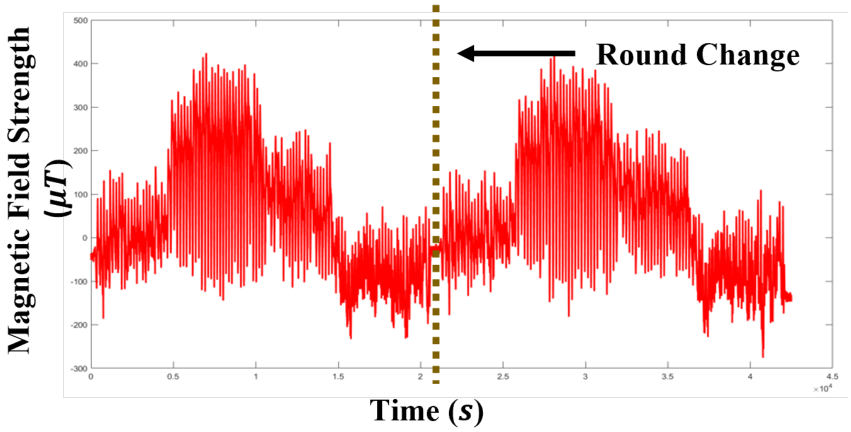

(a)

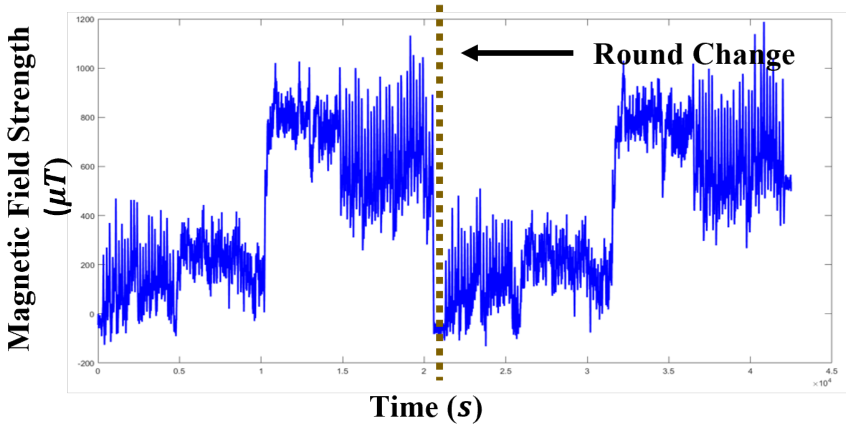

(b)

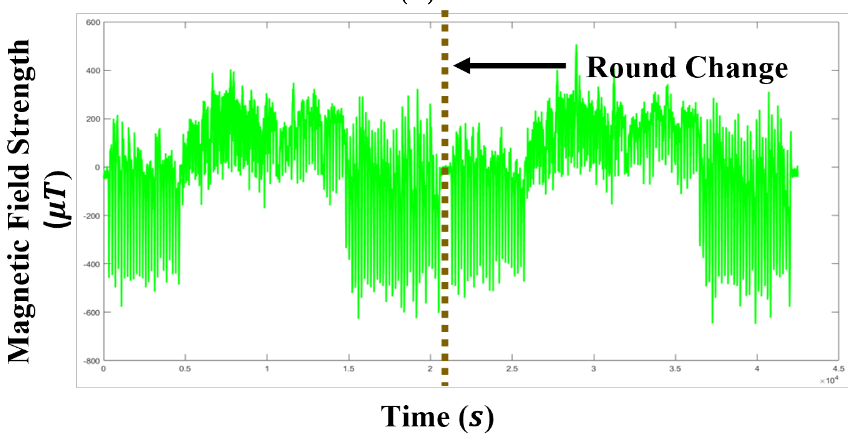

(c)

Figure 4.11: *Measurement of tri-axis magnetic field strength for participant 4 ($\hat{m}^4$) during both rounds of the SA walking route, depicted by (a) $\hat{m}^4_x$ (x-axis), (b) $\hat{m}^4_y$ (y-axis), and (c) $\hat{m}^4{}_z$ (z-axis) with the dashed line indicating the starting point for round 2.*

pant across both rounds of the SA walking route, along with the respective computed mean ϵ ($\bar{\epsilon}$) after applying the proposed MF matching method for updating individual position (refer to Section 3.4.6). The results demonstrate a significant decrease in cumulative positioning errors for all participants using the proposed MF matching method based on individual MF data, compared to the ZA-INS method. Figure 4.12 demonstrates the identification of the transition point between round 1 and round 2 at the walking step 125 for participant 4 where the computed DTW cost using the MF data points from step 125 and step 246 (the final step of round 2) exhibit the minimum DTW cost. This underscores the efficacy of the proposed method in accurately pinpointing the same positions between rounds based on the MF data points.

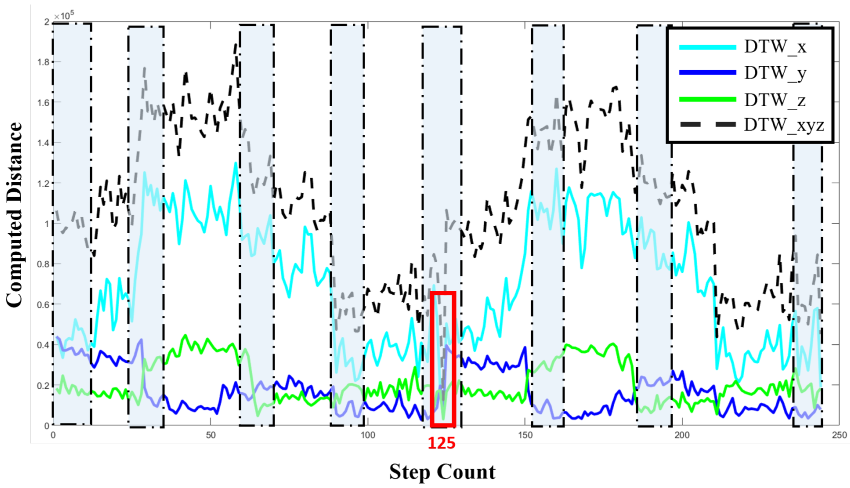

Figure 4.12: *Visualisation of participant 4's estimated DTW cost in SA, highlighting the identification of the transition point between rounds at step 125, showing the minimum DTW cost (DTW_xyz) computed using the MF data points from step 125 and step 246 (the final step of round 2).*

The positioning results for participant 4 are depicted in Fig. 4.13. Initially, significant misalignment was observed between reference points' positioning from round 1 to round 2 (see Fig. 4.13a). Nevertheless, the implementation of the proposed method led to a substantial reduction in positioning errors,

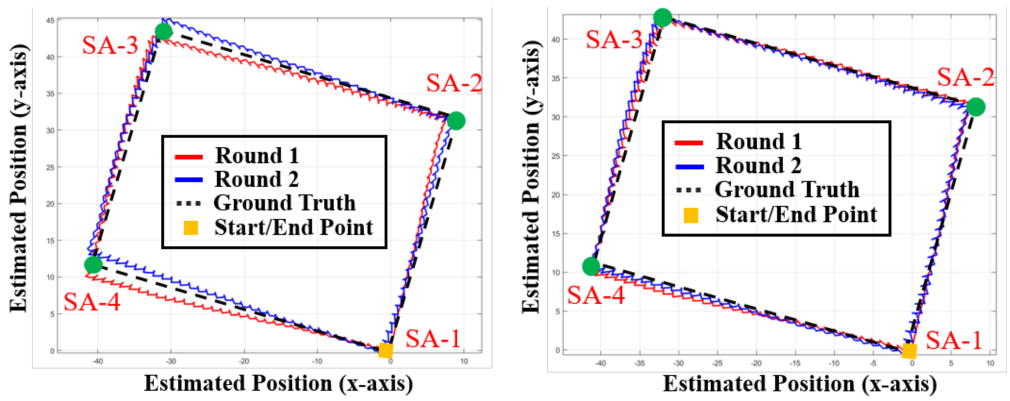

(a) (b)

Figure 4.13: *Plotting of (a) initial estimated SA walking route and (b) estimated SA walking route with the proposed positioning error reduction method for participant 4.*

including adjustment to the positioning heading (see Fig. 4.13b), resulting in decreased cumulative positioning errors across consecutive rounds.

Test B - Multi-Person Localisation

In contrast to Test A, this experiment involves all participants from each group completing a single round of walking along the SA route simultaneously, with each group conducting identical experiments on two separate days. Participant positions are updated using a cross-update approach that utilises each participant's MF data points. The update process involves determining the lowest DTW cost with the MF data points at each landmark from both self and other participants. For example, when participant 3 reaches the landmark SA-1 (the second landmark from the starting point), their DTW costs are initially computed with the MF points from participants 1, 2, and 4. Subsequently, participant 3's position at the specific landmark is updated using the landmark position from the respective participant with the minimum DTW cost.

Table 4.10 illustrates the positioning error comparison of each participant at every landmark. The results demonstrate an overall reduction in errors using the proposed method ($\bar{\epsilon} = 1.739$ m) compared to the ZA-INS method ($\bar{\epsilon} = 4.573$ m). Here, participants 1, 4, 5, 6, and 8 exhibit reduced positioning errors at all landmarks, with participant 8 showing the lowest mean error of $\bar{\epsilon} = 0.724$m which also presents the highest improvement rate among others.

Table 4.10: Comparison of Multi-Person Positioning Errors ($\bar{\epsilon}$ in Meter [m] Unit) for SA Walking Route at Each Landmark

Landmark	SA-1		SA-2		SA-3		SA-4		Mean	
Participant ID	ZA-INS	Ours	ZA-INS	Ours	ZA-INS	Ours	ZA-INS	Ours	ZA-INS	Ours
1	4.489	**3.610**	14.858	**1.380**	4.878	**0.030**	4.242	4.242	7.117	**2.315**
2	1.999	1.999	**3.218**	3.445	3.307	**2.233**	3.492	**1.523**	3.003	**2.301**
3	1.693	**1.593**	1.007	**0.014**	1.407	1.407	**1.675**	2.422	1.445	**1.359**
4	5.679	**1.575**	5.233	5.233	8.813	**7.031**	7.664	**4.943**	6.847	**4.696**
5	1.577	**1.216**	1.745	**0.076**	0.975	0.975	2.476	**1.413**	1.693	**0.920**
6	4.174	**0.315**	3.117	**0.291**	2.211	**1.388**	2.985	**1.152**	3.122	**0.787**
7	4.000	**0.324**	3.294	**0.167**	2.068	**1.473**	**1.148**	1.281	2.627	**0.811**
8	5.756	**1.310**	7.861	**0.109**	14.597	**0.352**	14.707	**1.126**	10.73	**0.724**
Mean	3.671	**1.493**	5.042	**1.339**	4.782	**1.861**	4.799	**2.263**	4.573	**1.739**

Even though there are overall improvements in the mean positioning errors of each participant, ZA-INS method shows relatively better performance for participants 2 and 4 in the landmark SA-2, and participants 3 and 7 in the landmark SA-4. These differences may be due to the noise generated during the online generation process of MF data (see Section 3.4.5), which utilises MF data points from different participants. It shows that there are possibility of increases the probability distribution error when utilising MF data points from different participants for computing the DTW costs. The overview of the estimated positions for each group of participants on the SA walking route using both the proposed method and the ZA-INS method is presented in Fig. 4.14.

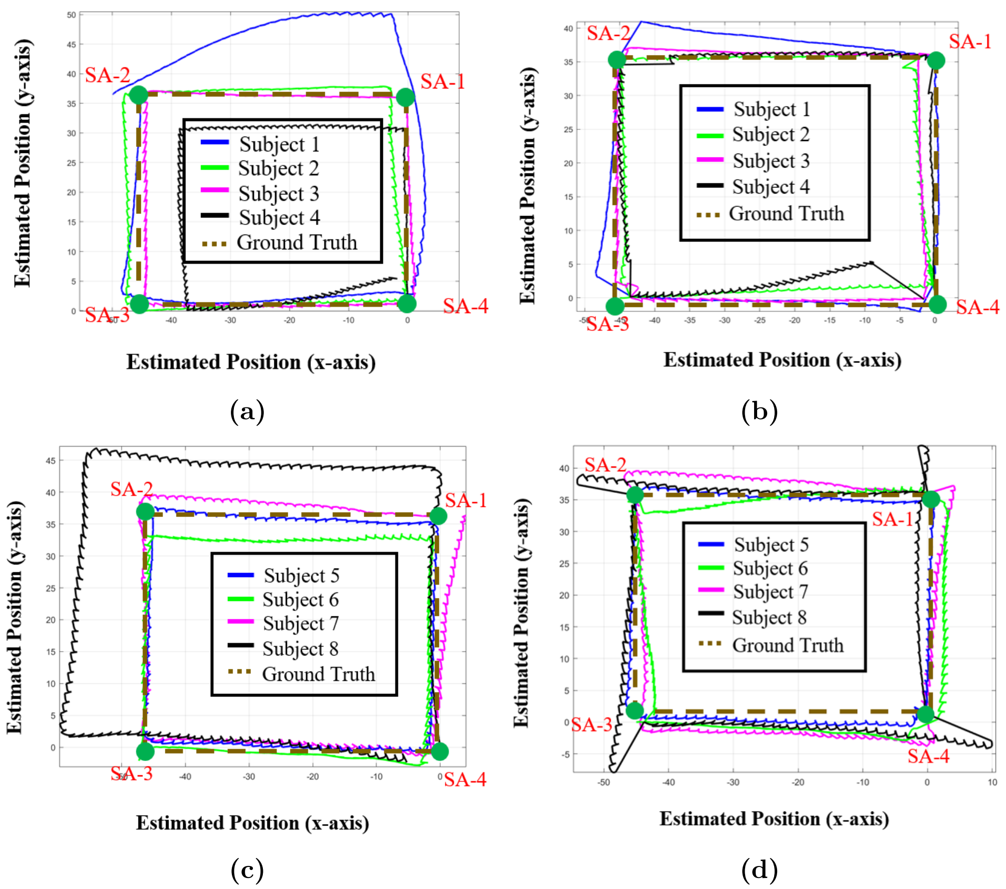

Figure 4.14: *Comparison of the estimated positions for the SA walking route for (a) G1 using the ZA-INS method, (b) G1 using the proposed method, (c) G2 using the ZA-INS method, and (d) G2 using the proposed method.*

4.4.2 Scenario B

Meanwhile, another set of experiments was conducted in a different building with an annular sector walking route (see Fig. 3.27b) aimed to further verify the effectiveness of the proposed multi-person positioning update method. Table 4.11 presents the positioning error comparison of each participant at every landmark for SB. The results indicate an overall reduction in errors using the proposed method ($\bar{\epsilon}$ = 1.263 m) compared to the ZA-INS method ($\bar{\epsilon}$ = 7.556 m). Participants 1, 2, 3, 5, 6, and 8 exhibited lower positioning errors at all landmarks, with participant 8 showing the most significant improvement from $\bar{\epsilon}$ = 21.548 m with the ZA-INS method to $\bar{\epsilon}$ = 1.324 m with the proposed method. Video observations revealed that participant 8 exhibited more tiny walking steps compared to other participants, as verified through the highest total MF data points generated (see Table 4.9). This further highlights the strength of the proposed method in coping with walking patterns characterised by tiny steps, where the ZA-INS method is not capable.

Table 4.11: Comparison of Multi-Person Positioning Errors ($\bar{\epsilon}$ in Meter [m] Unit) for SB Walking Route at Each Landmark

Landmark	SB-1		SB-2		SB-3		SB-4		Mean	
Participant ID	ZA-INS	Ours	ZA-INS	Ours	ZA-INS	Ours	ZA-INS	Ours	ZA-INS	Ours
1	4.908	**0.840**	3.876	**1.986**	3.704	**1.384**	2.976	**0.178**	3.866	**1.097**
2	3.394	**0.848**	11.104	**3.542**	5.558	**1.279**	0.146	**0.015**	5.050	**1.421**
3	12.391	**2.059**	4.809	**2.964**	10.889	**1.430**	6.086	**0.051**	8.544	**1.626**
4	0.949	**0.336**	**3.489**	3.790	16.170	**1.092**	14.560	**0.423**	8.792	**1.410**
5	3.851	**1.474**	4.620	**0.208**	3.343	**0.433**	3.786	**2.979**	3.900	**1.274**
6	5.963	**1.624**	3.817	**0.327**	2.575	**0.397**	4.566	**1.542**	4.230	**0.972**
7	6.607	**1.512**	7.500	**0.323**	2.615	**0.533**	**1.347**	1.541	4.517	**0.977**
8	50.498	**0.928**	2.176	2.176	8.939	**0.192**	24.581	**1.999**	21.548	**1.324**
Mean	11.070	**1.203**	5.174	**1.915**	6.724	**0.843**	7.256	**1.091**	7.556	**1.263**

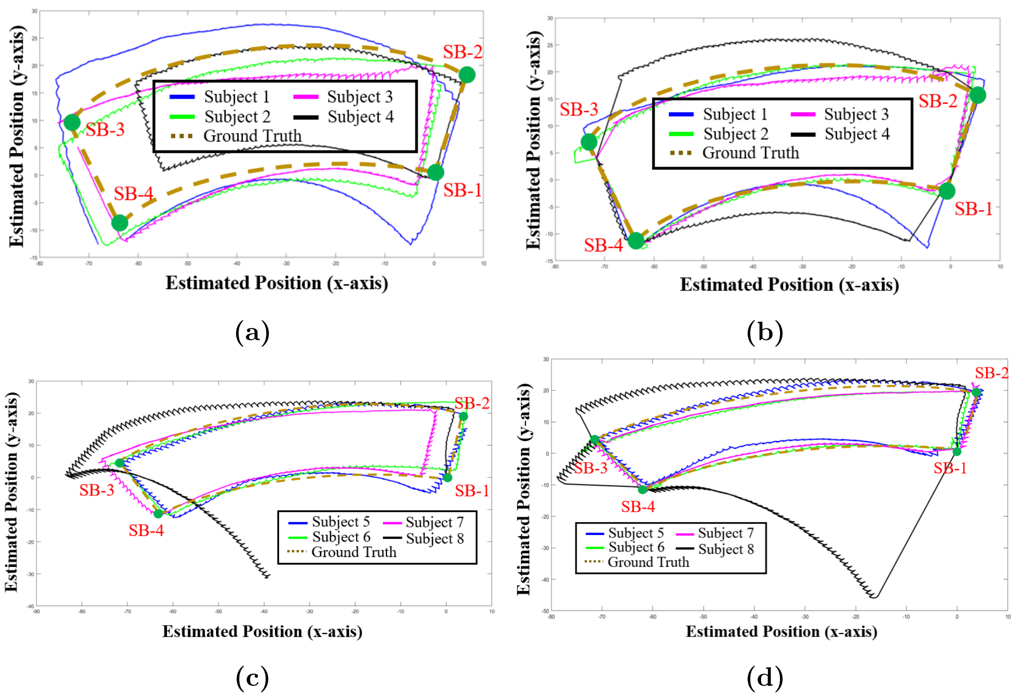

Figure 4.15: *Comparison of the estimated positions for the SB walking route for (a) G1 using the ZA-INS method, (b) G1 using the proposed method, (c) G2 using the ZA-INS method, and (d) G2 using the proposed method.*

Similarly, even though there have been overall improvements in the mean positioning errors of each participant, the ZA-INS method demonstrates relatively better performance for participant 4 at landmark SB-2 and participant 7 at landmark SB-4. Interestingly, participant 7 shows reduced positioning error at both landmarks SA-4 and SB-4 when using the ZA-INS method, where these landmarks represent the starting points of participant 7 in different buildings. A similar trend is observed for participant 3 at landmark SA-4, where the ZA-INS method outperforms, while the proposed method exhibits better performance at landmark SB-4. Fig. 4.15 illustrates the estimated positions for each group of participants on the SB walking route using both methods.

Lastly, Fig. 4.16 illustrates the computed DTW costs during the cross-update process for participant 3 upon reaching landmark SB-2. These costs are computed from the MF data points between participant 1 and 3. The minimum DTW cost is pinpointed at step 2, accurately recognising the current position as landmark SB-2 which the landmark SB-2 is the starting point for participant 1.

4.4.3 Discussion

The study introduces multi-INS, a novel infrastructure-free and self-contained multi-person inertial navigation system designed to address the research problems of accurate indoor positioning of multiple individuals. It presents innovative self-update and cross-update MF matching approaches which are useful for applications in scenarios where individual positions need updates without prior information. The MF matching methods involve selecting and processing target MFs which are important for identifying landmarks in indoor locations, suitable for time-critical tasks like localising firefight-

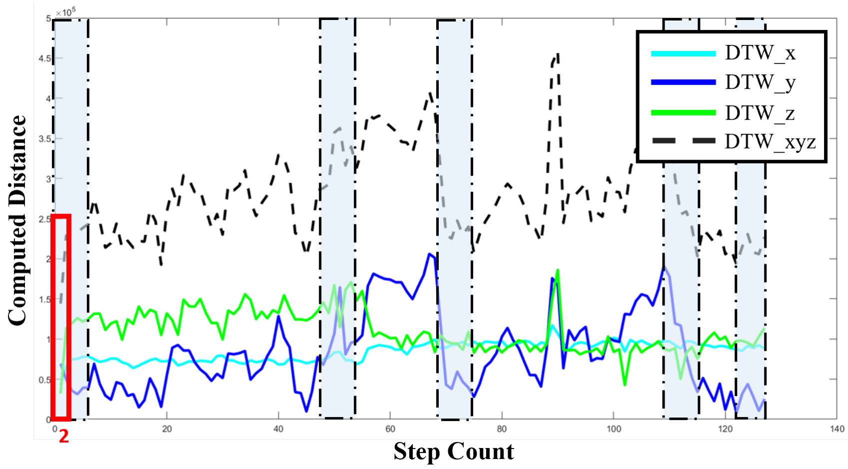

Figure 4.16: *Visualisation of the computed DTW costs during the cross-update process, utilising MF data points from participant 1 and 3 as participant 3 reaches landmark SB-2. The minimum DTW cost is located at step 2, correctly identifying the current position of participant 3 is landmark SB-2. Note that the landmark SB-2 is the starting position for participant 1.*

ers, elders, and lost children.

Table 4.12 compares the proposed method with existing studies, highlighting its merits in various aspects. Unlike existing works that often require predefined landmarks for positioning [120, 126], the proposed method generates MF data online, reducing dependency on the data pre-collection process. It also achieves lower positioning errors and reduced processing complexity compared to methods such as dual-foot-based INS [186]. The design of a "cloud"-based MF pool enables individuals to share MF data among multi-person, improving the effectiveness and reducing the processing complexities of the multi-person indoor positioning. Moreover, the method effectively addresses loop closure issues and demonstrates robustness to changes in the environment, validated through the results obtained in this study, outperformed the existing studies [135, 180]. This study also gathers a relatively large sample size, covering individuals with diverse walking patterns in two different scenarios and days, further validating its adaptability and robustness.

Table 4.12: Comparison with Existing Studies

Ref.	Sensors	Methodology	Experiment Scenarios	Performance
[186]	IMU	Centroid-based dual foot fusion	"U" shape corridor	RMSE > 3 m
[126]	IMU	Magnetic field data based trajectory calibration	1615.18 m (hybrid indoor & outdoor)	CEP (95%) = 2.5 m
[120]	IMU	Trajectory matching and manual loop-point closure	3200 m^2 space	RMS = 0.45 m
[135]	IMU	Offline magnetic field detection and online magnetic field data matching	Two different indoor spaces	RMSE > 3.5m
[180]	IMU	Magnetic offset enhancement based on the differences between magnetic field intensity	500 m^2 space	RMSE < 2 m
Ours	IMU	Online MF selection and positioning update with multi-person MFs data	2500 m^2 and 3000 m^2 spaces	RMSE < 1.5 m

Several limitations of this study are evident. Firstly, the performance evaluation of the proposed method relies on metrics from the state-of-the-art works [36, 120, 185, 196], which calculate the horizontal ϵ between estimated positions and predefined landmarks. These studies assume participants remain in the middle of the self-defined route throughout walking experiments, forming the basis for ground truth positions. Secondly, experiments are limited to narrow walking routes, as seen in some recent works [185, 197], leading to simpler ground truth data derivation compared to wider spaces. Generating ground truth data in wider indoor spaces necessitates complex and costly equipment for experiment setup [198, 199]. While some studies utilise the GNSS for high precision ground truth data, this method is only suitable for outdoor environments [200]. Moreover, studies indicate that ground truth positioning data derived from visual-inertial localisation systems also exhibit cumulative errors [201, 202]. These challenges emphasise the need for addressing ground truth data derivation in indoor positioning research.

4.5 Summary

This Chapter presents the experimental results of each study. The visualisation of trajectory and map and the quantity metrics for positioning error are presented specifically. The experimental results show improved performance of presented studies achieved. The discussions of each study are also described to enhance the significance and relevance of the results.

Chapter 5

Conclusion

This chapter provides a comprehensive summary of the research work presented in this thesis. The limitations and prospects for future research are discussed accordingly.

5.1 Summary of Work

Throughout the work presented in this thesis, this research aims to explore the advanced multi-person DR positioning method using sensor fusion to address the prevailing problems in this area. Specifically, five studies are conducted with the objectives of enhancing positioning accuracy, reconstructing maps and integrating multi-person trajectories in order to answer these questions.

Considering **RQ1**, three studies are formulated to answer this question from various research perspectives.

RQ1: What practical techniques can mitigate the cumulative errors in inertial based DR methods?

Study 1 identifies the characteristics of changes in heading direction during each walking pattern and devises a method to eliminate drifting using GD and RTE methods. In doing so, the heading bias error is decreased during each gait. Compared with the traditional method, the LCE value and heading error decrease which indicates enhanced performance for positioning.

Study 2 focuses on the dual foot zero-velocity detection by analysing the GLRT sequence. The utilisation of a fixed threshold in zero velocity detection often leads to imprecise determination of the motion phase, increasing positioning error. To address this problem, **Study 2** develops a dual foot synergistic method that identifies the phase in each instant by conjunction points of dual foot GLRT sequences. This algorithm calculates the motion phases by combining two IMU measurements which perform dynamic thresholds for zero-velocity detection in each gait cycle.

Study 3 focuses on stride length constraint in the polar model in the calculation of dual foot trajectory optimisation. The optimisation based on a fixed threshold disregards variations in stride length during the gait among different scenarios and users, resulting in inaccurate positioning outcomes. The dual foot trajectory is also combined and adjusted using the CBoM to improve the accuracy of the positioning. **Study 3** innovatively employs ultrasonic sensors to measure the smallest distance in each gait, which in turn calculates the corresponding minimum threshold for the centroid constraint in the EKF platform. The RMSE of the trajectory indicates that the dynamic thresholding proposed in this study enhances the accuracy of positioning compared to the conventional fixed threshold based methods. In summary, these three studies emphasise the importance of gait analysis in the field of DR methods, as it reduces the cumulative error by enhancing the precision of each positioning calculation using gait analysis based algorithms.

After achieving accurate positioning, surrounding map generation will emphasise the understanding and quality of trajectory visualisation.
RQ2: What techniques can be utilised to reconstruct the layout of the surroundings in the DR method?

Study 4 focuses on **RQ2** by exploring the surrounding reconstruction. This study is implemented upon the framework of **Study 3**. Considering the environmental factors and sensor physical characteristics, ultrasonic sensors are identified as the most suitable range finder sensors in burning buildings **Study 4**. The polar projection method utilises geometric calculations based on the individual's position, attitude and surrounding distance data obtained from the ultrasonic sensor to determine the coordinates of map points. The computed S-OGM results exhibit a structural representation of the environment that is highly consistent with the ground truth layout of the surroundings.

Considering the advancement achieved, **Study 5** aims to answer the ultimate question:

RQ3: What techniques can DR methods adopt to effectively update positioning results via common attributes from multiple persons?

Inspired by magnetic field based localisation, **Study 5** explores the use of magnetic fingerprints as the common characteristics to segment a continuous trajectory into distinct fingerprints. The DTW based matching strategy is designed to identify the optimal matching and timing for trajectory integration. The trajectories from multiple users are combined using an EKF framework, which incorporates specific pseudo-measurement data to update the position. A total of ten individuals are evenly distributed into two groups for data collection. The integrated trajectory results exhibit precise tracking performance for both individual and multi-person situations, achieved through individual self-update and multi-person cross-update methods, respectively.

5.2 Key Contributions

Based on the body of work, the details of these contributions are shown below.

1. **Improving Heading Estimation based on Gait Analysis**
   In **Study 1**, a new gait-aided DR system is explored to enhance localisation accuracy by utilising an adaptive heading estimation technique. This study examines various cases during the gait that are associated with the possible factors that influence the accuracy of heading estimation. This study presents significant insights in the field of DR research by examining the clamping angle of the foot and achieving enhanced positioning results.

2. **Improving Step Detection and Optimisation using Sensor Fusion**
   Study 2 and **Study 3** explore sensor fusion techniques by using dynamic thresholding approaches for detecting precise motion phases and optimising dual-foot positioning. These methods contribute to enhancing the positioning accuracy of DR methods by replacing inadequate configurations in the positioning calculation. Compared with

conventional fixed threshold based DR methods, the dual foot synergistic method and minimum stride length constrain method adaptively eliminate the positioning error among different users.

3. **Surrounding Map Reconstruction in DR Methods**

   Study 4 develops a novel map reconstruction algorithm in the DR system. This algorithm innovatively calculates the coordinates of map points using polar projection integrating range measurement from ultrasonic sensor and trajectory from DR system. By doing so, a surrounding map can be conducted while tracking users' positions. This map enhances the comprehension of trajectory and expands the potential use of the DR method in situations where layout information, such as in firefighting scenarios, is not previously known.

4. **Development of Multi-person Localisation**

   Based on the improvement approaches presented above, **Study 5** explores a novel approach for multi-person positioning updates by employing an online magnetic fingerprint matching technique. This approach updates the position of individuals by leveraging pseudo-measurements obtained from matched MFs from themselves or other individuals. The multi-person INS system proposed in this study has demonstrated remarkable performance in addressing the challenges of individual loop closure and the integration of multiple trajectories. This innovation has led to a substantial enhancement in the quantitative performance of inertial based DR method. Notably, to the best of our knowledge, this is the first multi-person method in the DR research field that has been documented in the literature. This approach surpasses most existing methods by its online MF matching capability, obviating the need for pre-installed landmark and WSN setups which brings important technical solutions to the application of DR methods in emergency services.

In summary, this thesis proposes a set of novel approaches that address significant problems in the DR research field. Five studies contribute to improving the accuracy of positioning, developing surrounding mapping and enabling multi-person usage, which makes up the research gap of indoor firefighting navigation. Specifically, the gait analysis, polar projection and online magnetic fingerprint inspire new research interests in DR related studies which enhance DR systems to adapt to harsh and dynamic environments. Additionally, the designed low-cost sensor fusion solutions will promote the industry development potential of application cases.

5.3 Limitations and Future Works

5.3.1 Optimisation of Multi-person Positioning

The multi-person positioning method described in this thesis comprises a two-phase computation. The initial phase involves the system establishing the online fingerprint, while the subsequent phase entails the system executing fingerprint matching and trajectory updating. The calculation process is both time-consuming and resource-intensive, resulting in delays in real-time applications. In order to address this issue, future work will incorporate multi-trajectory integration within a multi-threaded computing framework. A heuristic algorithm for fingerprint matching will be developed to optimise calculation speed and conserve memory by reducing unnecessary matching attempts. The learning-based approaches are potentially utilised for improving the adaptivity of system parameters. To investigate the positioning performance influenced by hardware quality factors, different IMU sensors e.g. Xsens IMU will be adopted in the future study.

5.3.2 Evaluation Benchmarking

The studies presented in this thesis do not have a comprehensive benchmark for evaluating the performance of positioning and mapping compared with a standard ground truth. Despite the overall results and quantity evaluation criteria, the majority of literature relies on loop closing RMSE and subjective visualisation comparison for evaluation, which limits the reliability of positioning and mapping assessment. In addition, the ground truth references of DR based methods are not continual while its measurements are easily affected by human subjective factors (e.g. individual ground truth measurement bias and irregular walking patterns [203]) and environmental factors (e.g. magnetic interference, visibility and temperature [204, 205]). This limitation will challenge the confidence of the DR system evaluation quality. Future work will adhere to the standards of building surveying in order to create a thorough evaluation system that includes ground truth determination, benchmark formulation, and evaluation metrics. The total station, WSN method, and SLAM based method will be utilised for benchmark development. By doing this, it is anticipated that a standardised objective quality assessment will be provided, allowing researchers in this field to compare the performance of their methods against a comprehensive standard.

5.3.3 Seamless Indoor-Outdoor Positioning

For the DR method, the calculation of positioning necessitates an initial position, commonly designated as (0,0) in the experiment. This initialisation often presents challenges in representing positions in a standard map. Hence, a standard geographical coordinate of the initial point is required to convert the coordinate system from a body frame coordinate to the Earth-centered, Earth-fixed coordinate system (ECEF) in order to ensure a standardised and consistent representation of position. In order to address this issue, future work would focus on exploring a seamless indoor-outdoor positioning system through the integration of GNSS positioning and DR positioning. By utilising the ECEF position obtained from GNSS, it is possible to ascertain the initial position of the DR method. In addition, this design has the capability to establish initial positions for multiple individuals at various starting points, thereby improving the efficiency of multi-person localisation.

List of Publications

Journals

[1] Wu R, Lee B G, Pike M, et al. IOAM: A Novel Sensor Fusion-Based Wearable for localisation and Mapping[J]. Remote Sensing, 2022, 14(23): 6081.

[2] Wu R, Pike M, Lee B G, et al. Multi-INS: A Novel Approach Integrating Online Magnetic Fingerprints for Multi-Person Inertial Navigation Systems [J]. IEEE Transactions on Systems, Man and Cybernetics: Systems. (Under Review)

[3] Wu R, Pike M, Lee B G. DT-SLAM: dynamic thresholding based corner point extraction in SLAM system[J]. IEEE Access, 2021, 9: 91723-91729.

[4] Chai X, Wu R, Pike M, et al. Smart wearables with sensor fusion for fall detection in firefighting[J]. Sensors, 2021, 21(20): 6770.

[5] Zhu L, Wu R, Lee B G, et al. FEGAN: A Feature-Oriented Enhanced GAN for Enhancing Thermal Image Super-Resolution[J]. IEEE Signal Processing Letters, 2024.

[6] Chai X, Lee B G, Pike M, Wu R, et al. Pre-impact Firefighter Fall Detection Using Machine Learning on the Edge[J]. IEEE Sensors Journal, 2023.

Conference Proceedings

[1] Wu R, Pike M, Chai X, et al. "GA-PDR: Using Gait Analysis for Heading Estimation in PDR Based Indoor localisation System," IECON 2023- 49th Annual Conference of the IEEE Industrial Electronics Society, Singapore, Singapore, 2023, pp. 1-6, doi: 10.1109/IECON51785.2023.10312643.

[2] Wu R, Lee B G, Pike M, et al. "Enhancing DF-INS for Accurate Zero-Velocity Detection in ILBS: A Dual Foot Synergistic Method," 2023

IEEE SENSORS, Vienna, Austria, 2023, pp. 1-4, doi: 10.1109/SENSORS56945.2023.10325168.

[3] Wu R, Pike M, Chai X, et al. SLAM-ING: A Wearable SLAM Inertial NaviGation System[C]//2022 IEEE Sensors. IEEE, 2022: 01-04.

[4] Wu R, Lee B G, Pike M, et al. Enhancing DF-INS for Accurate Zero-Velocity Detection in ILBS: A Dual Foot Synergistic Method[C]//2023 IEEE SENSORS. IEEE, 2023: 1-4.

[5] Lee B G, Wu R, Xu F, et al. "Comparative Analysis of Wireless Transmission Methods for Firefighting Communication in Challenging Indoor Environments," TENCON 2023 - 2023 IEEE Region 10 Conference (TENCON), Chiang Mai, Thailand, 2023, pp. 1070-1075, doi: 10.1109/TENCON58879.2023.10322361.

Patents

[1] Boon Giin Lee, Renjie Wu, Xiaoqing Chai, et al. A new type of infrared thermal imaging glasses. Publication date:2023-08-25 publication no.:CN219590611U (Chinese patent, Granted)

[2] Renjie Wu, Boon Giin Lee, Matthew Pike, et al. A shoe with a positioning function. Publication date: 2022-08-12 Publication no.:CN217161226U (Chinese patent, Granted)

[3] Boon Giin Lee, Renjie Wu, Matthew Pike, An ultrasound-based indoor inertial guidance mapping method and system. Publication date:2022-06-03 Publication no.:CN114577206A (Chinese patent, Granted)

[4] Boon Giin Lee, Shuhe Zhang, Renjie Wu, et al. A multi-user cooperative positioning method, apparatus, electronic device and storage medium. Publication date:2022-07-07 Publication no.:CN116399336A (Chinese patent)

[5] Boon Giin Lee, Renjie Wu, Matthew Pike, et al. A method, device and system for determining a motion trajectory. Publication date:2022-05-13 Publication no.:CN114485647A (Chinese patent)

[6] Boon Giin Lee, Shuhe Zhang, Renjie Wu, et al. A multi-user cooperative positioning method, apparatus, electronic device and storage

medium. Publication date: 2022-07-07 Publication no.:CN116399336A (Chinese patent)

[7] Boon Giin Lee, Renjie Wu, Matthew Pike. Ultrasonic Wave-Based Indoor Inertial Navigation Mapping Method and System. Application date 2023-02-21 Application no.:18/112,143 (US patent)

Bibliography

[1] C. Zhang, "University of nottingham thesis template for phd degree," https://www.overleaf.com/latex/templates/university-of-nottingham-thesis-template-for-phd-degree/yhdfrftcbgbk, 2019.

[2] M. A. Al-Ammar, S. Alhadhrami, A. Al-Salman, A. Alarifi, H. S. Al-Khalifa, A. Alnafessah, and M. Alsaleh, "Comparative survey of indoor positioning technologies, techniques, and algorithms," in *2014 International Conference on Cyberworlds*. IEEE, 2014, pp. 245–252.

[3] N. Zhu, J. Marais, D. Bétaille, and M. Berbineau, "Gnss position integrity in urban environments: A review of literature," *IEEE Transactions on Intelligent Transportation Systems*, vol. 19, no. 9, pp. 2762–2778, 2018.

[4] J. Jämsä, M. Luimula, S. Pieskä, V. Brax, O. Saukko, and P. Verronen, "Indoor positioning with laser scanned models in the metal industry," in *2010 Ubiquitous Positioning Indoor Navigation and Location Based Service*. IEEE, 2010, pp. 1–9.

[5] Q. Wang, Y. Guo, L. Yang, and M. Tian, "An indoor positioning system based on ibeacon," *Transactions on Edutainment XIII*, pp. 262–272, 2017.

[6] G. Yang, S. Zhu, Q. Li, and K. Zhao, "Uwb/ins based indoor positioning and nlos detection algorithm for firefighters," in *2020 IEEE 22nd International Conference on High Performance Computing and Communications; IEEE 18th International Conference on Smart City; IEEE 6th International Conference on Data Science and Systems (HPCC/SmartCity/DSS)*. IEEE, 2020, pp. 909–916.

[7] B. Lee, D.-M. Woo, M.-K. Park, and S. Kim, "Development of self-localizer using collaboration of trilateration and triangulation," in *2014 11th International Conference on Fuzzy Systems and Knowledge Discovery (FSKD)*. IEEE, 2014, pp. 729–733.

[8] C. Yang and H.-R. Shao, "Wifi-based indoor positioning," *IEEE Communications Magazine*, vol. 53, no. 3, pp. 150–157, 2015.

[9] A. Thaljaoui, T. Val, N. Nasri, and D. Brulin, “Ble localization using rssi measurements and iringla,” in *2015 IEEE international conference on industrial technology (ICIT)*. IEEE, 2015, Conference Proceedings, pp. 2178–2183.

[10] L. Zwirello, T. Schipper, M. Harter, and T. Zwick, “Uwb localization system for indoor applications: Concept, realization and analysis,” *Journal of Electrical and Computer Engineering*, vol. 2012, pp. 1–11, 2012.

[11] J. Zhou and J. Shi, “Rfid localization algorithms and applications—a review,” *Journal of intelligent manufacturing*, vol. 20, no. 6, pp. 695–707, 2009.

[12] Q. Song, S. Guo, X. Liu, and Y. Yang, “Csi amplitude fingerprinting-based nb-iot indoor localization,” *IEEE Internet of Things Journal*, vol. 5, no. 3, pp. 1494–1504, 2017.

[13] G. Grisetti, R. Kümmerle, C. Stachniss, and W. Burgard, “A tutorial on graph-based slam,” *IEEE Intelligent Transportation Systems Magazine*, vol. 2, no. 4, pp. 31–43, 2010.

[14] A. A. B. Pritsker, *Introduction to Simulation and SLAM II*. Halsted Press, 1984.

[15] O. Mezentsev, G. Lachapelle, and J. Collin, “Pedestrian dead reckoning—a solution to navigation in gps signal degraded areas?” *Geomatica*, vol. 59, no. 2, pp. 175–182, 2005.

[16] L. Ojeda and J. Borenstein, “Non-gps navigation with the personal dead-reckoning system,” in *Unmanned systems technology ix*, vol. 6561. SPIE, 2007, pp. 110–120.

[17] I. A. Kazerouni, L. Fitzgerald, G. Dooly, and D. Toal, “A survey of state-of-the-art on visual slam,” *Expert Systems with Applications*, vol. 205, p. 117734, 2022.

[18] M. U. Khan, S. A. A. Zaidi, A. Ishtiaq, S. U. R. Bukhari, S. Samer, and A. Farman, “A comparative survey of lidar-slam and lidar based sensor technologies,” in *2021 Mohammad Ali Jinnah University International Conference on Computing (MAJICC)*. IEEE, 2021, pp. 1–8.

[19] Y. S. Park, Y.-S. Shin, J. Kim, and A. Kim, “3d ego-motion estimation using low-cost mmwave radars via radar velocity factor for pose-graph slam,” *IEEE Robotics and Automation Letters*, vol. 6, no. 4, pp. 7691–7698, 2021.

[20] B. H. O. Pinto, H. A. de Oliveira, and E. J. Souto, “Factor optimization for the design of indoor positioning systems using a probability-based algorithm,” *Journal of Sensor and Actuator Networks*, vol. 10, no. 1, p. 16, 2021.

[21] X. Hou and J. Bergmann, "Pedestrian dead reckoning with wearable sensors: A systematic review," *IEEE Sensors Journal*, vol. 21, no. 1, pp. 143–152, 2020.

[22] A. K. Paul and T. Sato, "Localization in wireless sensor networks: A survey on algorithms, measurement techniques, applications and challenges," *Journal of sensor and actuator networks*, vol. 6, no. 4, p. 24, 2017.

[23] D. L. Smith, "Firefighter fitness: improving performance and preventing injuries and fatalities," *Current sports medicine reports*, vol. 10, no. 3, pp. 167–172, 2011.

[24] K. Akkaya, M. Younis, and W. Youssef, "Positioning of base stations in wireless sensor networks," *IEEE Communications Magazine*, vol. 45, no. 4, pp. 96–102, 2007.

[25] T. Augustin and D. Ossmann, "Enhanced pedestrian dead reckoning sensor fusion for firefighting," *Engineering Proceedings*, vol. 58, no. 1, p. 24, 2023.

[26] R. Wu, M. Pike, and B.-G. Lee, "Dt-slam: Dynamic thresholding based corner point extraction in slam system," *IEEE Access*, vol. 9, pp. 91 723–91 729, 2021.

[27] N. Ahmad, R. A. R. Ghazilla, N. M. Khairi, and V. Kasi, "Reviews on various inertial measurement unit (imu) sensor applications," *International Journal of Signal Processing Systems*, vol. 1, no. 2, pp. 256–262, 2013.

[28] B. Wagstaff and J. Kelly, "Lstm-based zero-velocity detection for robust inertial navigation," in *2018 International Conference on Indoor Positioning and Indoor Navigation (IPIN)*. IEEE, 2018, pp. 1–8.

[29] R. Wu, B. G. Lee, M. Pike, L. Zhu, X. Chai, L. Huang, and X. Wu, "Ioam: A novel sensor fusion-based wearable for localization and mapping," *Remote Sensing*, vol. 14, no. 23, p. 6081, 2022.

[30] R. Liu, C. Yuen, T.-N. Do, D. Jiao, X. Liu, and U.-X. Tan, "Cooperative relative positioning of mobile users by fusing imu inertial and uwb ranging information," in *2017 IEEE International Conference on Robotics and Automation (ICRA)*. IEEE, 2017, pp. 5623–5629.

[31] M. O. Wong, H. Zhou, H. Ying, and S. Lee, "A voice-driven imu-enabled bim-based multi-user system for indoor navigation in fire emergencies," *Automation in Construction*, vol. 135, p. 104137, 2022.

[32] I. Skog, J.-O. Nilsson, and P. Händel, "An open-source multi inertial measurement unit (mimu) platform," in *2014 International Symposium on Inertial Sensors and Systems (ISISS)*. IEEE, 2014, pp. 1–4.

[33] D. Roetenberg, H. Luinge, and P. Slycke, "Xsens mvn: Full 6dof human motion tracking using miniature inertial sensors," *xsens motion technologies bv*, 2009.

[34] D. Feng, C. Wang, C. He, Y. Zhuang, and X.-G. Xia, "Kalman-filter-based integration of imu and uwb for high-accuracy indoor positioning and navigation," *IEEE Internet of Things Journal*, vol. 7, no. 4, pp. 3133–3146, 2020.

[35] H. Leppäkoski, J. Collin, and J. Takala, "Pedestrian navigation based on inertial sensors, indoor map, and wlan signals," *Journal of Signal Processing Systems*, vol. 71, pp. 287–296, 2013.

[36] J. Chen, B. Zhou, S. Bao, X. Liu, Z. Gu, L. Li, Y. Zhao, J. Zhu, and Q. Li, "A data-driven inertial navigation/bluetooth fusion algorithm for indoor localization," *IEEE Sensors Journal*, vol. 22, no. 6, pp. 5288–5301, 2021.

[37] J. Jankovic, W. Jones, J. Burkhart, and G. Noonan, "Environmental study of firefighters," *The Annals of occupational hygiene*, vol. 35, no. 6, pp. 581–602, 1991.

[38] T. L. Guidotti, "Human factors in firefighting: ergonomic-, cardiopulmonary-, and psychogenic stress-related issues," *International archives of occupational and environmental health*, vol. 64, pp. 1–12, 1992.

[39] I. Skog, P. Handel, J.-O. Nilsson, and J. Rantakokko, "Zero-velocity detection—an algorithm evaluation," *IEEE transactions on biomedical engineering*, vol. 57, no. 11, pp. 2657–2666, 2010.

[40] S. Thrun, "Learning occupancy grid maps with forward sensor models," *Autonomous robots*, vol. 15, no. 2, pp. 111–127, 2003.

[41] H. Obeidat, W. Shuaieb, O. Obeidat, and R. Abd-Alhameed, "A review of indoor localization techniques and wireless technologies," *Wireless Personal Communications*, vol. 119, pp. 289–327, 2021.

[42] S. Zhang and H. Zhang, "A review of wireless sensor networks and its applications," in *2012 IEEE international conference on automation and logistics*. IEEE, 2012, pp. 386–389.

[43] J. Kuriakose, S. Joshi, R. Vikram Raju, and A. Kilaru, "A review on localization in wireless sensor networks," *Advances in signal processing and intelligent recognition systems*, pp. 599–610, 2014.

[44] S.-H. Fang and T. Lin, "Principal component localization in indoor wlan environments," *IEEE Transactions on Mobile Computing*, vol. 11, no. 1, pp. 100–110, 2011.

[45] A. Thaljaoui, T. Val, N. Nasri, and D. Brulin, "Ble localization using rssi measurements and iringla," in *2015 IEEE international conference on industrial technology (ICIT)*. IEEE, 2015, pp. 2178–2183.

[46] M. Sugano, T. Kawazoe, Y. Ohta, and M. Murata, "Indoor localization system using rssi measurement of wireless sensor network based on zigbee standard." *Wireless and optical communications*, vol. 538, pp. 1–6, 2006.

[47] Q. Z. Ahmed, M. Hafeez, F. A. Khan, and P. Lazaridis, "Towards beyond 5g future wireless networks with focus towards indoor localization," in *2020 IEEE Eighth International Conference on Communications and Networking (ComNet)*. IEEE, 2020, pp. 1–5.

[48] J. Zhou and J. Shi, "Rfid localization algorithms and applications—a review," *Journal of intelligent manufacturing*, vol. 20, pp. 695–707, 2009.

[49] A. Basiri, E. S. Lohan, T. Moore, A. Winstanley, P. Peltola, C. Hill, P. Amirian, and P. F. e Silva, "Indoor location based services challenges, requirements and usability of current solutions," *Computer Science Review*, vol. 24, pp. 1–12, 2017.

[50] S. Pan, Z. Xie, and Y. Jiang, "Sweeping robot based on laser slam," *Procedia Computer Science*, vol. 199, pp. 1205–1212, 2022.

[51] A. Singandhupe and H. M. La, "A review of slam techniques and security in autonomous driving," in *2019 third IEEE international conference on robotic computing (IRC)*. IEEE, 2019, pp. 602–607.

[52] J. Polvi, T. Taketomi, G. Yamamoto, A. Dey, C. Sandor, and H. Kato, "Slidar: A 3d positioning method for slam-based handheld augmented reality," *Computers & Graphics*, vol. 55, pp. 33–43, 2016.

[53] J. Song, J. Wang, L. Zhao, S. Huang, and G. Dissanayake, "Misslam: Real-time large-scale dense deformable slam system in minimal invasive surgery based on heterogeneous computing," *IEEE Robotics and Automation Letters*, vol. 3, no. 4, pp. 4068–4075, 2018.

[54] A. Gupta and X. Fernando, "Simultaneous localization and mapping (slam) and data fusion in unmanned aerial vehicles: Recent advances and challenges," *Drones*, vol. 6, no. 4, p. 85, 2022.

[55] T. Taketomi, H. Uchiyama, and S. Ikeda, "Visual slam algorithms: A survey from 2010 to 2016," *IPSJ Transactions on Computer Vision and Applications*, vol. 9, no. 1, pp. 1–11, 2017.

[56] Y.-S. Shin and A. Kim, "Sparse depth enhanced direct thermal-infrared slam beyond the visible spectrum," *IEEE Robotics and Automation Letters*, vol. 4, no. 3, pp. 2918–2925, 2019.

[57] M. U. Khan, S. A. A. Zaidi, A. Ishtiaq, S. U. R. Bukhari, S. Samer, and A. Farman, "A comparative survey of lidar-slam and lidar based sensor technologies," in *2021 Mohammad Ali Jinnah University International Conference on Computing (MAJICC)*. IEEE, 2021, Conference Proceedings, pp. 1–8.

[58] N. Mandischer, S. C. Eddine, M. Huesing, and B. Corves, "Radar slam for autonomous indoor grinding," in *2020 IEEE Radar Conference (RadarConf20)*. IEEE, 2020, Conference Proceedings, pp. 1–6.

[59] W. Chen, R. Chen, Y. Chen, H. Kuusniemi, and J. Wang, "An effective pedestrian dead reckoning algorithm using a unified heading error model," in *IEEE/ION Position, Location and Navigation Symposium*. IEEE, 2010, pp. 340–347.

[60] A. Manos, I. Klein, and T. Hazan, "Gravity-based methods for heading computation in pedestrian dead reckoning," *Sensors*, vol. 19, no. 5, p. 1170, 2019.

[61] Q. Fan, H. Zhang, P. Pan, X. Zhuang, J. Jia, P. Zhang, Z. Zhao, G. Zhu, and Y. Tang, "Improved pedestrian dead reckoning based on a robust adaptive kalman filter for indoor inertial location system," *Sensors*, vol. 19, no. 2, p. 294, 2019.

[62] A. Wahdan, J. Georgy, W. F. Abdelfatah, and A. Noureldin, "Magnetometer calibration for portable navigation devices in vehicles using a fast and autonomous technique," *IEEE Transactions on Intelligent Transportation Systems*, vol. 15, no. 5, pp. 2347–2352, 2014.

[63] J. W. Kim, H. J. Jang, D.-H. Hwang, and C. Park, "A step, stride and heading determination for the pedestrian navigation system," *Journal of Global Positioning Systems*, vol. 3, no. 1-2, pp. 273–279, 2004.

[64] S. Qiu, Z. Wang, H. Zhao, K. Qin, Z. Li, and H. Hu, "Inertial/magnetic sensors based pedestrian dead reckoning by means of multi-sensor fusion," *Information Fusion*, vol. 39, pp. 108–119, 2018.

[65] R. Ashkar, M. Romanovas, V. Goridko, M. Schwaab, M. Traechtler, and Y. Manoli, "A low-cost shoe-mounted inertial navigation system with magnetic disturbance compensation," in *International Conference on Indoor Positioning and Indoor Navigation*. IEEE, 2013, pp. 1–10.

[66] D. Wu, L. Xia, and J. Geng, "Heading estimation for pedestrian dead reckoning based on robust adaptive kalman filtering," *Sensors*, vol. 18, no. 6, p. 1970, 2018.

[67] W. Zhang, D. Wei, H. Yuan, and G. Yang, "Cooperative positioning method of dual foot-mounted inertial pedestrian dead reckoning systems," *IEEE Transactions on Instrumentation and Measurement*, vol. 70, pp. 1–14, 2021.

[68] Q. Wang, H. Luo, H. Xiong, A. Men, F. Zhao, M. Xia, and C. Ou, "Pedestrian dead reckoning based on walking pattern recognition and online magnetic fingerprint trajectory calibration," *IEEE Internet of Things Journal*, vol. 8, no. 3, pp. 2011–2026, 2020.

[69] B. Wang, X. Liu, B. Yu, R. Jia, and X. Gan, "Pedestrian dead reckoning based on motion mode recognition using a smartphone," *Sensors*, vol. 18, no. 6, p. 1811, 2018.

[70] B. Wu, C. Ma, S. Poslad, and D. R. Selviah, "An adaptive human activity-aided hand-held smartphone-based pedestrian dead reckoning positioning system," *Remote Sensing*, vol. 13, no. 11, p. 2137, 2021.

[71] S. Tateno, Y. Cho, D. Li, H. Tian, and P. Hsiao, "Improvement of pedestrian dead reckoning by heading correction based on optimal access points selection method," in *2017 56th Annual Conference of the Society of Instrument and Control Engineers of Japan (SICE)*. IEEE, 2017, pp. 321–326.

[72] P. Chen, Y. Kuang, and X. Chen, "A uwb/improved pdr integration algorithm applied to dynamic indoor positioning for pedestrians," *Sensors*, vol. 17, no. 9, p. 2065, 2017.

[73] J. Borenstein and L. Ojeda, "Heuristic drift elimination for personnel tracking systems," *The Journal of Navigation*, vol. 63, no. 4, pp. 591–606, 2010.

[74] A. R. Jiménez, F. Seco, F. Zampella, J. C. Prieto, and J. Guevara, "Improved heuristic drift elimination (ihde) for pedestrian navigation in complex buildings," in *2011 International Conference on Indoor Positioning and Indoor Navigation*. IEEE, 2011, pp. 1–8.

[75] M. N. Muhammad, Z. Salcic, I. Kevin, and K. Wang, "Indoor pedestrian tracking using consumer-grade inertial sensors with pztd heading correction," *IEEE Sensors Journal*, vol. 18, no. 12, pp. 5164–5172, 2018.

[76] Y. Wu, H. Zhu, Q. Du, and S. Tang, "A pedestrian dead-reckoning system for walking and marking time mixed movement using an shss scheme and a foot-mounted imu," *IEEE Sensors Journal*, vol. 19, no. 5, pp. 1661–1671, 2018.

[77] K. Britting, *Inertial Navigation Systems Analysis*. Wiley-Interscience, 2010.

[78] A. Alarifi, A. Al-Salman, M. Alsaleh, A. Alnafessah, S. Al-Hadhrami, M. A. Al-Ammar, and H. S. Al-Khalifa, "Ultra wideband indoor positioning technologies: Analysis and recent advances," *Sensors*, vol. 16, no. 5, 2016. [Online]. Available: https://www.mdpi.com/1424-8220/16/5/707

[79] C. Yang and H.-r. Shao, "Wifi-based indoor positioning," *IEEE Communications Magazine*, vol. 53, no. 3, pp. 150–157, 2015.

[80] R. Faragher and R. Harle, "An analysis of the accuracy of bluetooth low energy for indoor positioning applications," in *Proceedings of the 27th International Technical Meeting of The Satellite Division of the Institute of Navigation (ION GNSS+ 2014)*, 2014, pp. 201–210.

[81] M. Uradzinski, H. Guo, X. Liu, and M. Yu, "Advanced indoor positioning using zigbee wireless technology," *Wirel. Pers. Commun.*, vol. 97, no. 4, p. 6509–6518, dec 2017. [Online]. Available: https://doi.org/10.1007/s11277-017-4852-5

[82] Q. Song, S. Guo, X. Liu, and Y. Yang, "Csi amplitude fingerprinting-based nb-iot indoor localization," *IEEE Internet of Things Journal*, vol. 5, no. 3, pp. 1494–1504, 2018.

[83] X. Niu, Y. Li, J. Kuang, and P. Zhang, "Data fusion of dual foot-mounted imu for pedestrian navigation," *IEEE Sensors Journal*, vol. 19, no. 12, pp. 4577–4584, 2019.

[84] R. Harle, "A survey of indoor inertial positioning systems for pedestrians," *IEEE Communications Surveys & Tutorials*, vol. 15, no. 3, pp. 1281–1293, 2013.

[85] A. Kharb, V. Saini, Y. Jain, and S. Dhiman, "A review of gait cycle and its parameters," *IJCEM International Journal of Computational Engineering & Management*, vol. 13, 01 2011.

[86] S. Godha and G. Lachapelle, "Foot mounted inertial system for pedestrian navigation," *Measurement Science and Technology*, vol. 19, no. 7, p. 075202, may 2008. [Online]. Available: https://dx.doi.org/10.1088/0957-0233/19/7/075202

[87] B. Krach and P. Robertson, "Integration of foot-mounted inertial sensors into a bayesian location estimation framework," in *2008 5th Workshop on Positioning, Navigation and Communication*, 2008, pp. 55–61.

[88] L. Ojeda and J. Borenstein, "Non-gps navigation for security personnel and first responders," *The Journal of Navigation*, vol. 60, no. 3, p. 391–407, 2007.

[89] I. Skog, P. Handel, J.-O. Nilsson, and J. Rantakokko, "Zero-velocity detection—an algorithm evaluation," *IEEE Transactions on Biomedical Engineering*, vol. 57, no. 11, pp. 2657–2666, 2010.

[90] H. Qi and J. B. Moore, "Direct kalman filtering approach for gps/ins integration," *IEEE Transactions on Aerospace and Electronic Systems*, vol. 38, no. 2, pp. 687–693, 2002.

[91] M. S. Grewal and A. P. Andrews, *Kalman filtering: Theory and Practice with MATLAB*. John Wiley & Sons, 2014.

[92] J. Woods and C. Radewan, "Kalman filtering in two dimensions," *IEEE transactions on Information theory*, vol. 23, no. 4, pp. 473–482, 1977.

[93] A. R. Jiménez, F. Seco, J. C. Prieto, and J. Guevara, "Indoor pedestrian navigation using an ins/ekf framework for yaw drift reduction and a foot-mounted imu," in *2010 7th workshop on positioning, navigation and communication*. IEEE, 2010, pp. 135–143.

[94] J. Wahlström and I. Skog, "Fifteen years of progress at zero velocity: A review," *IEEE Sensors Journal*, vol. 21, no. 2, pp. 1139–1151, 2020.

[95] F. Woyano, S. Lee, and S. Park, "Evaluation and comparison of performance analysis of indoor inertial navigation system based on foot mounted imu," in *2016 18th International Conference on Advanced Communication Technology (ICACT)*. IEEE, 2016, pp. 792–798.

[96] M. Bloesch, S. Omari, M. Hutter, and R. Siegwart, "Robust visual inertial odometry using a direct ekf-based approach," in *2015 IEEE/RSJ international conference on intelligent robots and systems (IROS)*. IEEE, 2015, pp. 298–304.

[97] H. Zhao, Z. Wang, S. Qiu, Y. Shen, L. Zhang, K. Tang, and G. Fortino, "Heading drift reduction for foot-mounted inertial navigation system via multi-sensor fusion and dual-gait analysis," *IEEE Sensors Journal*, vol. 19, no. 19, pp. 8514–8521, 2018.

[98] M. Zhu, Y. Wu, and S. Luo, "A pedestrian navigation system by low-cost dual foot-mounted imus and inter-foot ranging," in *2020 DGON Inertial Sensors and Systems (ISS)*. IEEE, 2020, pp. 1–20.

[99] G. Prateek, R. Girisha, K. Hari, and P. Händel, "Data fusion of dual foot-mounted ins to reduce the systematic heading drift," in *2013 4th International Conference on Intelligent Systems, Modelling and Simulation*. IEEE, 2013, pp. 208–213.

[100] G. Hu, S. Gao, and Y. Zhong, "A derivative ukf for tightly coupled ins/gps integrated navigation," *ISA transactions*, vol. 56, pp. 135–144, 2015.

[101] Y. Tang, J. Jiang, J. Liu, P. Yan, Y. Tao, and J. Liu, "A gru and akf-based hybrid algorithm for improving ins/gnss navigation accuracy during gnss outage," *Remote Sensing*, vol. 14, no. 3, p. 752, 2022.

[102] F. Li and L. Chang, "Mekf with navigation frame attitude error parameterization for ins/gps," *IEEE Sensors Journal*, vol. 20, no. 3, pp. 1536–1549, 2019.

[103] J.-O. Nilsson, I. Skog, P. Händel, and K. Hari, "Foot-mounted ins for everybody-an open-source embedded implementation," in *Proceedings of the 2012 IEEE/ION Position, Location and Navigation Symposium*. Ieee, 2012, pp. 140–145.

[104] J.-O. Nilsson, A. K. Gupta, and P. Händel, "Foot-mounted inertial navigation made easy," in *2014 International Conference on Indoor Positioning and Indoor Navigation (IPIN)*. IEEE, 2014, pp. 24–29.

[105] A. Norrdine, Z. Kasmi, and J. Blankenbach, "Step detection for zupt-aided inertial pedestrian navigation system using foot-mounted permanent magnet," *IEEE Sensors Journal*, vol. 16, no. 17, pp. 6766–6773, 2016.

[106] H. Li, H. Guo, Y. Qi, L. Deng, and M. Yu, "Research on multi-sensor pedestrian dead reckoning method with ukf algorithm," *Measurement*, vol. 169, p. 108524, 2021.

[107] Q. Wang, M. Cheng, A. Noureldin, and Z. Guo, "Research on the improved method for dual foot-mounted inertial/magnetometer pedestrian positioning based on adaptive inequality constraints kalman filter algorithm," *Measurement*, vol. 135, pp. 189–198, 2019.

[108] A. A. Abdallah, C.-S. Jao, Z. M. Kassas, and A. M. Shkel, "A pedestrian indoor navigation system using deep-learning-aided cellular signals and zupt-aided foot-mounted imus," *IEEE Sensors Journal*, vol. 22, no. 6, pp. 5188–5198, 2021.

[109] I. Kingma, H. M. Toussaint, D. A. Commissaris, M. J. Hoozemans, and M. J. Ober, "Optimizing the determination of the body center of mass," *Journal of biomechanics*, vol. 28, no. 9, pp. 1137–1142, 1995.

[110] Y.-C. Pai and J. Patton, "Center of mass velocity-position predictions for balance control," *Journal of biomechanics*, vol. 30, no. 4, pp. 347–354, 1997.

[111] G. Pavei, E. Seminati, D. Cazzola, and A. E. Minetti, "On the estimation accuracy of the 3d body center of mass trajectory during human locomotion: inverse vs. forward dynamics," *Frontiers in physiology*, vol. 8, p. 129, 2017.

[112] C. X. Yang, "Low-cost experimental system for center of mass and center of pressure measurement (june 2018)," *IEEE Access*, vol. 6, pp. 45 021–45 033, 2018.

[113] G. Pavei, F. Salis, A. Cereatti, and E. Bergamini, "Body center of mass trajectory and mechanical energy using inertial sensors: a feasible stride?" *Gait & posture*, vol. 80, pp. 199–205, 2020.

[114] G. Zhang, D. Zhang, Y. He, J. Chen, F. Zhou, and Y. Chen, "Multi-person passive wifi indoor localization with intelligent reflecting surface," *IEEE Transactions on Wireless Communications*, 2023.

[115] H. Qian, X. Yang, X. Zhang, Y. Ding, and L. Zhang, "Pla-jpda for indoor multi-person tracking using ir-uwb radars," in *2020 IEEE Radar Conference (RadarConf20).* IEEE, 2020, pp. 1–6.

[116] C. Wu, F. Zhang, B. Wang, and K. R. Liu, "mmtrack: Passive multi-person localization using commodity millimeter wave radio," in *IEEE INFOCOM 2020-IEEE Conference on Computer Communications.* IEEE, 2020, pp. 2400–2409.

[117] T. Yang, P. Guo, W. Liu, X. Liu, and T. Hao, "Enhancing pir-based multi-person localization through combining deep learning with domain knowledge," *IEEE Sensors Journal*, vol. 21, no. 4, pp. 4874–4886, 2020.

[118] C. Randell, C. Djiallis, and H. Muller, "Personal position measurement using dead reckoning," in *Seventh IEEE International Symposium on Wearable Computers, 2003. Proceedings.* IEEE Computer Society, 2003, Conference Proceedings, pp. 166–166.

[119] W. Zhang, X. Li, D. Wei, X. Ji, and H. Yuan, "A foot-mounted pdr system based on imu/ekf+ hmm+ zupt+ zaru+ hdr+ compass algorithm," in *2017 International conference on indoor positioning and indoor navigation (IPIN).* IEEE, 2017, pp. 1–5.

[120] M. Kotaru, K. Joshi, D. Bharadia, and S. Katti, "Spotfi: Decimeter level localization using wifi," in *Proceedings of the 2015 ACM Conference on Special Interest Group on Data Communication*, 2015, Conference Proceedings, pp. 269–282.

[121] X. Wang, M. Jiang, Z. Guo, N. Hu, Z. Sun, and J. Liu, "An indoor positioning method for smartphones using landmarks and pdr," *Sensors*, vol. 16, no. 12, p. 2135, 2016.

[122] L. Gao and S. Konomi, "Indoor spatiotemporal contact analytics using landmark-aided pedestrian dead reckoning on smartphones," *Sensors*, vol. 23, no. 1, p. 113, 2022.

[123] F. Gu, X. Hu, M. Ramezani, D. Acharya, K. Khoshelham, S. Valaee, and J. Shang, "Indoor localization improved by spatial context—a survey," *ACM Computing Surveys (CSUR)*, vol. 52, no. 3, pp. 1–35, 2019.

[124] A. R. Jiménez, F. Zampella, and F. Seco, "Improving inertial pedestrian dead-reckoning by detecting unmodified switched-on lamps in buildings," *Sensors*, vol. 14, no. 1, pp. 731–769, 2014.

[125] Q. Liang, Y. Sun, L. Wang, and M. Liu, "A novel inertial-aided visible light positioning system using modulated leds and unmodulated lights as landmarks," *IEEE Transactions on Automation Science and Engineering*, vol. 19, no. 4, pp. 3049–3067, 2021.

[126] Q. Wang, H. Luo, H. Xiong, A. Men, F. Zhao, M. Xia, and C. Ou, "Pedestrian dead reckoning based on walking pattern recognition and online magnetic fingerprint trajectory calibration," *IEEE Internet of Things Journal*, vol. 8, no. 3, pp. 2011–2026, 2020.

[127] Q. Wang, H. Luo, F. Zhao, and W. Shao, "An indoor self-localization algorithm using the calibration of the online magnetic fingerprints and indoor landmarks," in *2016 international conference on indoor positioning and indoor navigation (IPIN)*. IEEE, 2016, Conference Proceedings, pp. 1–8.

[128] Q. Wang, M. Cheng, A. Noureldin, and Z. Guo, "Research on the improved method for dual foot-mounted inertial/magnetometer pedestrian positioning based on adaptive inequality constraints kalman filter algorithm," *Measurement*, vol. 135, pp. 189–198, 2019.

[129] M. Angermann, M. Frassl, M. Doniec, B. J. Julian, and P. Robertson, "Characterization of the indoor magnetic field for applications in localization and mapping," in *2012 International Conference on Indoor Positioning and Indoor Navigation (IPIN)*. IEEE, 2012, pp. 1–9.

[130] G. Ouyang and K. Abed-Meraim, "A survey of magnetic-field-based indoor localization," *Electronics*, vol. 11, no. 6, p. 864, 2022.

[131] H. Zhao, Z. Wang, S. Qiu, Y. Shen, L. Zhang, K. Tang, and G. Fortino, "Heading drift reduction for foot-mounted inertial navigation system via multi-sensor fusion and dual-gait analysis," *IEEE Sensors Journal*, vol. 19, no. 19, pp. 8514–8521, 2018.

[132] B. Kim and S.-H. Kong, "A novel indoor positioning technique using magnetic fingerprint difference," *IEEE Transactions on Instrumentation and Measurement*, vol. 65, no. 9, pp. 2035–2045, 2016.

[133] H. Luo, F. Zhao, M. Jiang, H. Ma, and Y. Zhang, "Constructing an indoor floor plan using crowdsourcing based on magnetic fingerprinting," *Sensors*, vol. 17, no. 11, p. 2678, 2017.

[134] A. Nikitin, C. Laoudias, G. Chatzimilioudis, P. Karras, and D. Zeinalipour-Yazti, "Indoor localization accuracy estimation from fingerprint data," in *2017 18th IEEE International Conference on Mobile Data Management (MDM)*. IEEE, 2017, pp. 196–205.

[135] D. Carrillo, V. Moreno, B. Úbeda, and A. F. Skarmeta, "Magicfinger: 3d magnetic fingerprints for indoor location," *Sensors*, vol. 15, no. 7, pp. 17 168–17 194, 2015.

[136] G. Wang, X. Wang, J. Nie, and L. Lin, "Magnetic-based indoor localization using smartphone via a fusion algorithm," *IEEE Sensors Journal*, vol. 19, no. 15, pp. 6477–6485, 2019.

[137] P. Senin, "Dynamic time warping algorithm review," *Information and Computer Science Department University of Hawaii at Manoa Honolulu, USA*, vol. 855, no. 1-23, p. 40, 2008.

[138] B. Wang, Q. Chen, L. T. Yang, and H.-C. Chao, "Indoor smartphone localization via fingerprint crowdsourcing: Challenges and approaches," *IEEE Wireless Communications*, vol. 23, no. 3, pp. 82–89, 2016.

[139] Y. Chen, M. Zhou, and Z. Zheng, "Learning sequence-based fingerprint for magnetic indoor positioning system," *Ieee Access*, vol. 7, pp. 163 231–163 244, 2019.

[140] J. Chen, G. Ou, A. Peng, L. Zheng, and J. Shi, "A hybrid dead reckon system based on 3-dimensional dynamic time warping," *Electronics*, vol. 8, no. 2, p. 185, 2019.

[141] S. Guo, G. Niu, Z. Wang, and M.-O. Pun, "Magnetic field strength sequence-based indoor localization using multi-level link-node models," in *ICC 2020-2020 IEEE International Conference on Communications (ICC)*. IEEE, 2020, pp. 1–6.

[142] X. Niu, T. Liu, J. Kuang, Q. Zhang, and C. Guo, "Pedestrian trajectory estimation based on foot-mounted inertial navigation system for multistory buildings in postprocessing mode," *IEEE Internet of Things Journal*, vol. 9, no. 9, pp. 6879–6892, 2021.

[143] Y. Wu, H.-B. Zhu, Q.-X. Du, and S.-M. Tang, "A survey of the research status of pedestrian dead reckoning systems based on inertial sensors," *International Journal of Automation and Computing*, vol. 16, pp. 65–83, 2019.

[144] J. Borenstein, L. Ojeda, and S. Kwanmuang, "Heuristic reduction of gyro drift in imu-based personnel tracking systems," in *Optics and Photonics in Global Homeland Security V and Biometric Technology for Human Identification VI*, vol. 7306. SPIE, 2009, pp. 244–254.

[145] Zidane-Han, "Pedestrian-dead-reckoning," https://github.com/Zidane-Han/Pedestrian-Dead-Reckoning, 2022.

[146] A. Abadleh, E. Al-Hawari, E. Alkafaween, and H. Al-Sawalqah, "Step detection algorithm for accurate distance estimation using dynamic step length," in *2017 18th IEEE international conference on mobile data management (MDM)*. IEEE, 2017, pp. 324–327.

[147] S. H. Shin and C. G. Park, "Adaptive step length estimation algorithm using optimal parameters and movement status awareness," *Medical engineering & physics*, vol. 33, no. 9, pp. 1064–1071, 2011.

[148] J. Karki, "Active low-pass filter design," *Texas Instruments application report*, 2000.

[149] M. Gdeisat and F. Lilley, "One-dimensional phase unwrapping problem," *signal*, vol. 4, p. 6, 2011.

[150] B. Sensortec, "Intelligent 9-axis absolute orientation sensor," *BNO055 datasheet, November*, 2014.

[151] S.-H. Cha, "Comprehensive survey on distance/similarity measures between probability density functions," *INTERNATIONAL JOURNAL OF MATHEMATICAL MODELS AND METHODS IN APPLIED SCIENCES*, vol. 1, 01 2007.

[152] I. J. Myung, "Tutorial on maximum likelihood estimation," *Journal of Mathematical Psychology*, vol. 47, no. 1, pp. 90–100, 2003. [Online]. Available: https://www.sciencedirect.com/science/article/pii/S0022249602000287

[153] E. Alessio, A. Carbone, G. Castelli, and V. Frappietro, "Second-order moving average and scaling of stochastic time series," *European Physical Journal B*, vol. 27, no. 2, pp. 197–200, 2002. [Online]. Available: http://www.sciengine.com/publisher/EDPSciences/journal/EuropeanPhysicalJournalB/27/2/10.1140/epjb/e20020150

[154] B. Chu, "Position compensation algorithm for omnidirectional mobile robots and its experimental evaluation," *International Journal of Precision Engineering and Manufacturing*, vol. 18, no. 12, pp. 1755–1762, 2017.

[155] O. Rukundo and H. Cao, "Nearest neighbor value interpolation," *arXiv preprint arXiv:1211.1768*, 2012.

[156] R. Girisha, G. Prateek, K. Hari, and P. Händel, "Fusing the navigation information of dual foot-mounted zero-velocity-update-aided inertial navigation systems," in *2014 International Conference on Signal Processing and Communications (SPCOM)*. IEEE, 2014, Conference Proceedings, pp. 1–6.

[157] I. Skog, P. Handel, J.-O. Nilsson, and J. Rantakokko, "Zero-velocity detection—an algorithm evaluation," *IEEE transactions on biomedical engineering*, vol. 57, no. 11, pp. 2657–2666, 2010.

[158] A. R. Jiménez, F. Zampella, and F. Seco, "Light-matching: A new signal of opportunity for pedestrian indoor navigation," in *International conference on indoor positioning and indoor navigation*. IEEE, 2013, Conference Proceedings, pp. 1–10.

[159] C. Fischer, P. T. Sukumar, and M. Hazas, "Tutorial: Implementing a pedestrian tracker using inertial sensors," *IEEE pervasive computing*, vol. 12, no. 2, pp. 17–27, 2012.

[160] S. Rajagopal, “Personal dead reckoning system with shoe mounted inertial sensors,” *Master’s Degree Project, Stockholm, Sweden*, 2008.

[161] E. Foxlin, “Pedestrian tracking with shoe-mounted inertial sensors,” *IEEE Computer graphics and applications*, vol. 25, no. 6, pp. 38–46, 2005.

[162] C. Bector and S. Chandra, “On incomplete lagrange function and saddle point optimality criteria in mathematical programming,” *Journal of mathematical analysis and applications*, vol. 251, no. 1, pp. 2–12, 2000.

[163] W. Gander, “Least squares with a quadratic constraint,” *Numerische Mathematik*, vol. 36, no. 3, pp. 291–307, 1980.

[164] C. K. Liew, “Inequality constrained least-squares estimation,” *Journal of the American Statistical Association*, vol. 71, no. 355, pp. 746–751, 1976.

[165] M. Jacquelin Perry, “Gait analysis: normal and pathological function,” *New Jersey: SLACK*, 2010.

[166] J. K. Aggarwal and Q. Cai, “Human motion analysis: A review,” *Computer vision and image understanding*, vol. 73, no. 3, pp. 428–440, 1999.

[167] M. Posa, C. Cantu, and R. Tedrake, “A direct method for trajectory optimization of rigid bodies through contact,” *The International Journal of Robotics Research*, vol. 33, no. 1, pp. 69–81, 2014.

[168] R. W. P. C.-G. L. Wu, “Slam-ing: A wearable slam inertial navigation system,” in *2022 IEEE SENSORS conference*, 2022, Conference Proceedings.

[169] M. W. Whittle, “Three-dimensional motion of the center of gravity of the body during walking,” *Human Movement Science*, vol. 16, no. 2-3, pp. 347–355, 1997.

[170] p. https://en.wikipedia.org/wiki/File:BodyPlanes.jpg, 2007.

[171] T. Komura, A. Nagano, H. Leung, and Y. Shinagawa, “Simulating pathological gait using the enhanced linear inverted pendulum model,” *IEEE Transactions on biomedical engineering*, vol. 52, no. 9, pp. 1502–1513, 2005.

[172] F. L. Buczek, K. M. Cooney, M. R. Walker, M. J. Rainbow, M. C. Concha, and J. O. Sanders, “Performance of an inverted pendulum model directly applied to normal human gait,” *Clinical Biomechanics*, vol. 21, no. 3, pp. 288–296, 2006.

[173] L. Zhou and J. Liu, "A method of the body of mass trajectory for human gait analysis," *Information Technology*, vol. 40, no. 8, pp. 147–150, 2016.

[174] Y. Shi, L. Meng, and D. Chen, "Human standing-up trajectory model and experimental study on center-of-mass velocity," in *IOP Conference Series: Materials Science and Engineering*, vol. 612. IOP Publishing, 2019, Conference Proceedings, p. 022088.

[175] F. Tsai and W. Philpot, "Derivative analysis of hyperspectral data," *Remote sensing of environment*, vol. 66, no. 1, pp. 41–51, 1998.

[176] H. A. Burger, "Use of euler-rotation angles for generating antenna patterns," *IEEE Antennas and Propagation Magazine*, vol. 37, no. 2, pp. 56–63, 1995.

[177] E. W. Weisstein, "Euler angles," *https://mathworld. wolfram. com/*, 2009.

[178] Z. Qiu, Y. Lu, and Z. Qiu, "Review of ultrasonic ranging methods and their current challenges," *Micromachines*, vol. 13, no. 4, p. 520, 2022.

[179] Bresenham and E. J., "Algorithm for computer control of a digital plotter," *Ibm Systems Journal*, vol. 4, no. 1, pp. 25–30, 1965.

[180] B. Kim and S.-H. Kong, "A novel indoor positioning technique using magnetic fingerprint difference," *IEEE Transactions on Instrumentation and Measurement*, vol. 65, no. 9, pp. 2035–2045, 2016.

[181] H. Azami, K. Mohammadi, and B. Bozorgtabar, "An improved signal segmentation using moving average and savitzky-golay filter," *Journal of Signal and Information Processing*, vol. 3, no. 1, 2012.

[182] V. Renaudin, M. H. Afzal, G. Lachapelle *et al.*, "Complete triaxis magnetometer calibration in the magnetic domain," *Journal of sensors*, vol. 2010, 2010.

[183] M. Okawa, "Template matching using time-series averaging and dtw with dependent warping for online signature verification," *IEEE Access*, vol. 7, pp. 81 010–81 019, 2019.

[184] H. Zhang, Y. Dong, J. Li, and D. Xu, "Dynamic time warping under product quantization, with applications to time-series data similarity search," *IEEE Internet of Things Journal*, vol. 9, no. 14, pp. 11 814–11 826, 2021.

[185] F. De Cillis, L. Faramondi, F. Inderst, S. Marsella, M. Marzoli, F. Pascucci, and R. Setola, "Hybrid indoor positioning system for first responders," *IEEE Transactions on Systems, Man, and Cybernetics: Systems*, vol. 50, no. 2, pp. 468–479, 2017.

[186] R. Girisha, G. Prateek, K. Hari, and P. Händel, "Fusing the navigation information of dual foot-mounted zero-velocity-update-aided inertial navigation systems," in *2014 International Conference on Signal Processing and Communications (SPCOM).* IEEE, 2014, pp. 1–6.

[187] R. Girisha, G. V. Prateek, K. Hari, and P. Händel, "Fusing the navigation information of dual foot-mounted zero-velocity-update-aided inertial navigation systems," in *2014 International Conference on Signal Processing and Communications (SPCOM)*, 2014, pp. 1–6.

[188] T. Chai and R. R. Draxler, "Root mean square error (rmse) or mean absolute error (mae)," *Geoscientific Model Development Discussions*, vol. 7, no. 1, pp. 1525–1534, 2014.

[189] W. Shi, Y. Wang, and Y. Wu, "Dual mimu pedestrian navigation by inequality constraint kalman filtering," *Sensors*, vol. 17, no. 2, p. 427, 2017.

[190] Z. Wang, H. Zhao, S. Qiu, and Q. Gao, "Stance-phase detection for zupt-aided foot-mounted pedestrian navigation system," *IEEE/ASME Transactions On Mechatronics*, vol. 20, no. 6, pp. 3170–3181, 2015.

[191] C.-S. Jao, K. Stewart, J. Conradt, E. Neftci, and A. Shkel, "Zero velocity detector for foot-mounted inertial navigation system assisted by a dynamic vision sensor," in *2020 DGON Inertial Sensors and Systems (ISS).* IEEE, 2020, Conference Proceedings, pp. 1–18.

[192] B. Wagstaff, V. Peretroukhin, and J. Kelly, "Improving foot-mounted inertial navigation through real-time motion classification," in *2017 International Conference on Indoor Positioning and Indoor Navigation (IPIN).* IEEE, 2017, Conference Proceedings, pp. 1–8.

[193] C. Chen, P. Zhao, C. X. Lu, W. Wang, A. Markham, and N. Trigoni, "Deep-learning-based pedestrian inertial navigation: Methods, data set, and on-device inference," *IEEE Internet of Things Journal*, vol. 7, no. 5, pp. 4431–4441, 2020.

[194] C.-H. Chen, P.-W. Chen, P.-J. Chen, and T.-H. Liu, "Indoor positioning using magnetic fingerprint map captured by magnetic sensor array," *Sensors*, vol. 21, no. 17, p. 5707, 2021.

[195] C. Guo and D. Liu, "Quantitative analyses of magnetic field distributions for buildings of steel structure," in *2012 Sixth International Conference on Electromagnetic Field Problems and Applications.* IEEE, 2012, Conference Proceedings, pp. 1–4.

[196] M. Zhu, Y. Wu, and S. Luo, "f^{2}imu-r: pedestrian navigation by low-cost foot-mounted dual imus and interfoot ranging," *IEEE Transactions on Control Systems Technology*, vol. 30, no. 1, pp. 247–260, 2021.

[197] I. Silva, C. Pendão, J. Torres-Sospedra, and A. Moreira, "Trackinfactory: A tight coupling particle filter for industrial vehicle tracking in indoor environments," *IEEE Transactions on Systems, Man, and Cybernetics: Systems*, vol. 52, no. 7, pp. 4151–4162, 2021.

[198] J. Li, X. Zhou, S. Qiu, Y. Mao, Z. Wang, C. K. Loo, and X. Liu, "Learning based stance phase detection and multi-sensor data fusion for zupt-aided pedestrian dead reckoning system," *IEEE Internet of Things Journal*, 2023.

[199] H. Yao, X. Liang, R. Chen, X. Wang, H. Qi, L. Chen, and Y. Wang, "A benchmark of absolute and relative positioning solutions in gnss denied environments," *IEEE Internet of Things Journal*, 2023.

[200] Z. Chen and X. Pan, "A novel zero-velocity detector for pedestrian inertial navigation based on deep learning," in *2021 6th International Conference on Intelligent Computing and Signal Processing (ICSP)*. IEEE, 2021, pp. 807–811.

[201] Y. Wang, J. Kuang, X. Niu, and J. Liu, "Llio: Lightweight learned inertial odometer," *IEEE Internet of Things Journal*, vol. 10, no. 3, pp. 2508–2518, 2022.

[202] C. Chen, P. Zhao, C. X. Lu, W. Wang, A. Markham, and N. Trigoni, "Deep-learning-based pedestrian inertial navigation: Methods, data set, and on-device inference," *IEEE Internet of Things Journal*, vol. 7, no. 5, pp. 4431–4441, 2020.

[203] Y. Murata, K. Hiroi, K. Kaji, and N. Kawaguchi, "Pedestrian dead reckoning based on human activity sensing knowledge," in *Acm International Joint Conference on Pervasive Ubiquitous Computing: Adjunct Publication*, 2014, pp. 797–806.

[204] M. Hölzl, R. Neumeier, and G. Ostermayer, "Localization in an industrial environment: A case study on the difficulties for positioning in a harsh environment," *International Journal of Distributed Sensor Networks*, 2015.

[205] V. K. Vadlamani, M. Bhattarai, M. Ajith, and M. Martnez-Ramon, "A novel indoor positioning system for unprepared firefighting scenarios," 08 2020.

[206] N. Pirzada, M. Y. Nayan, F. Subhan, M. F. Hassan, and M. A. Khan, "Comparative analysis of active and passive indoor localization systems," *AASRI Procedia*, vol. 5, pp. 92–97, 2013.

[207] X. Yun, E. R. Bachmann, H. Moore, and J. Calusdian, "Self-contained position tracking of human movement using small inertial/magnetic sensor modules," in *Proceedings 2007 IEEE International Conference on Robotics and Automation.* IEEE, 2007, pp. 2526–2533.

[208] C.-S. Jao and A. M. Shkel, "Zupt-aided ins bypassing stance phase detection by using foot-instability-based adaptive covariance," *IEEE Sensors Journal*, vol. 21, no. 21, pp. 24 338–24 348, 2021.

[209] Z. Wang, H. Zhao, S. Qiu, and Q. Gao, "Stance-phase detection for zupt-aided foot-mounted pedestrian navigation system," *IEEE/ASME Transactions On Mechatronics*, vol. 20, no. 6, pp. 3170–3181, 2015.

[210] V. Zhmud, N. Kondratiev, K. Kuznetsov, V. Trubin, and L. Dimitrov, "Application of ultrasonic sensor for measuring distances in robotics," in *Journal of Physics: Conference Series*, vol. 1015, no. 3. IOP Publishing, 2018, p. 032189.

[211] O. Rukundo and H. Cao, "Nearest neighbor value interpolation," *arXiv preprint arXiv:1211.1768*, 2012.

[212] S. Choi, J.-Y. Lee, and W. Yu, "Fast any-angle path planning on grid maps with non-collision pruning," in *2010 IEEE International Conference on Robotics and Biomimetics.* IEEE, 2010, pp. 1051–1056.

Appendix A

List of Abbreviations

IPS	Indoor Positioning System
DR	Dead Reckoning
WSN	Wireless Sensor Network
INS	Inertial Navigation System
PDR	Pedestrian Dead Reckoning
SLAM	Simultaneous localisation and Mapping
vSLAM	visual SLAM
GNSS	Global Navigation Satellite System
MFM	Magnetic Field Matching
MF	Magnetic Fingerprint
LDM	Light Density Matching
IMU	Inertial Measurement Unit
MIMUs	Magneto-inertial measurement units
Multi-INS	Multi-person INS
GA-PDR	Gait Analysis-based PDR
GLRT	General Likelihood Ratio Test
FT-INS	Foot-mounted INS
DF-INS	Dual Foot-mounted INS
IOAM	Inertial Odometry and Mapping
ZUPT	Zero-velocity Update
ZARU	Zero Angular Rate Update
ZV	Zero Velocity
MCD	Minimum Centroid Distance

KF	Kalman Filter
EKF	Extended Kalman Filter
UKF	Unscented Kalman filter
DTF	Dual Trajectory Fusion
UAV	Unmanned Aerial Vehicles
CBoM	Center Body of Mass
S-OGM	surrounding Occupancy Grid Map
RMSE	Root Mean Square Error
MSE	Mean Square Error
ORB	Oriented Fast and Rotated Brief
LIDAR	Light Detection and Ranging
RADAR	Radio Detection and Ranging
GAN	Generative Adversarial Networks
RF	Radio Frequency
MEMS	Micro-Electro-Mechanical System
LCE	Loop Closing Error
DTW	Dynamic Time Wrapping
MFI	Magnetic Field Intensity
MWR	Millimeter Wave Radio
PIR	Pyroelectric infrared
IoT	Internet of Things
HDE	Heuristic Drift Elimination
GA	Gait Analysis
GD	Gait Detection
RTE	Redundant Turn Elimination
CEP	circular error probable
ROI	Region-of-interest
SP	Step Pattern
ECEF	Earth-fixed coordinate system

Appendix B

SLAM-ING: A Wearable SLAM Inertial NaviGation System

ILBS shows great research promotions with wide applications e.g., indoor firefighting, cave exploration, parking and market guide. FT-INS, one approach of ILBS, lacks a reference map of the environment, resulting in poor trajectory recognition. This paper introduces SLAM-ING, a novel wearable type SLAM via a ZARU aided Inertial NaviGation. SLAM-ING proposes a gravity centre calculation method, merging the dual (left and right) foot trajectories. Moreover, the proposed polar projection and occupancy grid map method determines the map boundary, enabling the fusion of the trajectory and ultrasonic range. The mapping results of SLAM-ING are demonstrated with the ground truth. The location performance is validated using a self-created database, the results of which indicate lower horizontal and spherical error compared with the traditional INS in all scenarios.

B.1 Introduction

ILBS[49] is an actively explored research topic in the field of Geographic Sciences (GS). However, due to the characteristics and materials used in modern buildings, GNSS, a commonly used global localisation system, is unsuitable for indoor localisation. Other passive localisation methods include UWB [10]; Wi-Fi [120]; BLE [126]; and radio frequency identification (RFID) [11]. However, many existing solutions rely upon pre-existing infrastructure such as sensors and access points to be installed for localisation to work accurately – limiting their potential for more widespread usage. Therefore, alternatives which function without existing infrastructure are desirable for a broad range of use cases, including emergency response and home applications. Active localisation and mapping is one such approach in which users carry sensors on their person [206].

INS is a popular active localisation method in ILBS [207] with lower environmental limitations compared with vSLAM [26] and LiDAR SLAM [57]. Using INS, a user's current position is computed based on their last known position. Foot-mounted INS has been shown to achieve high accuracy [208] due to its ability to measure inertia. In addition, the Zero-velocity UPdaTe (ZUPT) and Zero Angular Rate Update (ZARU) can only be applied in the foot-mounted system when the user is stationary [209]. OpenShoe [103, 104] is an embedded foot-mounted INS utilising ZUPT. However, the tracking performance of these methods with a single IMU is easily affected by mechanical and measurement errors arising from its electronic components.

At present, to reduce heading drift, many approaches have considered using a dual foot-mounted design. Multiple sensors reduce the impact electrical component noise has on overall tracking performance. Similarly, multiple sensors allow for kinematic analysis of user motion, which, in turn, can help constrain growing position errors. Prateek et al. [99] proposed a sphere limit algorithm built upon the OpenShoe model to merge dual-foot INS data. Zhao et al. [97] proposed a dual gait analysis approach to optimise step length estimation. Wang et al. [128] proposed an adaptive inequality constraint using Kalman filter for dual-foot sensor fusion. Dual foot-mounted INS systems have been shown to improve tracking performance dramatically. However, the lack of a reference map of the environment makes it difficult to recognise the trajectory in unfamiliar scenarios like indoor firefighting.

To address the lack of an environment map, this paper proposes SLAM-ING, a SLAM approach which utilises INS and ultrasonic sensors to generate a dynamic map of the environment by measuring the distance between the user and the surrounding environment. A gravity centre calculation and an occupancy grid mapping approach is applied to model the map points. ultrasonic sensor works stably under smoke and vapour-filled environments, playing scenario and power-friendly roles among kinds of ranging methods [154, 178].

B.2 ZUPT and ZARU Aided INS for Dual Foot Fusion

B.2.1 Initialization

The sampling rate of an ultrasonic sensor is lower than that of an IMU, because of the physical transmission properties of sound [210]. A nearest neighbour interpolation method [211] is adapted to align the range data to the sampling rate of the IMU.

$$u^{(i)} = interp\left(\hat{u}^{(i)}, \frac{Ts\left(imu^{(i)}\right)}{Ts\left(\hat{u}^{(i)}\right)}\right) \tag{B.1}$$

where $\hat{u}^{(i)}$and $u^{(i)}$represent the original and interpolated ultrasonic range signal. $i \in \{R,\ L\}$represents the sensor mounted on right or left foot. $Ts()$ computes the sampling rate of the sensor. Two data sequences from the sensors on each foot are synchronised. The IMU data is defined as:

$$D_k^{(i)} \triangleq \left[a_k^{(i)} \quad \omega_k^{(i)}\right]^T, D_k^{(i)} \in \mathbb{R}^6 \tag{B.2}$$

B.2.2 EKF

The IMU state in the navigation system at time $k \in \mathbb{N}^+$is defined as [156]:

$$\hat{x}_k^{(i)} \triangleq \left[\hat{p}_k^{(i)} \ \hat{\mathrm{v}}_k^{(i)} \ \hat{\theta}_k^{(i)}\right] \tag{B.3}$$

where $\hat{p}_k^{(i)} \in \mathbb{R}^3$,$\hat{v}_k^{(i)} \in \mathbb{R}^3$and $\hat{\theta}_k^{(i)} \in \mathbb{R}^3$represent the position, velocity and pose in 3-axis [97, 99]. The INS process for state transforming from the last known state is defined as:

$$\hat{x}_k^{(i)} = f\left(\hat{x}_{k-1}^{(i)}, \widetilde{e}_{k-1}^{(i)}\right) \tag{B.4}$$

where f denotes a 9-dimension state transforming function, $\widetilde{e}_{k-1}^{(i)}$denotes the error covariance variable of navigation system. And the time dynamics of error $\delta\hat{x}_k^{(i)}$ for $\hat{x}_k^{(i)}$is modeled as:

$$\delta\hat{x}_k^{(i)} = \left[\delta\hat{p}_k^{(i)} \ \delta\hat{v}_k^{(i)} \ \delta\hat{\theta}_k^{(i)} \ \delta a_k^{(i)} \ \delta\omega_k^{(i)}\right] \tag{B.5}$$

$$\delta\hat{x}_k^{(i)} = F_k^{(i)}\delta\hat{x}_{k-1}^{(i)} + G_k^{(i)}w_k^{(i)} \tag{B.6}$$

where $\delta\hat{p}_k^{(i)}$, $\delta\hat{v}_k^{(i)}$ and $\delta\hat{\theta}_k^{(i)}$ indicate error covariance of position, velocity and pose, $\delta a_k^{(i)}$ and $\delta\omega_k^{(i)}$represents the hardware bias of the accelerometer and gyroscope. $F_k^{(i)}$and $G_k^{(i)}$ denote the state transition and noise gain matrix. The state covariance matrix is described by:

$$P_k^{(i)} = F_k^{(i)}P_k^{(i)}\left(F_k^{(i)}\right)^T + G_k^{(i)}Q_k^{(i)}\left(G_k^{(i)}\right)^T \tag{B.7}$$

B.2.3 ZUPT and ZARU

A step detector [157] classifies each data sample according to its gait state, being either: moving and stationary. When a stationary standing phase is detected, the navigation system sets pseudo-measurements in the Kalman filter framework to correct $\hat{x}_k^{(i)}$ as explained in [103, 159, 161]. The Kalman gain is computed by:

$$K_k^{(i)} = P_k^{(i)} \left(H_k\right)^T \left[H_k P_k^{(i)} \left(H_k\right)^T + R_k\right]^{-1} \tag{B.8}$$

$$H_k = \begin{bmatrix} H_v \\ H_\omega \end{bmatrix} = \begin{bmatrix} 0_{3\times3} & I_{3\times3} & 0_{3\times3} & 0_{3\times3} & 0_{3\times3} \\ 0_{3\times3} & 0_{3\times3} & 0_{3\times3} & 0_{3\times3} & I_{3\times3} \end{bmatrix} \tag{B.9}$$

where $I_{3\times3}$ denotes identity matrix and $0_{3\times3}$ denotes zero matrix. H_k is the observation transition matrix with pseudo-measurement. R_k denotes the noise covariance matrix of H_k. Updating the prediction variable in the Kalman filter platform to correct the navigation state:

$$\hat{x}_k^{(i)} = \hat{x}_k^{(i)} + K_k^{(i)} \left[\left[\delta\hat{v}_k^{(i)} \ \delta\omega_k^{(i)}\right]^T - H_k \hat{x}_k^{(i)}\right] \tag{B.10}$$

Finally, correct the state covariance matrix to complete the EKF loop:

$$P_k^{(i)} = \left[I_{15\times9} - K_k H_k\right] P_k^{(i)} \tag{B.11}$$

The position of the dual foot is fused by the centroid method [157] in Kalman filter.

B.3 Ultrasonic Mapping

B.3.1 Gravity Center Calculation

In SLAM-ING, to simplify the visualization of the trajectory, the user is defined as being a rigid body [166, 167]. The gravity centre of the carrier is calculated by merging the dual foot position estimation using a weight fusion method:

$$p_c = g\left[p^{(R)} \quad \mathrm{p}^{(L)}\right] = \alpha p^{(R)} + \beta p^{(L)}, \ \alpha + \beta = 1 \tag{B.12}$$

where $p_c \in \mathbb{R}^3$ indicates the position of the hypothetical gravity centre of the carrier's body. α and β are weight parameters for right and left foot INS, respectively.

B.3.2 Ultrasonic Scanning Projection

The coordinates of ultrasonic mapping points are calculated based on the reference position and pose i.e., the INS. The ranging direction of the ultrasonic sensor is parallel to the x-axis of IMU in each foot.

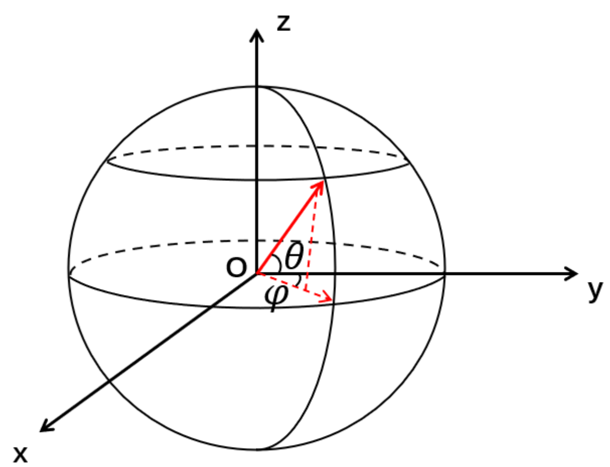

Figure B.1: *The schematic of polar projection.*

To project the 3D scanning to 2D XOY coordinate, a polar transform method is shown in Fig. B.1. The proposed method is described below [176, 177]:

$$M\left(r_k^{(j)}\right) = \begin{bmatrix} \cos\theta\cos\varphi \\ \cos\theta\sin\varphi \\ sin\theta\} \end{bmatrix} \tag{B.13}$$

where θ and φ denote the pitch and yaw angles in the sphere coordinate. The coordinate of ultrasonic mapping points $M\left(r_k^{(j)}\right)$ under maximum covering principle is calculated as below:

$$Up_k^{(i)} = \left[Ux_k^{(i)}\ Uy_k^{(i)}\ Uz_k^{(i)}\right]^T = p_k^{(i)} + \left[u_k^{(i)} diag(1,1,1) M\left(r_k^{(i)}\right)\right] \tag{B.14}$$

The ultrasonic range is mapped via occupancy grid map algorithm (see Fig. B.2) [40]. The grid mapping via Bresenham [212] algorithm is defined as (B.15)

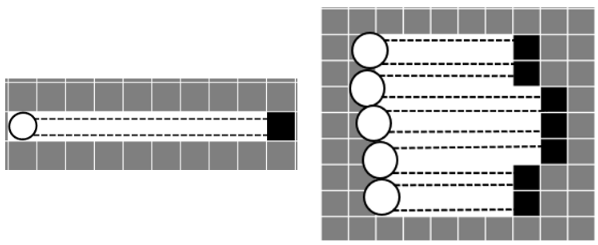

Figure B.2: *Schematic of single scanning [40] (a) and continual scanning (b). The white circle is the position of ultrasonic sensor, black, gray and white cells denote boundary, unavailable area and empty area, respectively.*

$$B\left(p_k^{(j)}, Up_k^{(j)}\right) \tag{B.15}$$

where $p_k^{(j)}$ and $Up_k^{(j)}$ indicate the ultrasonic placement position and the boundary position of ultrasonic scanning, respectively.

B.4 Experiment and Discussion

SLAM-ING prototype system utilised a MPU9250 IMU (200Hz), a HC-SR04 ultrasonic sensor (15Hz), and an ESP32 dual core micro-computing unit. SLAM-ING were mounted to the front, and outer side of each shoe. Sensor data is transmitted via Wi-Fi to a nearby terminal, as shown in Fig. B.3.

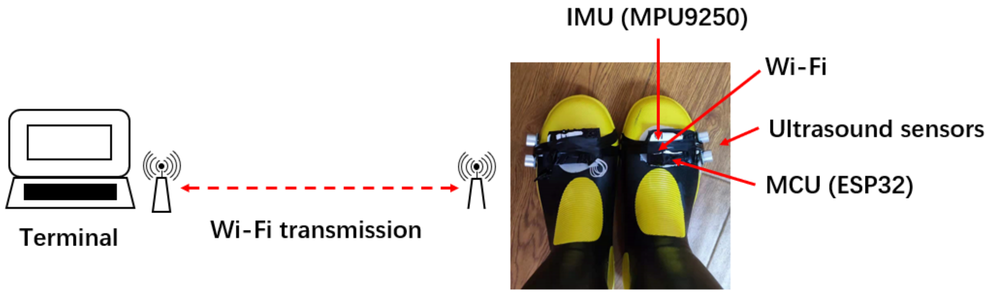

Figure B.3: *The inner design and hardware placing of the SLAM-ING data collector.*

Data collection to evaluate the system was held in an office-like building. Scenario 1 featured a 10m straight corridor and scenario 2 had a 40m "L" shape route. The gravity centre weights are $\alpha = 0.5$ and $\beta = 0.5$. The ground truth of the corridor boundary is measured by a laser range finder.

The gravity centre calculation (see Fig.B.4a and B.4c) fuses the dual foot trajectories, eliminating the dynamic stride length interference which simplifies the user's track visualisation to a single line. The ultrasonic mapping of this approach demonstrates good consistency with the ground truth. A few of the map areas derive from the boundary because of the ultrasonic measurement noise and human's physiological activity.

INS trajectory performance is measured via horizontal and spherical error [187]. Our method showed lower error because the ZARU further constrains the drift of pose estimation. In general, SLAM-ING shows good performance in localisation and mapping which is promising to specific application.

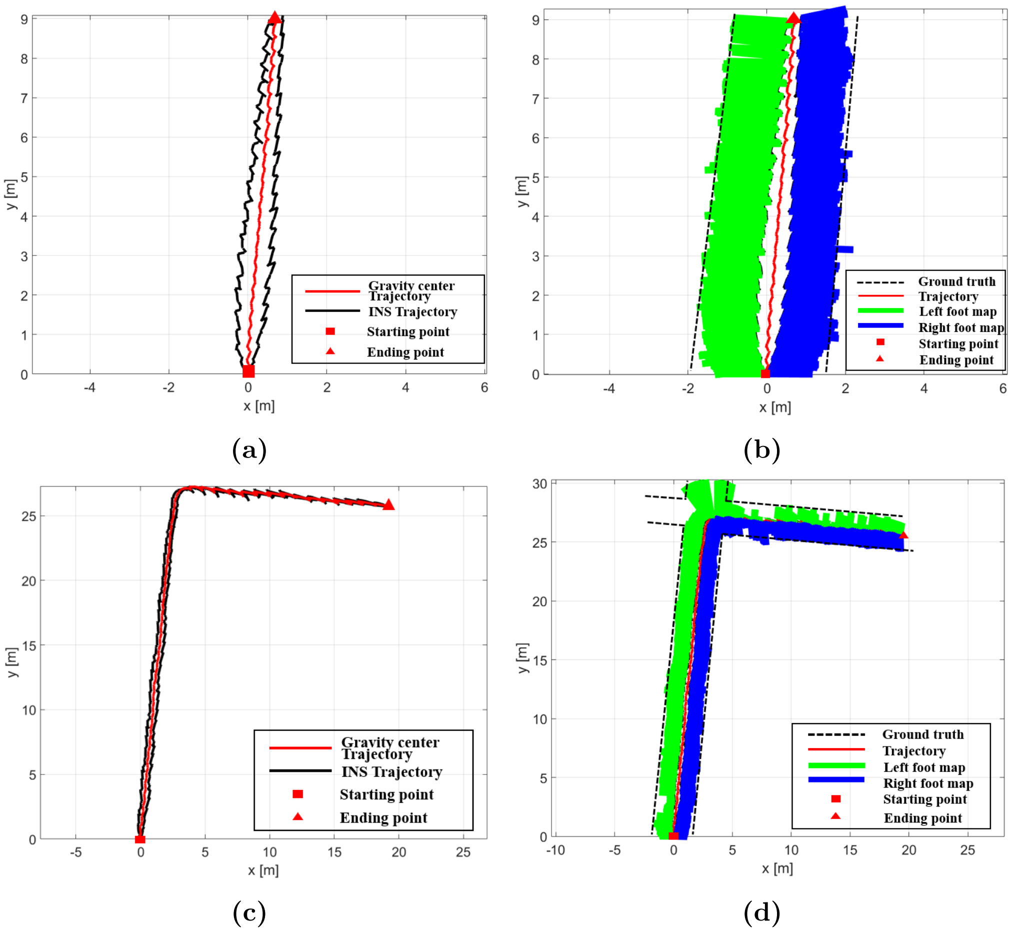

Figure B.4: *2D plotting the gravity centre fusion and INS trajectory of Scenario 1 and Scenario 2 (a)(c) and ultrasonic mapping (b)(d) for the left foot (green area) and right foot (blue area).*

Table B.1: Comparison of Horizontal and Spherical Error of INS With/Without ZARU

Scenarios	Error type [m]	ZARU (Ours)	No ZARU [187]
Scenario1	Horizontal	**9.1301**	9.6376
	Spherical	**9.9232**	10.169
Scenario2	Horizontal	**32.097**	32.609
	Spherical	**33.167**	34.126

Two limitations were identified in the current implementation of SLAM-ING. First, the physical specifications of ultrasonic sensor limit the resolution and range of mapping. Second, the proposed method adopts a rectangle shape ultrasonic sensing model which limits the measurement accuracy at uneven boundary areas.

B.5 Conclusion

This study proposes SLAM-ING, a novel localisation and mapping approach utilising INS and ultrasonic sensors. The primary contributions of this system include a gravity centre calculation method for dual foot trajectory fusion and an ultrasonic mapping method using polar projection. A ZARU method is also adopted for stable pose estimation. This study demonstrated improved localisation performance with lower error rates relative to ZUPT-only approaches. Future work will explore the application of high-quality ultrasonic sensors and a cone-shaped ultrasonic sensing model for more accurate mapping performance.